ALMA MATER STUDIORUM
UNIVERSITÀ DI BOLOGNA

DOTTORATO DI RICERCA IN

Ingegneria e tecnologia dell'informazione per il monitoraggio strutturale e ambientale e la gestione dei rischi - EIT4SEMM

Ciclo XXXVI

Settore Concorsuale: ICAR08

Settore Scientifico Disciplinare: 08B2

Advances in the design of carpet cloaks for surface elastic waves

Presentata da: *Zinon Chatzopoulos*

Coordinatore Dottorato

Luca De Marchi

Supervisore

Alessandro Marzani

Co-Supervisore

Antonio Palermo

Esame finale anno 2024

Abstract of thesis entitled

Advances in the design of carpet cloaks for surface elastic waves

submitted by

Zinon Chatzopoulos

for the degree of Doctor of Philosophy

at University of Bologna

The objective of this Ph.D. thesis pertains to the conception and design of an innovative device, called elastic carpet cloak, to protect structures from surface elastic waves, i.e. Love and Rayleigh waves. The cloak smoothly redirects surface waves around objects, without any scattering or energy loss by adjusting its material properties based on transformational elastodynamics principles. Initially, we delve into cloaking of Love waves within an isotropic layered medium. By leveraging the form invariance of the governing equation, we derive the requisite anisotropic mechanical characteristics of ideal cloaks to hide triangular and parabolic-shaped defects. We validate our approach through dispersion analyses and harmonic simulations, matching ideal cloaks with pristine mediums. Then, for triangular defects, we adapt the ideal properties into layered cloaks of monoclinic double-material unit cells, demonstrating great convergence with ideal case, as the unit cell size decreases. Next, we explore cloaking of Rayleigh waves in homogeneous mediums. By utilizing transformation elastodynamics and assuming identity gauge for the displacements, we obtain the effective cloaking properties, characterized by non-symmetric elastic tensors. To address this, we employ a symmetrization technique to approximate the non-symmetric behavior by symmetric, yet anisotropic, composites. Symmetrized cloaks with triangular and semi-circular shapes are evaluated through simulations and dispersion analyses, with a semi-circular design exhibiting superior performance. Finally, we construct 3-D cloaks for Rayleigh and Love waves, pointing out the distinctions between 3-D cloaking with the superposition of Love and Rayleigh waves and its impact on symmetrization. In particular, prismatic, and cylindrical cloaks are designed according to symmetrization method driven by the weak form solution of Love waves. Time-harmonic simulations and dispersive analyses show that a symmetrized cylindrical cloak, constructed by the "Maximal" mean, provides significant cloaking protection across all computed frequencies. This study advances the design of feasible and efficient broadband elastic cloaks for surface waves.

Acknowledgments

I would like to express my deep gratitude and appreciation to all those who have supported me throughout my journey in completing this doctoral thesis. The realization of this work would not have been possible without their invaluable support, encouragement, motivation and contribution.

First and foremost, I would like to thank Prof. Alessandro Marzani, who gave me the opportunity to be a part of his spectacular scientific lab. His never ending guidance, deep expertise and also patience have been indispensable in developing this research. As an incredible mentor, he significantly enhanced not only my academic experience, but also inspired me to push myself past my limits and encouraged me on my research and daily life.

I am also very grateful to my co-supervisor Prof. Antonio Palermo for his insightful comments and suggestions through every step of this work. His outstanding research skills, passion for science and knowledge, paved the way for me to fly above all the obstacles arose in my study. I want to express my sincere gratitude to Prof. Sebastien Guenneau for his extremely valuable ideas and support as an expert in cloaking, that culminated in two published research works. Also, I want to thank deeply Prof. Andre Diatta, whose mathematical talents assisted the publication of the findings of Chapter 3.

,I thank all my wonderful colleagues in our Lab for making those 3 years unforgettable: Xingbo Pu, Farhad Zeighami, Masoud Mohammadgholiha, Soroosh Kamali, Ata Kalantari, Kemeng Cui, Yifei Xu. Additionally, I want to thank Prof. Oreste S. Bursi, Dr. Fabrizio Alosci, Tugberk Guner, Dr. Panagiotis Koutsogiannakis, Dr. Roberto Andreotti, for their kind hospitality during my secondmend period at Univeristy of Trento.

Special thanks to the European Union's Horizon 2020 research and innovation program under the Marie Skłodowska Curie grant agreement No. 813424 for this prestigious fellowship that supported me during my Ph.D. studies. Massive thanks to the legendary Prof. Gazetas and Prof. Antoniadis for the concept and architecture of the ITN Inspire project. Also, I cannot thank enough Dr. Marianna Loli for the perfect organization and all the great ESRs and colleagues in this project.

Finally, I am forever grateful to my loving parents, my family and my amazing friends, for their love, moral support, understanding, and unwavering belief in my abilities during this arduous but worth-exploring journey of the concept of cloaking.

Zinon Chatzopoulos,
University of Bologna,
31 October 2023

Contents

1 Introduction 7
- 1.1 Cloaking & invisibility: an overview . . . 7
- 1.2 Thesis objective & Contribution . . . 14

2 Cloaking of Love waves **28**
- 2.1 Introduction . . . 29
- 2.2 Statement of the problem . . . 32
- 2.3 Ideal cloaks: two illustrative examples . . . 37
- 2.4 Cloak realization via composite media . . . 45
- 2.5 Conclusion . . . 51
- 2.6 Appendix A. Distribution of the effective shear modulus. . . . 52
- 2.7 Appendix B. Inverse homogenization-Genetic Algorithm . . . 53

3 Cloaking of Rayleigh waves **65**
- 3.1 Introduction . . . 66
- 3.2 Governing Equations for 2-D Elasticity . . . 68
- 3.3 Carpet cloaking for Rayleigh waves: Transformation . . . 71
- 3.4 Carpet cloaking for Rayleigh waves: Symmetrization . . . 76
- 3.5 Numerical results and comparisons . . . 78
- 3.6 Conclusion . . . 88
- 3.7 Appendix A. Transformations with offset parameter ε. . . . 89

4 3-D Elastic cloaking **98**
- 4.1 Introduction . . . 99
- 4.2 Governing Equations . . . 102
- 4.3 3-D cloaking vs out-of-plane and in-plane cloaking . . . 109
- 4.4 Carpet cloaking for Surface elastic waves: Symmetrization . . . 113
- 4.5 Numerical Results and comparisons . . . 115
- 4.6 Conclusion . . . 127

5 Conclusions & future outlook **140**

Listing of figures

1.1 (a) 2D microwave cloaking structure with a plot of the material parameters that are implemented. (b) The design of the non-resonant elements and the relation between the unit cell geometry and the effective index. (c) Snapshots of time-dependent, steady-state electric field patterns. The fields shown are **(A)** the simulation of the cloak with the exact material properties, **(B)** the simulation of the cloak with the reduced material properties, **(C)** the experimental measurement of the bare conducting cylinder, and **(D)** the experimental measurement of the cloaked conducting cylinder. The right-hand scale indicates the instantaneous value of the field. (d) 2D field mapping (E-field) of the perturbation and ground-plane cloaked perturbation, illuminated by the waves from the left side **(A)** perturbation and **(B)** ground-plane cloaked perturbation. Reproduced with permission from [71,63] 9

1.2 Design of the discrete mass-spring polar lattice for a carpet cloak. (a) Geometric transformation for realizing a carpet cloak concealing a triangular void; (b) The mass-spring lattice is designed using the discrete transformation. For the design, $\alpha = 60$, and the lengths of springs, k_1, k_2, k_3, and the rigid masses are $\alpha[1-\frac{2\sqrt{3}}{3}tan\theta]$, $\alpha[1-\frac{\sqrt{3}}{3}tan\theta]$, $\alpha[1-\frac{\sqrt{3}}{3}tan\theta]$, and $\frac{2\sqrt{3}\alpha}{3}tan\theta$, respectively; ($c$) Zero-mode of the transformed lattice is equivalent to the rigid rotation of the virtual lattice. Reproduced with permission from [14]. 12

1.3 Hexachiral lattices. (a) Nonresonant lattice: black circles are rigid masses and black segments are massless elastic rods; contact points are perfect hinges. The highlighted angle is the twisting angle γ. (b) Isotropic zero mode: the lattice expands (black) from its reference configuration (gray) without stretching any rods. (c) Polar metamaterial: black disks are embedded resonators; colored coating is elastic and massless. (d) Resonance modes under imposed outer displacement: translational to the left and rotational to the right. Reproduced with permission from [53] 12

1.4 The incompressible neo-Hookean cylindrical annulus is pre-stressed as depicted on the right. This annulus then creates a cloak when slotted into a cylindrical cavity in an unbounded elastic medium, as illustrated on the left. Reproduced with permission from [60] 13

1.5 (a) Blueprint of the circular elastic cloak (only one-quarter is shown). White parts correspond to PVC, black parts to PDMS. The table on the right-hand side gives the elastic moduli (real parts) for the 16 different metamaterials in 20 concentric rings. The clamped region to be cloaked is shown in red, the surrounding region with homogeneous porosity ($f = 40\%$ PVC filling fraction) is highlighted in yellow. The plate thickness is $h = 1mm$. (b) Oblique-view photograph of a cloak before filling with PDMS. 14

2.1 (a) Reference configuration virtual domain. (b) A generic carpet-pinched cloak (purple region ψ) to conceal a defect (white region) from the propagating surface Love waves (real domain). (c) Schematic of a triangular pinched-carpet cloak in a layered isotropic medium. (d) Schematic of a parabolic pinched-carpet cloak in an isotropic heterogeneous medium characterized by a parabolic velocity profile along the depth of the half space. (e) Schematic of the FE model domain used in the simulations (not in scale). 34

2.2 Displacement fields of the Reference $(a)-(b)$, Ideal Cloak $(c)-(d)$ and Obstacle $(e)-(f)$ configurations, for the triangular pinched cloak case of section 3.1 computed at frequencies $\omega^\star = 1$ and $\omega^\star = 2$. (g) Dispersive curves (first 4 modes) for the Reference (blue lines) and the Ideal Cloak (red lines) configurations, as obtained by considering the unit cell in the schematic (R and IC), respectively. The analytical solution for the reference configuration is also presented (black lines). See Table 2.1 for the shear velocity C_{si} and density ρ_i of homogeneous isotropic layer i in R. 40

2.3 Displacement fields for the Reference $(a)-(b)$, Ideal Cloak $(c)-(d)$ and Obstacle $(e)-(f)$ configurations, considering the parabolic pinched cloak case of section 3.2 computed at frequencies $\omega^\star = 1$ and $\omega^\star = 2$. (g) Dispersive curves (first 2 modes) for the Reference (blue lines) and the Ideal Cloak (red lines) configurations, as obtained by considering the unit cell in the schematic (R and IC), respectively. 44

2.4 (a) Details of the monoclinic unit cell and (b-c) schematic representation of the layered cloaks. 45

2.5 Comparison between the Ideal (IC) and the Layered Cloak (LC) displacement fields, for a cloak fully contained inside the first layer (1^{st} column, panels (a) and (c)) and for a cloak exceeding the first layer (2^{nd} column, panels (b) and (d)). The harmonic simulations are performed at two different normalized frequencies $\omega^\star = [1-2]$. . . . 48

2.6 Parametric study on the dispersion curves with respect to the unit cell dimension of the layered cloaks. The dispersion of the Ideal cloak is provided for reference. . . . 56

2.7 Contour plots of the transformed shear moduli coefficients over a rectangular domain $(-c, c) \times (-b, 0)$, for the triangular $(a)-(c)$ and the parabolic $(d)-(f)$ shaped cloaks, respectively. 57

2.8 Results of the genetic algorithm, including the fitness value, the value of each parameter, the fitness of each individual and the time of convergence. 58

3.1 (a) Reference configuration (virtual domain) of the triangular cloak. (b) Deformed configuration (physical domain) obtained by the action of (Ξ^T) that maps the (virtual domain) into a defect (white region) surrounded by the cloak (purple region). (c) Reference configuration (virtual domain) of the semi-circular cloak. (d) Deformed configuration (physical domain) obtained by the action of (Ξ^{C_i}) that maps the (virtual domain) into a defect (white region) surrounded by the cloak (blue region). (e) Schematic representation of the FEM model. 73

3.2 Displacement fields for the Reference $(a)-(b)$, Ideal Cloak $(c)-(f)$ and Obstacle $(g)-(j)$ configurations, of the triangular T and the circular C_i type of cloaks, computed at frequencies $f^\star = [1, 2]$, respectively. (k) Performance of the ideal cloaks and the obstacle cases, computed by using the average of the total displacement of the transmitted field along the surface beyond the cloaked region. 79

3.3 Schematics of the unit cells for the reference R (a), triangular T (b) and circular C_i (c) cloak configurations, respectively. (d)-(e) Dispersion curves for the reference (diamond dots) and the ideal cloaks (contour circle dots) configurations, respectively. (f) Snapshots of surface modes displacement field, as obtained for the triangular T (left) and the circular C_2 (right) ideal cloaks, respectively. 80

3.4 Displacement field of the symmetrized cloaks for the T (a)-(b), C_1 (c)-(d), C_2 (e)-(f) and C_3 (g)-(h) class of transformations, computed at frequencies $f^\star = 1.5$ and $f^\star = 2$, respectively. (i) Performance of the cloaks using the ratio of the transmitted field of the symmetrized cloak over the ideal one, calculated at normalized frequencies $f^\star = [0.5 - 2.5]$. 86

3.5 Dispersion curves for the Triangular T (a) and Circular Symmetrized cloaks of C_1 (b), C_2 (c) and C_3 (d) type of transformation, respectively, as obtained from the IPR method. (e) Snapshots of particular surface modes of the displacement fields, as obtained for the triangular T (Left) and the Circular C_2 (Right) symmetrized cloaks, respectively. 87

4.1 (a) 3-D Schematic of a triangular carpet-pinched cylindrical cloak. (b) In-plane ($X_3 = 0$) model representation. (c) 3-D Schematic of a semi-circular carpet cylindrical cloak. (d) In-plane ($X_3 = 0$) model representation. 106

4.2 Out-of-plane Displacement fields for the Reference $(a1)-(a3)$, Ideal Cloak $(b1)-(c3)$ and Obstacle $(d1)-(e3)$ configurations, of the triangular T and the circular C type of cloaks, computed at frequencies $f^\star = [1, 1.5, 2]$, respectively. (f) Performance of the ideal cloaks and the obstacle cases, computed by using the average of the total displacement of the transmitted field along the surface beyond the cloaked region at 21 frequencies in the range $f^\star = [0.5, 1.5, 2]$. 117

4.3 In-plane Displacement fields for the Reference $(a1)-(a3)$, Ideal Cloak $(b1)-(c3)$ and Obstacle $(d1)-(e3)$ configurations, of the triangular T and the circular C type of cloaks, computed at frequencies $f^* = [1, 1.5, 2]$, respectively. (f) Performance of the ideal cloaks and the obstacle cases, computed by using the average of the total displacement of the transmitted field along the surface beyond the cloaked region at 21 frequencies in the range $f^* = [0.5, 0.1, 2.5]$. 118
4.4 Schematics of the cross-section of the unit cell for the reference R (a), triangular $T(b)$ and circular C_2 (c) cloak configurations, respectively. All the unit cells have thickness d. 119
4.5 Dispersion curves of Love wave surface modes for the reference (diamond dots), and ideal cloaks (contour circle dots) of triangular (left column) and semi-circular cross-sections (right column), respectively, computed at different angles of incidence $\varphi = [0°, 30°, 45°]$ 121
4.6 Dispersion curves of Rayleigh wave surface modes for the reference (diamond dots), and ideal cloaks (contour circle dots) of triangular (left column) and semi-circular cross-sections (right column), respectively, computed at different angles of incidence $\varphi = [0°, 30°, 45°]$ 122
4.7 (a)-(d) Performance of the cloaks using the ratio of the transmitted field of the symmetrized cloaks over the ideal one, for Love (a)-(b) and Rayleigh (c)-(d) waves, respectively. (e)-(f) Scattering percentage ratio of the symmetrized cloaks over the obstacle configuration for the triangular (e) and the semi-circular (f) shaped cloaks, respectively. The results are calculated at normalized frequencies $f^* = [0.5 - 2.5]$. 128
4.8 In-plane Displacement fields for the Reference $(a1)-(a3)$, and symmetrized cloaks obtained through the 'Arithmetic' $(p = 1)$ $(b1) - (c3)$, 'Quadratic' $(p = 2)$ $(d1) - (e3)$ and 'Maximum' mean $(p = \infty)$ $(f1) - (g3)$, of triangular and semi-circular cross sections, respectively. The harmonic simulations are performed at 3 different normalized frequencies $f^* = [1, 1.5, 2]$. 129
4.9 Dispersion curves of Love (Left column) and Rayleigh (right column) surface modes, for the reference (diamond dots) and the symmetrized $(p = \infty)$ semi-circular C_2 cloak (contour circle dots), respectively, computed at different angles of incidence $\varphi = [0°, 30°, 45°]$ 130

To my parents

1

Introduction

1.1 Cloaking & invisibility: an overview

In this thesis, we delve into the challenge of cloaking surface elastic waves using the principles of transformational elastodynamics.

Wave cloaking is the ability to reroute waves around an object/region without any scattering effects or loss of energy. As a result, it stands as a fundamental objective within the realm of solid me-

chanics. The concept of invisibility has been a subject of profound research in recent years. Pioneering contributions by Pendry et al.[61] and Leonhart[41] established theoretical frameworks for cloaking electromagnetic waves, building upon the invariance of Maxwell's equations under arbitrary coordinate transformations[77]. Furthermore, Schurig et at.[71] and Liu et al.[63] fuelled the research interest in cloaking by demonstrating the possibility of a practical electromagnetic cloaking device (Fig. 1.1). The notion of transformation optics[28,29,37,10,47,15] emerged due to an earlier fundamental result by Greenleaf et al.[1,30], pertaining singular transformations with cloaking applications in conductivity. The traditional approach to cloaking via transformation theory entails mapping a single point, such as the origin, to an inner boundary corresponding to a specific geometric shape (e.g., a circle), and to an outer boundary (e.g., larger circle) that maps to itself, thus forming the cloak's structure. However, such transformation becomes singular at the origin, resulting in singular material properties, that are challenging, if not impossible, to realize in practise. Addressing this issue, Greenleaf et al.[27] proposed the strategy of finite energy solutions of the Helmholtz and Maxwell's equations for such singular electromagnetic parameters. In the same work, an identity between the transformed scalar wave equation and the metric of the deformed configuration was derived, aiding the calculation of the effective materials properties of the cloak. Alternatively, to overcome the singularity in the transformed domain, Kohn et al.[39] proposed a near-cloaking transformation, which maps a small ball of finite radius instead of the origin.

In the spirit of acoustics, Norris[57] formulated the theory of acoustic cloaking by showing that for perfect cloaking efficiency the total mass of the cloaking region must be infinite. However, he pointed out that this could be circumvented by imposing the density and the elastic properties of the cloak to be anisotropic. Cummer et al.[19] verified the existence of transformation-type solutions for the 2D acoustic equations with anisotropic mass density. Building upon those ideas Chen et al.[12] proposed a scheme to realize a two dimensional (2D) acoustic cloak via acoustic metamaterials, which was further expanded to 3D acoustic cloaking. Additionally, Cummer et al.[18] modeled a 3-D

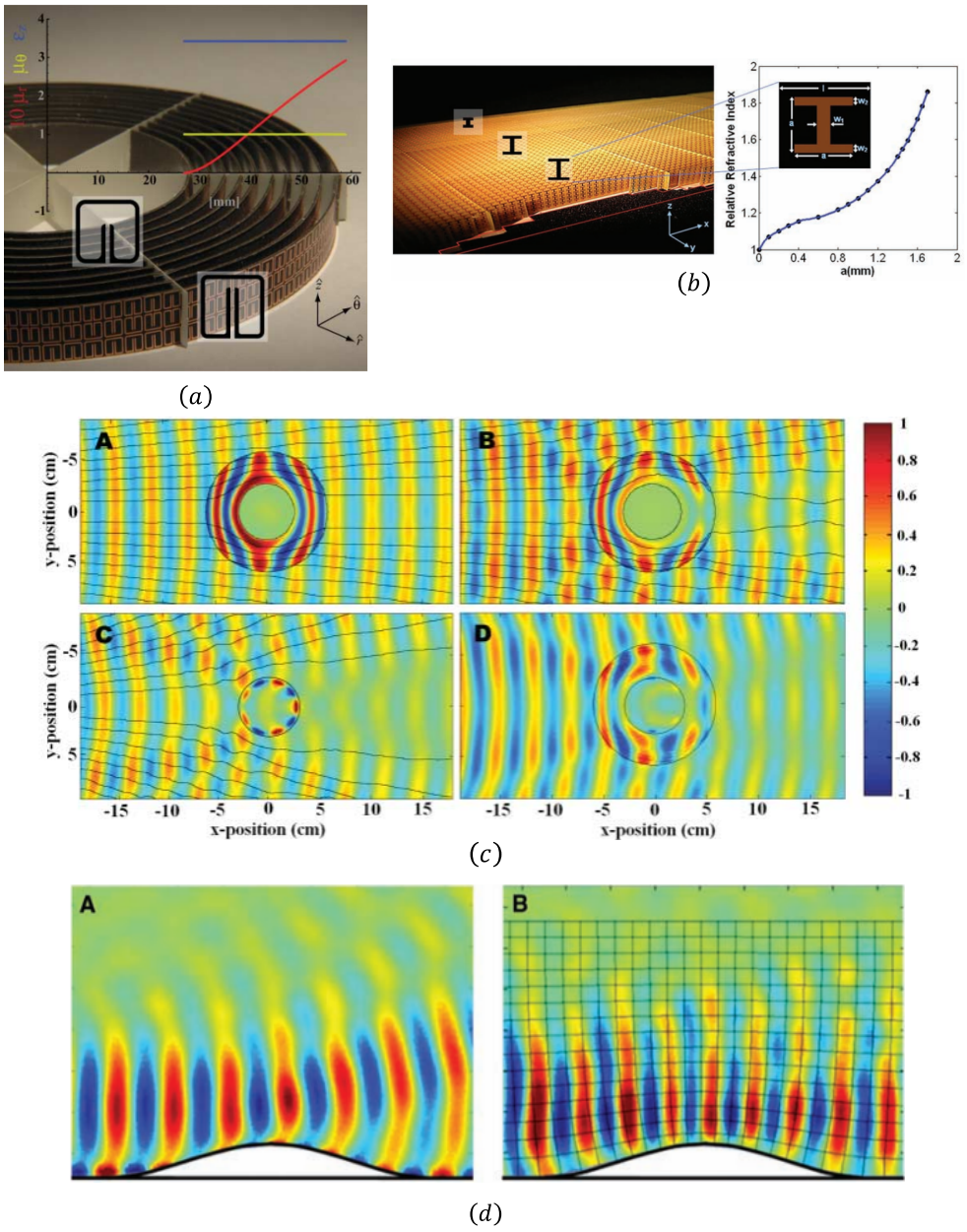

Fig. 1.1: (*a*) 2D microwave cloaking structure with a plot of the material parameters that are implemented. (*b*) The design of the non-resonant elements and the relation between the unit cell geometry and the effective index. (*c*) Snapshots of time-dependent, steady-state electric field patterns. The fields shown are **(A)** the simulation of the cloak with the exact material properties, **(B)** the simulation of the cloak with the reduced material properties, **(C)** the experimental measurement of the bare conducting cylinder, and **(D)** the experimental measurement of the cloaked conducting cylinder. The right-hand scale indicates the instantaneous value of the field. (*d*) 2D field mapping (E-field) of the perturbation and ground-plane cloaked perturbation, illuminated by the waves from the left side **(A)** perturbation and **(B)** ground-plane cloaked perturbation. Reproduced with permission from [71,63]

acoustic cloaking shell through scattering theory capable of bending the pressure and velocity fields around the object. Naturally, the idea of cloaking extends to various scientific domains, such as thermodynamics[79,55,33,72,81,11,70], quantum mechanics[85,26,43,42,44,23], diffusion[32,66,31] and fluid mechanics[82,88,54,34,35,76,86]. Extended reviews on transformation optics in metamaterials in different fields, with a focus on experimental results, are extensively covered in[24,25,36,64,62].

The first ideas around invisibility can be traced back in 1949, when Reissner et al.[65] designed reinforced holes in a plane sheet in order to maintain the same displacement and stress fields of the structure as it was before the inclusion. This technique paved the way for the concept of neutral inclusions introduced by Mansfield[46], that has been studied extensively in the past decades, see for instance[49,67]. It includes the insertion of an inclusion in a medium subjected to a uniform stress field so it does not disturb the original outside field. The inclusion is surrounded by a coating of a specific geometric shape, such as a sphere made of an isotropic material. In the same vein, similar shielding results with neutral holes can be obtained with the idea of neutral inhomogeneities, which involves the introduction of a foreign body in a host solid and modifying the contact mechanism between them so as to leave the stress field in the host solid undisturbed. This modification can be achieved, for example, by a suitably designed thick or thin interphase between them. As a result, the importance of the concept of neutral inhomogeneities in the design of composite structures and in its relevance with cloaking has been investigated my many researchers in[68,4,6,3,5,13,75]. However, the characteristics and the shape of the inclusion and the coating itself are inherently dependent on the imposed external load. This represents the main distinction with cloaking.

The formal cloaking scheme for elasticity was first investigated in 2006 by Milton et al.[48]. Surprisingly, the authors found that the Navier elastodynamic equations are not form invariant under an arbitrary curvilinear transformation and are mapped to a more general system with non-scalar density and additional third-order tensors. As a result, all three components of the elastic waves are fully coupled in the transformed medium, making the cloaking problem in elasticity far more challenging

than in optics or acoustics. However, the same authors[48] demonstrated that, for a particular choice of gauge between the displacement fields, a more general constitutive model (the so-called Willis model) remains invariant under an arbitrary coordinate transformation yielding symmetric stress but tensorial density. Notably, the choice of the map between the displacements and their transformed counterpart directly affects the symmetry of the stress tensor. Brun et al.[8] realized that choosing an identity map to connect the displacement fields (gauge) makes the Navier equation retain its form invariance, but breaks the minor symmetries of the transformed elasticity tensor. Norris et al.[56] further generalised those ideas by deriving a more general system of transformed equations that depend on both the transformation and the choice of gauge. In particular. the transformed equations can either be of Willis-form, where the elastic stress is symmetric but with the presence of third-order tensors, or of Cosserat form, where the transformed equations retain their structure but contain non-symmetric constitutive relations. As a result, both cases possess severe constraints toward the realization of a 3-D elastodynamic cloak.

A notable approach to address this challenge pertains to the adoption of the so-called Cosserat or micropolar materials of chiral (i.e. non-centrosymmetric) behaviour for cloaking applications[52,53,51,14,87,78] (Fig. 1.2*a*). Those engineered lattice-based materials, see[22] for a review, can establish the necessary non-symmetric stress tensor by introducing an additional rotational degree of freedom, realized through mechanism like a body torque torque[51,80] (Fig. 1.2*b*) or rotational resonance[53,83] (Fig. 1.3). Similarly, mechanical cloaking designs enforcing direct lattice transformation have shown promising cloaking applications in the static[9,69] and dynamic[38] regimes, respectively.

In 2012, Parnell[58] introduced an alternative technique for elastic cloaking in the form of elastic pre-stress (Fig. 1.4). In particular, he showed that cloaking objects from anti-plane waves can be achieved by applying elastic pre-stress upon neo-Hookean[59] or Mooney–Rivlin[60] type of nonlinear materials. It turns out that the equation governing antiplane waves in the pre-stressed medium is equivalent to the antiplane equation in an unstressed medium with inhomogeneous and anisotropic

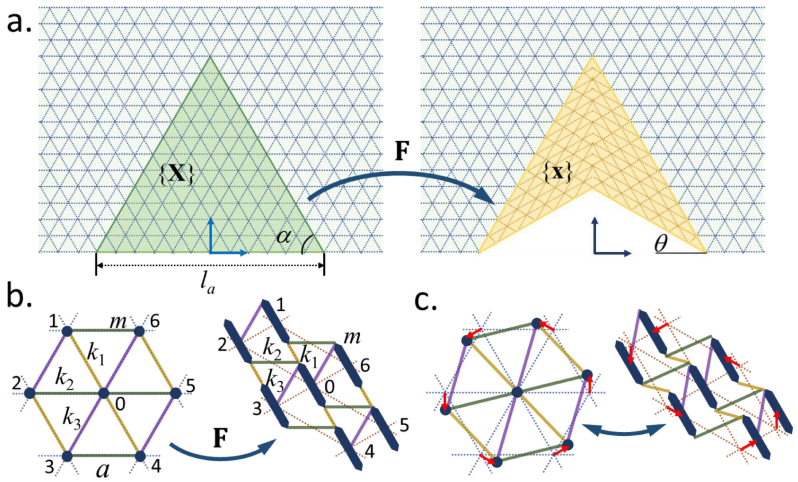

Fig. 1.2: Design of the discrete mass-spring polar lattice for a carpet cloak. (a) Geometric transformation for realizing a carpet cloak concealing a triangular void; (b) The mass-spring lattice is designed using the discrete transformation. For the design, $\alpha = 60$, and the lengths of springs, k_1, k_2, k_3, and the rigid masses are $\alpha[1 - \frac{2\sqrt{3}}{3}tan\theta]$, $\alpha[1 - \frac{\sqrt{3}}{3}tan\theta]$, $\alpha[1 - \frac{\sqrt{3}}{3}tan\theta]$, and $\frac{2\sqrt{3}\alpha}{3}tan\theta$, respectively; ($c$) Zero-mode of the transformed lattice is equivalent to the rigid rotation of the virtual lattice. Reproduced with permission from [14].

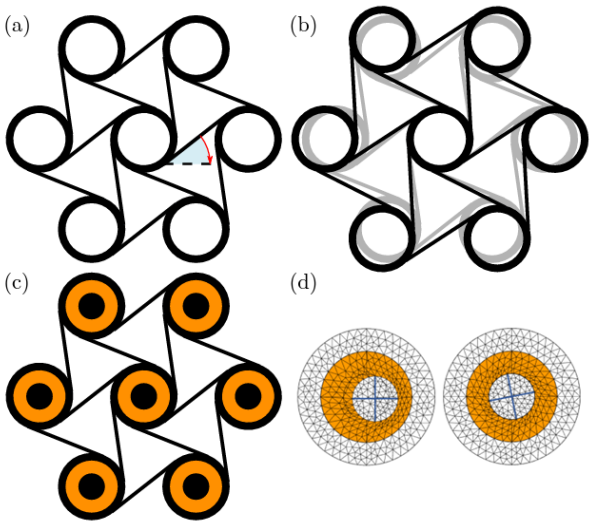

Fig. 1.3: Hexachiral lattices. (a) Nonresonant lattice: black circles are rigid masses and black segments are massless elastic rods; contact points are perfect hinges. The highlighted angle is the twisting angle γ. (b) Isotropic zero mode: the lattice expands (black) from its reference configuration (gray) without stretching any rods. (c) Polar metamaterial: black disks are embedded resonators; colored coating is elastic and massless. (d) Resonance modes under imposed outer displacement: translational to the left and rotational to the right. Reproduced with permission from [53]

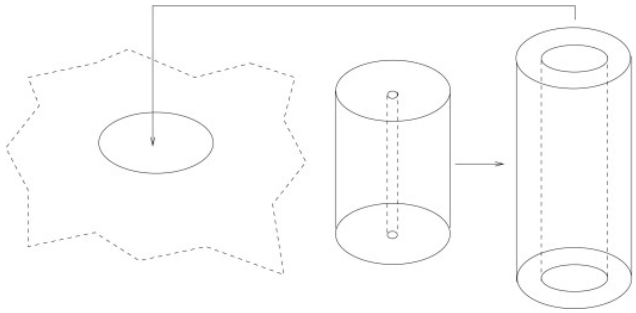

Fig. 1.4: The incompressible neo-Hookean cylindrical annulus is pre-stressed as depicted on the right. This annulus then creates a cloak when slotted into a cylindrical cavity in an unbounded elastic medium, as illustrated on the left. Reproduced with permission from [60]

shear modulus and isotropic scalar mass density. Notably, this approach was successfully applied in the development of ground cloaks [84] and periodic structures [2].

Surprisingly, there are certain geometric configurations in elasticity where the governing equations retain their form, such as the case of elastic thin plates. Indeed, Farhat et al. [21] introduced a cylindrical cloak to control bending waves in thin plates by exploiting the form invariance of the biharmonic equation (adopting the hypothesis of von Kármán). It was shown that a heterogeneous orthotropic cloak with an anisotropic Young modulus and a radially dependent isotropic mass density was sufficient to make object surrounded by such a coat neutral for flexural waves in thin elastic plates. Although those material properties are tougher to realize than conventional ones, one can easily mimic such behaviour by structuring the plate with concentric layers of piece-wise isotropic homogeneous materials by means of homogenization theory as shown in [20]. Building upon this idea, Stenger et al. [73], provided an experimental proof of this cloak using homogeneous and locally isotropic rings, achieving a fractional bandwidth of around one octave (Fig. 1.5). Several other approaches in the context of elastic plates involve non-linear [45] or conformal [40] mappings, wave conversion techniques [74], omnidirectional cloaking designs [50] and 'push-out' tranformations [17]. In the spirit or push-out' transformations, Colquitt et al. [16] and Brun et al. [7] both showed that a formulation for flexural waves in a Kirchhoff-Love plate, after the cloaking transformation, includes additional terms in the governing

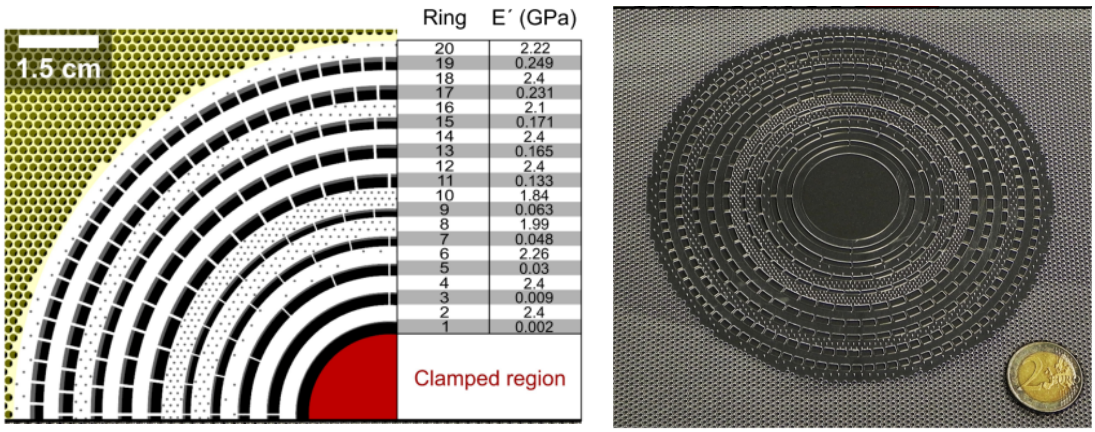

(*a*) (*b*)

Fig. 1.5: (*a*) Blueprint of the circular elastic cloak (only one-quarter is shown). White parts correspond to PVC, black parts to PDMS. The table on the right-hand side gives the elastic moduli (real parts) for the 16 different metamaterials in 20 concentric rings. The clamped region to be cloaked is shown in red, the surrounding region with homogeneous porosity ($f = 40\%$ PVC filling fraction) is highlighted in yellow. The plate thickness is $h = 1mm$. (*b*) Oblique-view photograph of a cloak before filling with PDMS.

equation in the form of in-plane body forces and pre-stress. This is in contrast with the work of Farhat et al.[21], where the biharmonic fourth order equation retained its form.

1.2 Thesis objective & Contribution

While extensive research has been conducted on cloaking methods for elastic waves, there remains a significant gap in exploring applications related to elastic surface waves. This thesis aims to address this gap by investigating the potential for cloaking Love and Rayleigh-type elastic surface waves.

Rayleigh and Love are elastic waves that propagate along the surface of a medium. In stratified or heterogeneous media both types of waves exhibit dispersive characteristics, where their velocity depends on the wavelength. The concept of bending these surface waves around an object has been of major interest due to its numerous applications in engineering. Notably, Rayleigh and Love waves are the primary surface waves generated during earthquake events, which can potentially lead to structural

damage or failure on the Earth's surface. Thus, having the possibility to cloak objects from these waves represents a tremendous advancement in seismic protection.

In Chapter 2, we investigate the novel concept of hiding surface defects from Love waves, a scenario that has not previously been studied. Love waves are antiplane shear waves traveling along a heterogeneous medium's free surface. These waves are guided by an elastic layer over a stiffer substrate and exhibit unique properties due to their layered, semi-infinite nature. Our study involves two key steps: designing ideal carpet cloaks for surface defects and their practical realization. We create carpet pinched cloaks for surface-level defects within profiles of depth-increasing shear velocity, using coordinate transformation and mapping techniques based on the form-invariance property of the Helmholtz equation. We validate our approach with dispersion analysis and simulations, revealing that the cloaked defects have minimal scattering, demonstrating the invariance of Love waves dispersive properties.

In Chapter 3, we address the challenge of cloaking an object on the free surface of an elastic medium from Rayleigh waves. Unlike other cloaking scenarios, we must consider full in-plane elasticity due to the vector nature of Rayleigh waves. We derive transformed equations for in-plane elasticity by assuming a Cosserat gauge between the displacement fields in the virtual (reference) and the transformed (cloaked) domain, and subsequently substitute the non-symmetric components of the elasticity tensor with symmetrized ones using the arithmetic mean. Our goal is to assess how this symmetrization affects the cloaking of Rayleigh waves. We investigate various cloaking designs, including a triangular and semi-circular cloaks with different radial transformations. We evaluate their performance by comparing wave fields and dispersion relations between symmetrized and ideal cloaking designs. Our analysis employs the inverse participation ratio (IPR) to quantify displacement field localization and surface mode identification. Furthermore, we use harmonic simulations to compare transmitted displacement fields after the cloak in both symmetrized and ideal scenarios. Finally, our investigation culminates in the examination of the requirements for a symmetric elastic tensor in the

context of circular cloaks, specifically analyzing the necessary conditions for each type of radial transformation (C_i). Our investigation reveals that a symmetrized semi-circular cloak with effective properties obtained from a quadratic transformation offers the best cloaking performance among the designs studied.

In Chapter 4, we explore the potential for creating 3-D cloaks to effectively reroute both Rayleigh and Love waves around an object of interest. Again, we adopt a Cosserat kinematic relation for the displacements to acquire the necessary non-symmetric mechanical properties for cloaking. We design 3-D cloaks by using the cylindrical analogue of the 2-D transformations studied in the previous Chapter, i.e. of triangular and semi-circular cross-sections, respectively. Importantly, the 3-D problem differs from the superposition of Love and Rayleigh waves due to its need for a heterogeneous system, primarily because Love waves propagate exclusively in layered media, leading to Rayleigh waves with dispersive characteristics. In addition, by comparing the weak formulation of the 3-D equation of motion with the separate weak forms of Love and Rayleigh waves, we identify an extra set of coefficients in the transformed elasticity tensor that didn't appear in the previous cases. Furthermore, the symmetrization of the elasticity tensor has a direct consequence on the effective shear moduli required for cloaking Love waves. This phenomenon did not appear in Chapter 2 since the transformation of the scalar Helmholtz equation does not produce non-symmetric mechanical properties. To avoid this, we introduced a symmetrization strategy, constraining related symmetric coefficients to match the weak-form solution of Love waves and symmetrizing the remaining terms using the generalized mean. This approach aimed to find the ideal combination of symmetrization and cloak geometry for optimal cloaking efficiency. To verify the effectiveness of our designs, we conducted time-harmonic simulations and dispersion analyses, specifically examining how the proposed cloaks performed under different symmetrization schemes and various angles of incidence. Our findings revealed that a symmetrized semi-circular cylindrical cloak constructed using the "Maximal" mean offered substantial cloaking protection across all tested frequencies.

Finally, Chapter 5 summarizes the main contributions of the previous chapters, and provides possible directions for future developments of the topic of elastic cloaking.

References

[1] A., G., M., L., & G., U. (2003). On nonuniqueness for calderon's inverse problem. *Mathematical Research Letters*, 10.

[2] Barnwell, E. G., Parnell, W. J., & David Abrahams, I. (2016). Antiplane elastic wave propagation in pre-stressed periodic structures; tuning, band gap switching and invariance. *Wave Motion*, 63, 98–110.

[3] Benveniste, Y. & Chen, T. (2001). On the saint-venant torsion of composite bars with imperfect interfaces. *Proceedings of the Royal Society of London. Series A: Mathematical, Physical and Engineering Sciences*, 457(2005), 231–255.

[4] Benveniste, Y. & Miloh, T. (1999). Neutral inhomogeneities in conduction phenomena. *Journal of the Mechanics and Physics of Solids*, 47(9), 1873–1892.

[5] Benveniste, Y. & Miloh, T. (2007). Soft neutral elastic inhomogeneities with membrane-type interface conditions. *Journal of Elasticity*, 88(2), 87–111.

[6] Benveniste, Y. & Milton, G. (2003). New exact results for the effective electric, elastic, piezoelectric and other properties of composite ellipsoid assemblages. *Journal of the Mechanics and Physics of Solids*, 51(10), 1773–1813.

[7] Brun, M., Colquitt, D. J., Jones, I. S., Movchan, A. B., & Movchan, N. V. (2014). Transformation cloaking and radial approximations for flexural waves in elastic plates. *New Journal of Physics*, 16(9), 093020.

[8] Brun, M., Guenneau, S., & Movchan, A. B. (2009). Achieving control of in-plane elastic waves. *Applied Physics Letters*, 94(6), 061903.

[9] Bückmann, T., Kadic, M., Schittny, R., & Wegener, M. (2015). Mechanical cloak design by direct lattice transformation. *Proceedings of the National Academy of Sciences*, 112(16), 4930–4934.

[10] Cai, W., Chettiar, U. K., Kildishev, A. V., & Shalaev, V. M. (2007). Optical cloaking with metamaterials. *Nature Photonics*, 1(4), 224–227.

[11] Cassier, M., DeGiovanni, T., Guenneau, S., & Guevara Vasquez, F. (2021). Active thermal cloaking and mimicking. *Proceedings of the Royal Society A: Mathematical, Physical and Engineering Sciences*, 477(2249), 20200941.

[12] Chen, H. & Chan, C. T. (2007). Acoustic cloaking in three dimensions using acoustic metamaterials. *Applied Physics Letters*, 91(18), 183518.

[13] Chen, T., Benveniste, Y., & Chuang, P. C. (2002). Exact solutions in torsion of composite bars: thickly coated neutral inhomogeneities and composite cylinder assemblages. *Proceedings of the Royal Society of London. Series A: Mathematical, Physical and Engineering Sciences*, 458(2023), 1719–1759.

[14] Chen, Y., Nassar, H., & Huang, G. (2021). Discrete transformation elasticity: An approach to design lattice-based polar metamaterials. *International Journal of Engineering Science*, 168, 103562.

[15] Choi, J. S. & Howell, J. C. (2014). Paraxial ray optics cloaking. *Opt. Express*, 22(24), 29465–29478.

[16] Colquitt, D., Brun, M., Gei, M., Movchan, A., Movchan, N., & Jones, I. (2014). Transformation elastodynamics and cloaking for flexural waves. *Journal of the Mechanics and Physics of Solids*, 72, 131–143.

[17] Colquitt, D. J., Jones, I. S., Movchan, N. V., Movchan, A. B., Brun, M., & McPhedran, R. C. (2013). Making waves round a structured cloak: lattices, negative refraction and fringes. *Proceedings of the Royal Society A: Mathematical, Physical and Engineering Sciences*, 469(2157), 20130218.

[18] Cummer, S. A., Popa, B.-I., Schurig, D., Smith, D. R., Pendry, J., Rahm, M., & Starr, A. (2008). Scattering theory derivation of a 3d acoustic cloaking shell. *Phys. Rev. Lett.*, 100, 024301.

[19] Cummer, S. A. & Schurig, D. (2007). One path to acoustic cloaking. *New Journal of Physics*, 9(3), 45.

[20] Farhat, M., Guenneau, S., & Enoch, S. (2009a). Ultrabroadband elastic cloaking in thin plates. *Phys. Rev. Lett.*, 103, 024301.

[21] Farhat, M., Guenneau, S., Enoch, S., & Movchan, A. B. (2009b). Cloaking bending waves propagating in thin elastic plates. *Phys. Rev. B*, 79, 033102.

[22] Fernandez-Corbaton, I., Rockstuhl, C., Ziemke, P., Gumbsch, P., Albiez, A., Schwaiger, R., Frenzel, T., Kadic, M., & Wegener, M. (2019). New twists of 3d chiral metamaterials. *Advanced Materials*, 31(26), 1807742.

[23] Fleury, R. & Alù, A. (2013). Quantum cloaking based on scattering cancellation. *Phys. Rev. B*, 87, 045423.

[24] Fleury, R. & Alù, A. (2014). Cloaking and invisibility: A review. *Forum for Electromagnetic Research Methods and Application Technologies (FERMAT)*, 1(9).

[25] Fleury, R., Monticone, F., & Alù, A. (2015). Invisibility and cloaking: Origins, present, and future perspectives. *Phys. Rev. Appl.*, 4, 037001.

[26] Gevaux, D. (2009). Cloaking matters. *Nature Physics*, 5, 16.

[27] Greenleaf, A., Kurylev, Y., Lassas, M., & Uhlmann, G. (2007). Full-wave invisibility of active devices at all frequencies. *Communications in Mathematical Physics*, 275, 749–789.

[28] Greenleaf, A., Kurylev, Y., Lassas, M., & Uhlmann, G. (2009). Cloaking devices, electromagnetic wormholes, and transformation optics. *SIAM Review*, 51(1), 3–33.

[29] Greenleaf, A., Kurylev, Y., Lassas, M., & Uhlmann, G. (2011). Cloaking a sensor via transformation optics. *Phys. Rev. E*, 83, 016603.

[30] Greenleaf, A., Lassas, M., & Uhlmann, G. (2003). Anisotropic conductivities that cannot be detected by eit. *Physiological Measurement*, 24(2), 413.

[31] Guenneau, S., Diatta, A., Puvirajesinghe, T. M., & Farhat, M. (2017). Cloaking and anamorphism for light and mass diffusion. *Journal of Optics*, 19(10), 103002.

[32] Guenneau, S. & Puvirajesinghe, T. M. (2013). Fick's second law transformed: one path to cloaking in mass diffusion. *Journal of The Royal Society Interface*, 10(83), 20130106.

[33] Han, T., Bai, X., Gao, D., Thong, J. T. L., Li, B., & Qiu, C.-W. (2014). Experimental demonstration of a bilayer thermal cloak. *Phys. Rev. Lett.*, 112, 054302.

[34] Hua, Y., Qian, C., Chen, H., & Wang, H. (2022). Experimental topology-optimized cloak for water waves. *Materials Today Physics*, 27, 100754.

[35] Iida, T., Zareei, A., & Alam, M.-R. (2023). Water wave cloaking using a floating composite plate. *Journal of Fluid Mechanics*, 954, A4.

[36] Kadic, M., Bückmann, T., Schittny, R., & Wegener, M. (2013). Metamaterials beyond electromagnetism. *Reports on Progress in Physics*, 76(12), 126501.

[37] Kadic, M., Bückmann, T., Schittny, R., & Wegener, M. (2015). Experiments on cloaking in optics, thermodynamics and mechanics. *Philosophical Transactions of the Royal Society A: Mathematical, Physical and Engineering Sciences*, 373(2049), 20140357.

[38] Kadic, M., Wegener, M., Nicolet, A., Zolla, F., Guenneau, S., & Diatta, A. (2020). Elastodynamic behavior of mechanical cloaks designed by direct lattice transformations. *Wave Motion*, 92, 102419.

[39] Kohn, R. V., Lu, J., Schweizer, B., & Weinstein, M. I. (2014). A variational perspective on cloaking by anomalous localized resonance. *Communications in Mathematical Physics*, 328, 1432–0916.

[40] Lee, M. K. & Kim, Y. Y. (2016). Add-on unidirectional elastic metamaterial plate cloak. *Scientific Reports*, 6, 20731.

[41] Leonhardt, U. (2006). Optical conformal mapping. *Science*, 312(5781), 1777–1780.

[42] Lin, D.-H. (2010). Cloaking spin-$\frac{1}{2}$ matter waves. *Phys. Rev. A*, 81, 063640.

[43] Lin, D.-H. & Luan, P.-G. (2009). Cloaking of matter waves under the global aharonov-bohm effect. *Phys. Rev. A*, 79, 051605.

[44] Lin, D.-H. & Luan, P.-G. (2012). Cloaking matter waves around a dirac monopole. *Physics Letters A*, 376(5), 675–678.

[45] Liu, M. & Zhu, W. (2019). Nonlinear transformation-based broadband cloaking for flexural waves in elastic thin plates. *Journal of Sound and Vibration*, 445, 270–287.

[46] Mansfield, E. H. (1953). Neutral holes In plane sheet-reinforced holes which are elastically equivalent to the uncut sheet. *The Quarterly Journal of Mechanics and Applied Mathematics*, 6(3), 370–378.

[47] McCall, M. (2013). Transformation optics and cloaking. *Contemporary Physics*, 54(6), 273–286.

[48] Milton, G. W., Briane, M., & Willis, J. R. (2006). On cloaking for elasticity and physical equations with a transformation invariant form. *New Journal of Physics*, 8(10), 248–248.

[49] Milton, G. W. & Serkov, S. K. (2001). Neutral coated inclusions in conductivity and anti–plane elasticity. *Proceedings of the Royal Society of London. Series A: Mathematical, Physical and Engineering Sciences*, 457(2012), 1973–1997.

[50] Misseroni, D., Movchan, A. B., & Bigoni, D. (2019). Omnidirectional flexural invisibility of multiple interacting voids in vibrating elastic plates. *Proceedings of the Royal Society A: Mathematical, Physical and Engineering Sciences*, 475(2229), 20190283.

[51] Nassar, H., Chen, Y., & Huang, G. (2019). Isotropic polar solids for conformal transformation elasticity and cloaking. *Journal of the Mechanics and Physics of Solids*, 129, 229–243.

[52] Nassar, H., Chen, Y. Y., & Huang, G. L. (2018). A degenerate polar lattice for cloaking in full two-dimensional elastodynamics and statics. *Proceedings of the Royal Society A: Mathematical, Physical and Engineering Sciences*, 474(2219), 20180523.

[53] Nassar, H., Chen, Y. Y., & Huang, G. L. (2020). Polar metamaterials: A new outlook on resonance for cloaking applications. *Phys. Rev. Lett.*, 124, 084301.

[54] Newman, J. (2014). Cloaking a circular cylinder in water waves. *European Journal of Mechanics - B/Fluids*, 47, 145–150. Enok Palm Memorial Volume.

[55] Nguyen, D. M., Xu, H., Zhang, Y., & Zhang, B. (2015). Active thermal cloak. *Applied Physics Letters*, 107(12), 121901.

[56] Norris, A. & Shuvalov, A. (2011). Elastic cloaking theory. *Wave Motion*, 48(6), 525–538. Special Issue on Cloaking of Wave Motion.

[57] Norris, A. N. (2008). Acoustic cloaking theory. *Proceedings of the Royal Society A: Mathematical, Physical and Engineering Sciences*, 464(2097), 2411–2434.

[58] Parnell, W. J. (2012). Nonlinear pre-stress for cloaking from antiplane elastic waves. *Proceedings of the Royal Society A: Mathematical, Physical and Engineering Sciences*, 468(2138), 563–580.

[59] Parnell, W. J., Norris, A. N., & Shearer, T. (2012). Employing pre-stress to generate finite cloaks for antiplane elastic waves. *Applied Physics Letters*, 100(17), 171907.

[60] Parnell, W. J. & Shearer, T. (2013). Antiplane elastic wave cloaking using metamaterials, homogenization and hyperelasticity. *Wave Motion*, 50(7), 1140–1152. Advanced Modelling of Wave Propagation in Solids.

[61] Pendry, J. B., Schurig, D., & Smith, D. R. (2006). Controlling electromagnetic fields. *Science*, 312(5781), 1780–1782.

[62] Peralta, I., Fachinotti, V. D., & Álvarez Hostos, J. C. (2020). A brief review on thermal metamaterials for cloaking and heat flux manipulation. *Advanced Engineering Materials*, 22(2), 1901034.

[63] R, L., C, J., Y, M. J. J. C. J., J, C. T., & R, S. D. (2009). Broadband ground-plane cloak. *Science*, 323(5912), 366–369.

[64] Raza, M., Liu, Y., Lee, E. H., & Ma, Y. (2016). Transformation thermodynamics and heat cloaking: a review. *Journal of Optics*, 18(4), 044002.

[65] Reissner, H. & Morduchow, M. (1949). Reinforced circular cutouts in plane sheets. *National Advisory Committee for Aeronautics , Technical Note*, 1852, 1–60.

[66] Restrepo-Flórez, J. M. & Maldovan, M. (2017). Mass diffusion cloaking and focusing with metamaterials. *Applied Physics Letters*, 111(7), 071903.

[67] Richards, R. & Bjorkman, G. S. (1982). Neutral holes: Theory and design. *Journal of the Engineering Mechanics Division*, 108(5), 945–960.

[68] Ru, C.-Q. (1998). Interface design of neutral elastic inclusions. *International Journal of Solids and Structures*, 35(7), 559–572.

[69] Sanders, E. D., Aguiló, M. A., & Paulino, G. H. (2021). Optimized lattice-based metamaterials for elastostatic cloaking. *Proceedings of the Royal Society A: Mathematical, Physical and Engineering Sciences*, 477(2253), 20210418.

[70] Schittny, R., Kadic, M., Guenneau, S., & Wegener, M. (2013). Experiments on transformation thermodynamics: Molding the flow of heat. *Phys. Rev. Lett.*, 110, 195901.

[71] Schurig, D., Mock, J. J., Justice, B. J., Cummer, S. A., Pendry, J. B., Starr, A. F., & Smith, D. R. (2006). Metamaterial electromagnetic cloak at microwave frequencies. *Science*, 314(5801), 977–980.

[72] Shen, X., Li, Y., Jiang, C., Ni, Y., & Huang, J. (2016). Thermal cloak-concentrator. *Applied Physics Letters*, 109(3), 031907.

[73] Stenger, N., Wilhelm, M., & Wegener, M. (2012). Experiments on elastic cloaking in thin plates. *Phys. Rev. Lett.*, 108, 014301.

[74] Wang, X., Chen, H., Yin, Y., Ruan, Y., Zhu, S., Hu, C., & Chen, H. (2023). Multiband elastic waveguide cloak in thin plates. *Advanced Engineering Materials*, 25(12), 2300025.

[75] Wang, X. & Schiavone, P. (2012). Neutral coated circular inclusions in finite plane elasticity of harmonic materials. *European Journal of Mechanics - A/Solids*, 33, 75–81.

[76] Wang, Z., Li, C., Zatianina, R., Zhang, P., & Zhang, Y. (2017). Carpet cloak for water waves. *Phys. Rev. E*, 96, 053107.

[77] Ward, A. J. & Pendry, J. B. (1996). Refraction and geometry in maxwell's equations. *Journal of Modern Optics*, 43(4), 773–793.

[78] Wu, Q. & Huang, G. (2022). Omnidirectional wave polarization manipulation in isotropic polar solids. *International Journal of Solids and Structures*, 241, 111481.

[79] Xu, H., Shi, X., Gao, F., Sun, H., & Zhang, B. (2014). Ultrathin three-dimensional thermal cloak. *Phys. Rev. Lett.*, 112, 054301.

[80] Xu, X., Wang, C., Shou, W., Du, Z., Chen, Y., Li, B., Matusik, W., Hussein, N., & Huang, G. (2020). Physical realization of elastic cloaking with a polar material. *Phys. Rev. Lett.*, 124, 114301.

[81] Yue, X., Nangong, J., Chen, P., & Han, T. (2021). Thermal cloak: Theory, experiment and application. *Materials*, 14(24).

[82] Zareei, A. & Alam, M.-R. (2015). Cloaking in shallow-water waves via nonlinear medium transformation. *Journal of Fluid Mechanics*, 778, 273–287.

[83] Zhang, H., Chen, Y., Liu, X., & Hu, G. (2020a). An asymmetric elastic metamaterial model for elastic wave cloaking. *Journal of the Mechanics and Physics of Solids*, 135, 103796.

[84] Zhang, P. & Parnell, W. J. (2018). Hyperelastic antiplane ground cloaking. *The Journal of the Acoustical Society of America*, 143(5), 2878–2885.

[85] Zhang, S., Genov, D. A., Sun, C., & Zhang, X. (2008). Cloaking of matter waves. *Phys. Rev. Lett.*, 100, 123002.

[86] Zhang, Z., He, G., Wang, W., Liu, S., & Wang, Z. (2020b). Broadband cloaking of multiple truncated cylinders in water waves using the arrangement defects. *Physics of Fluids*, 32(6), 067111.

[87] Zhao, S., Chen, J., Chang, Z., & Huang, G. (2023). Microstructure realization of a lattice-based polar solid for arbitrary elastic waveguiding. *Journal of the Mechanics and Physics of Solids*, 173, 105226.

[88] Zou, S., Xu, Y., Zatianina, R., Li, C., Liang, X., Zhu, L., Zhang, Y., Liu, G., Liu, Q. H., Chen, H., & Wang, Z. (2019). Broadband waveguide cloak for water waves. *Phys. Rev. Lett.*, 123, 074501.

2

Cloaking of Love waves

The contents and the figures of the presented chapter are (except for Appendix B.2.7) adopted and reproduced with permission from [93] Copyright 2022, Elsevier Ltd.

Love waves are antiplane elastic waves which propagate along the surface of a heterogeneous medium. Under time-harmonic regime, they are governed by a scalar equation of the Helmholtz type. We exploit the invariance of this governing equation under an in-plane arbitrary coordinate transformation to design broadband cloaks for surface defects. In particular, we apply transforma-

tion elastodynamics to determine the anisotropic, position dependent, mechanical properties of ideal cloaks able to hide triangular and parabolic-shaped defects. Dispersion analysis and time-harmonic numerical simulations are employed to validate the proposed strategy. Next, we utilize layered monoclinic materials, with homogenized properties matching those of the ideal cloaks, to design feasible triangular-shaped cloaks. The performance of the layered cloaks is validated via parametric analysis of the dispersion curves, which converge to those of the ideal cloak when the unit cell-wavelength ratio vanishes. Finally, time-harmonic numerical simulations confirm a significant reduction of the defect-generated scattered fields by the layered cloaks.

2.1 Introduction

The prospect of rerouting the propagation of elastic waves around an object and isolate it from unwanted mechanical vibrations has fuelled the research interest towards the realization of elastic cloaking devices. A cloak is a region of a medium surrounding a defect, or a target object, purposely designed to make it scattering free from particular waves. Among the approaches existing to design a cloak, transformation elastodynamics has been extensively employed in recent works as it allows for the direct derivation of passive cloaks material properties [101]. In brief, transformation elastodynamics consists in a coordinate transformation to map (or stretch) a spatial region embedding a defect, the cloak, to a region as if no obstacle were there. In general, this coordinate transformation turns a homogeneous and isotropic material into an inhomogeneous and anisotropic material, posing some challenges for the practical realization of a cloak.

A necessary mathematical prerequisite for material-parameter transformation to work is that the underlying equations must be invariant with respect to general coordinate transformations. Milton et al. [110] showed that, in the general case of an elastic medium, the equations of motion are not form invariant under an arbitrary transformation, leading to non-scalar density and additional third-order

elastic tensors. Also, the choice of the map linking the displacements to their transformed counterpart is proven vital, since the symmetry of the stress tensor is dependent upon it. Brun et al.[92] realized that choosing an identity map linking these displacements makes the Navier equation transformation invariant, but breaks the minor symmetries of the transformed elasticity tensor. Norris et al.[115] considered multiple types of map (constant, identity, etc), that resulted in having materials breaking the stress symmetry. In these cases, the resulting material parameters are impractical and very difficult to handle. An ample number of ideas tackled those situations, including the adoption of the so-called Cosserat or micropolar cloaks with chiral behaviour. Chiral materials allow to obtain the required non-symmetric stress tensor, by enforcing an additional rotational degree of freedom in the form of a body torque [114,113,132] or rotational resonance [133]. As an extension, Chen et al.[94] proposed the use of discrete transformation elasticity upon an architected lattice-based material to achieve the chiral behavior required to design a cloak. Conversely, Achaoui et al.[89] considered a Willis medium as background material and, exploiting its form invariance[110], developed a Cosserat-Willis type cloak. Other strategies include the use of pentamode materials to achieve the required effective properties, although their mechanical instability is a considerable impedance factor for their practical manufacture[102].

Noteworthy, there are configurations where the governing equation retains its form under a coordinate transformation, such as antiplane elastic waves and bending waves in thin-plate geometries. For antiplane shear waves, Parnell et al.[119] proposed to exploit non-linear elastic pre-stress upon an incompressible neo-Hookean material to derive the required elastic properties for cloaking. Parnell and Shearer[120] extended this seminal work by considering a Mooney–Rivlin hyperelastic model to obtain a more feasible cloak design. Later, Zhang and Parnell[134] exploited hyperelastic materials to design a ground cloak for antiplane shear waves. More recently, a multi-layered cloak for antiplane shear waves was considered in[128] to account for the stiffness of the inclusion; results for cavities, elastic and rigid inclusions are given. For thin plates, Farhat et al.[97] proposed a cloak to control bending waves for a wide range of frequencies. Subsequently, Stenger et al.[125], building upon this theory, provided

an experimental proof by fabricating an elastic cloak using homogeneous and locally isotropic rings. Further experiments by Misseroni et al.[111,112] showed the possibility of cloaking flexural vibrations in structured plates. However, control of flexural pulse dynamics remains a further challenge[122,127]. We remark that most of the above literature concerns passive cloaking designs, since it exploits the concept of geometric transformation, in the tracks of what was earlier proposed for electromagnetic waves[104]. Some alternative path to cloaking using active sources can reduce the plate design complexity in the time harmonic regime[117]. Active cloaking has been proposed for acoustic and transverse elastic waves[129,130].

Besides the rich literature on passive and active cloaking for elastic waves, applications for surface waves are still rare. The most relevant studies, to the best of our knowledge, are those that exploit micropolar materials[103] or near-cloaking techniques[124] to hide surface defects from Rayleigh waves.

In this work, we explore the possibility of cloaking surface defects from waves of the Love type, a scenario that has not been considered yet. Love waves are antiplane shear waves propagating at the free surface of a heterogeneous medium with a stiffness profile increasing with depth. They share the same scalar governing equation of antiplane shear bulk waves, but are characterized by a dispersive and multi-modal nature due to the layered and semi-infinite nature of the support. Addressing the capabilities of a cloak to preserve the dispersive and multi-modal nature of Love waves can have a significant technological/engineering relevance in various fields, spanning from seismology to the design of lab-on-chip devices. We note that some control of Love waves has been achieved using locally resonant elements atop the air-soil interface[118,107], but these works do not make use of the concept of artificial anisotropy, as required by geometric (non conformal) transforms. Here instead, by exploiting the invariant form of antiplane shear waves, we apply transformation elastodynamics to design cloaks for surface defects. In particular, we focus our attention on carpet pinched cloaks able to hide a defect placed at the surface of the domain.

First, we apply transformation elastodynamics to normally dispersive profiles, i.e., with increasing

shear speed for increasing depth of the medium, to design ideal cloaks. We describe the proposed mapping and provide the space dependent anisotropic properties of the mapped material. We prove, via numerical finite element simulations, the validity of the proposed mapping, showing both the invariance of the dispersive properties of Love waves and the near zero scattering for configurations with cloaked defects.

Next, for a surface triangular defect, we apply a straightforward homogenization technique [91,109,90] to map the material properties of the ideal cloak onto a monoclinic double-material unit cell. The unit cell allows the realization of a layered cloak with a feasible microstructure. We confirm the validity of the adopted homogenization step by both comparing the harmonic wave fields of the layered and ideal cloaks, and showing the invariance of the dispersive properties of Love waves. We conclude by discussing the potential and limitations of the proposed strategy.

2.2 Statement of the problem

We present an approach to cloaking of Love waves that involves a coordinate stretch in the medium vertical plane, thus affecting the surface wave trajectory along the same plane, see Fig. **??**. This approach is in stark contrast to [118] where the wave control was achieved in the horizontal plane.

2.2.1 Antiplane surface waves in vertically heterogeneous media

Following the cloaking strategy proposed by Li and Pendry in the context of electromagnetic waves [104], we propose the design of a carpet cloak for Love waves by applying a geometric transformation at the free surface of the heterogeneous substrate. Our aim is to stretch this interface in such a way that Love waves propagate along a curved path without experiencing some scattering in the substrate. The reference configuration consists in an isotropic vertically heterogeneous half-space extending from $X_2 = 0$, to $X_2 = -\infty$ (see Fig. 2.1*a*.). The medium is characterized by shear modulus $\mu(X_2)$ and

density $\rho(X_2)$ which vary along the depth of the half-space only. We consider the propagation of time harmonic antiplane shear waves travelling along the X_1 direction and confined at the free surface of the medium, $X_2 = 0$. The displacement field is restricted to the out-of-plane component $\mathbf{U} = [U_1, U_2, U_3] = [0, 0, U_3]$ and the governing equation is given by the two-dimensional scalar equation:

$$\nabla_X \cdot (\mu(X_2)\nabla_X U_3(X_1, X_2)) + \omega^2 \rho(X_2) U_3(X_1, X_2) = 0 \tag{2.1}$$

where $\nabla_X = (\partial/\partial X_1, \partial/\partial X_2)^T$ is the gradient operator with respect to the coordinates X_1 and X_2 and ω the wave angular frequency.

Here, we restrict our investigation to normally dispersive profiles, i.e., vertically heterogeneous media with increasing shear velocity $c_s(X_2) = \sqrt{\frac{\mu(X_2)}{\rho(X_2)}}$ with depth, such that the velocity of propagation of surface waves decreases for increasing frequency [98]. The simplest normally dispersive configuration consists in a soft layer with shear velocity c_{s1} overlying a stiffer half-space with shear velocity $c_{s2} > c_{s1}$. Antiplane surface waves propagating in this double-layered medium are known as Love waves [105]. By extension, we use the same label for antiplane surface waves propagating in any normally dispersive half-space.

In what follows, we discuss how to hide a surface defect located in such heterogeneous, normally dispersive, half-space from the propagating Love waves.

2.2.2 Geometric transformation for carpet cloaking

Let us recall the fundamental results of transformation elastodynamic theory for an antiplane shear wave problem. Given the scalar nature of the governing equation in Eq. (2.1), we can mutate the approach developed for cloaking of acoustic waves [116]. Hence, we consider a point-wise invertible transformation χ that maps the reference configuration (virtual domain) $\mathbf{X} \in \Psi$ (in Fig. 2.1*a*) to the deformed region (real domain) as $\mathbf{x} = \chi(\mathbf{X}) \in \psi$ (in Fig. 2.1*b*). The deformation gradients for the

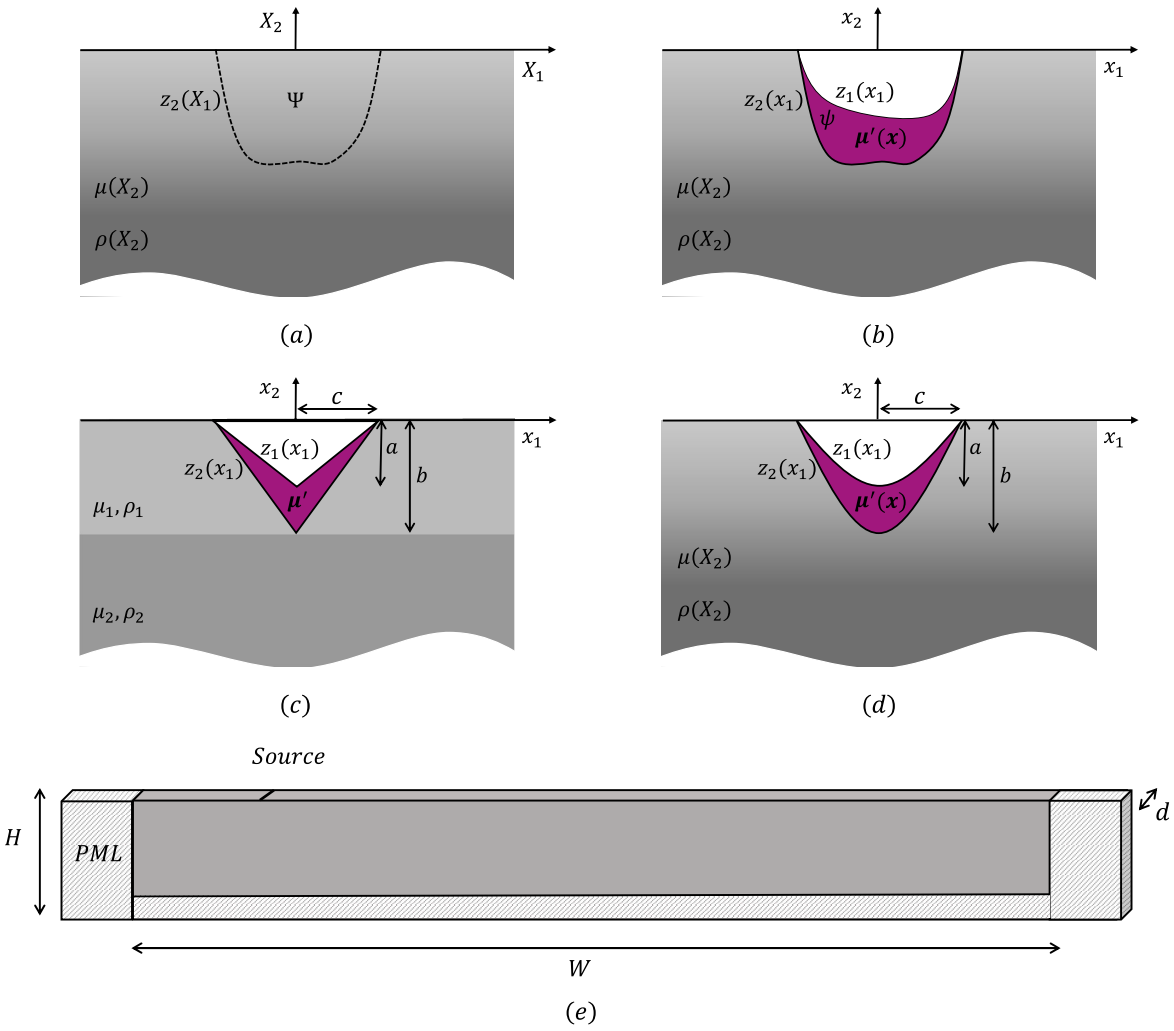

Fig. 2.1: (*a*) Reference configuration virtual domain. (*b*) A generic carpet-pinched cloak (purple region ψ) to conceal a defect (white region) from the propagating surface Love waves (real domain). (*c*) Schematic of a triangular pinched-carpet cloak in a layered isotropic medium. (*d*) Schematic of a parabolic pinched-carpet cloak in an isotropic heterogeneous medium characterized by a parabolic velocity profile along the depth of the half space. (*e*) Schematic of the FE model domain used in the simulations (not in scale).

transformed and the reference domain are $\mathbf{F} = \nabla_X x$ and $\mathbf{F}^{-1} = \nabla X$, respectively. Given $\mathbf{x} = \{x_1, x_2\}$ the coordinates for the transformed domain, the forward transformation gradient $\mathbf{F}$ reads:

$$\mathbf{F} = \nabla_X x = \begin{pmatrix} \frac{\partial x_1}{\partial X_1} & \frac{\partial x_1}{\partial X_2} \\ \frac{\partial x_2}{\partial X_1} & \frac{\partial x_2}{\partial X_2} \end{pmatrix} \tag{2.2}$$

and, by the chain rule, the relation between the gradient operator in both domains is given by [124]:

$$\nabla_x = \mathbf{F}^{-T} \nabla_X. \tag{2.3}$$

By using the identity [99]:

$$\nabla_X \cdot \nabla_X \to J \nabla_x \cdot (J^{-1} \mathbf{F} \mathbf{F}^T \nabla_x) \tag{2.4}$$

where $J = \det(\mathbf{F})$ is the determinant of the Jacobian matrix, we obtain the transformed governing Eq. (2.1) in the new coordinates $\mathbf{x}$ as:

$$\nabla_x \cdot \mu'(\mathbf{x}) \nabla_x u_3(\mathbf{x}) + \rho'(\mathbf{x}) \omega^2 u_3(\mathbf{x}) = 0 \tag{2.5}$$

with:

$$\mu'(\mathbf{x}) = \frac{\mathbf{F} \mu(\mathbf{x}(\mathbf{X})) \mathbf{F}^T}{J} = \frac{\mathbf{F} \mu(\mathbf{x}) \mathbf{F}^T}{J}, \quad \rho'(\mathbf{x}) = \frac{\rho(\mathbf{x}(\mathbf{X}))}{J} = \frac{\rho(\mathbf{x})}{J}. \tag{2.6}$$

Note that, in Eq. (2.6) the differentiation is applied with respect to the vector variable $\mathbf{x}$ and $u_3(\mathbf{x}(\mathbf{X})) = U_3(\mathbf{X})$. The anisotropic shear modulus $\mu'(\mathbf{x})$ and the density $\rho'(\mathbf{x})$ provided in Eq. (2.6) describe the properties of the cloak region in ψ with $\mu(\mathbf{x}(\mathbf{X})) = \mu(\mathbf{X})$ and $\rho(\mathbf{x}(\mathbf{X})) = \rho(\mathbf{X})$ being the isotropic shear modulus and density mapped from the virtual domain $\mathbf{X}$ to the real domain $\mathbf{x}(\mathbf{X})$.

Let us now specify our derivation for a two-dimensional carpet pinched cloak like the one shown in Fig. 2.1b. We denote with $z_1(x_1)$ and $z_2(x_1)$ the interior and exterior boundaries of the cloak,

respectively. The transformation χ that maps the region enclosed between two curves $(X_1; 0)$ and $(X_1; z_2(X_1))$ of the virtual domain to the one comprised between $(x_1; z_1(x_1))$ and $(x_1; z_2(x_1))$ of the real domain is:

$$\begin{cases} x_1 = X_1 \\ x_2 = (1 - \xi)X_2 + z_1(X_1) \end{cases} \tag{2.7}$$

where $\xi = \frac{z_1(X_1)}{z_2(X_1)}$. Note that $(X_1; 0)$ is mapped on $(x_1; z_1(x_1))$ while $(X_1; z_2(X_1))$ is point-wise fixed. The Jacobian of the transformation reads:

$$\mathbf{F} = \begin{bmatrix} 1 & 0 \\ L & 1 - \xi \end{bmatrix} \tag{2.8}$$

where $L = -\frac{\partial \xi(X_1)}{\partial X_1} X_2 + \frac{\partial z_1(X_1)}{\partial X_1}$. By means of Eqs. (2.6), we can obtain the transformed shear modulus and density within the carpet cloak as:

$$\mu'(\mathbf{x}) = \begin{bmatrix} \mu'_{11}(\mathbf{x}) & \mu'_{12}(\mathbf{x}) \\ \mu'_{12}(\mathbf{x}) & \mu'_{22}(\mathbf{x}) \end{bmatrix} = \begin{bmatrix} 1 & L \\ L & (L^2 + (1 - \xi)^2) \end{bmatrix} \frac{\mu(\mathbf{x})}{1 - \xi}, \quad \rho'(\mathbf{x}) = \frac{\rho(\mathbf{x})}{1 - \xi} \tag{2.9}$$

Note that carpet-cloak requires a material with an inhomogenous and anisotropic shear modulus and an inhomogenous density. The nature of material inhomogeneity depends on both the geometrical transformation and the vertically heterogeneity of the host material properties. Conversely, the degree of anisotropicity depends only on the geometrical transformation. In what follows, we elucidate these aspects with two illustrative examples. As an aside, we remind that the derived transformed shear moduli and density would work also in the case of bulk antiplane waves, although their investigation is out of the scope of this work.

2.3 Ideal cloaks: two illustrative examples

We analyse the propagation of Love waves in two distinct half-spaces: (i) a double-layered medium hosting a triangular-shaped defect (Fig. 2.1*c*); (ii) a heterogeneous medium with continuous varying shear velocity profile with a parabolic-shaped defect (Fig. 2.1*d*). For both configurations, carpet pinched cloaks obtained by stretching the geometry of surface defects are considered, in accordance with the geometrical transformation in Eq. (2.7).

2.3.1 Triangular pinched cloak

First, we present the simplest configuration where carpet-cloaking of Love waves can be tested, namely a triangular pinched cloak located inside the soft layer of a double-layered semi-infinite medium. The shear velocities in the soft layer (1) and the bottom half-space (2) are c_{s1} and c_{s2}, respectively, with $\gamma = \frac{c_{s1}}{c_{s2}} = 0.3$. The density ρ is assumed constant over the whole semi-infinite medium, $\rho_1 = \rho_2 = \rho$. We denote the depth of the soft layer by h_1. Numerical values of the above geometrical and mechanical quantities are collected in Table 2.1.

We consider a triangular defect with length $2c = 1.8h_1$ and depth $a = 0.6h_1$. The defect is surrounded by a cloak which extends up to the depth $b = h_1$. The boundaries of the cloak are thus marked by linear functions $z_1(X_1) = \frac{a}{c}|X_1| - a$ and $z_2(X_1) = \frac{b}{c}|X_1| - b$, where $|.|$ denotes the absolute value. The Jacobian matrix of the geometrical transformation

$$\mathbf{F} = \begin{bmatrix} 1 & 0 \\ \operatorname{sgn}(x_1)\frac{a}{c} & \frac{b-a}{b} \end{bmatrix} \tag{2.10}$$

is constant within each symmetric half of the cloak. Similarly, the shear modulus $\mu(\mathbf{x}) = \mu_1$ is constant within the cloak, since its geometry is fully contained within the first layer. Hence, according to Eq. (2.9), each symmetric half of the triangular-pinched cloak presents a homogeneous and

anisotropic effective shear modulus and homogeneous density given as:

$$\mu' = \begin{bmatrix} 1 & \operatorname{sgn}(x_1)\frac{a}{c} \\ \operatorname{sgn}(x_1)\frac{a}{c} & \frac{(ab)^2+(bc)^2+(ca)^2-2abc^2}{(bc)^2} \end{bmatrix} \mu_1 \frac{b}{b-a}, \quad \rho' = \rho \frac{b}{b-a} \tag{2.11}$$

The coefficients $\mu'_{11}, \mu'_{12}, \mu'_{22}$, as obtained from Eq. (2.11), are displayed in Appendix A (Fig. 2.7$(a)-(c)$). Note that in both transformations there are no singularities like in the case of semi-circular cloaks, where a small ball of radius ε must be considered. However, for the triangular cloak, the existence of sharp edges introduces the possibility of numerical errors that could affect the performance of the cloak, but such investigation is beyond the scope of this study.

To evaluate the cloaking capabilities of this configuration, we first perform time-harmonic simulations in a finite element environment (COMSOL Multiphysics) modeling a 3D strip of the medium with dimensions $W \times H \times d$ along the Cartesian axes (x_1, x_2, x_3), embedding the described cloak (see Fig. 2.1e). Fixed constraints are imposed at the bottom base of the model, continuity boundary conditions are imposed along the out-of-plane x_3 direction, and Perfectly Matched Layers (PML) are applied to suppress reflections from the model terminal sections. PML are used in numerical analyses to terminate finite element approximations of scattering problems. They can be derived through analytic continuation and coordinate transformation in the complex plane to convert oscillating waves into exponentially decaying ones (see[95]). Shear waves are generated by imposing at the surface of the model a time-harmonic line source along the x_3 direction located at $0.4W$ distance from the origin. The domain displacements components $u_2 = u_1 = 0$ are restrained to limit our investigation to antiplane waves $u_3 \neq 0$.

To generalize the results of our calculations, we introduce the following normalized quantities:

- $\omega^\star = \frac{\omega}{\omega_{c1}}$ the normalized circular frequency, where $\omega_{c1} = \frac{\pi}{h_1\sqrt{\frac{1}{\omega_1^2}-\frac{1}{\omega_2^2}}}$ is the cut-off frequency of the first higher-order Love wave mode;

- $k^\star = \frac{\omega_{c1}}{c_{s2}}$, the normalized wavenumber, so that $\lambda^\star = \frac{2\pi}{k^\star}$ is the normalized wavelength.

Accordingly, the dimensions of the model are chosen as $W = 8\lambda^\star$, $H \approx 0.69\lambda^\star$ and $d \approx 0.01\lambda^\star$.

We compare the results of harmonic simulations performed in (i) the pristine configuration, i.e., the domain with no defect ("Reference"), (ii) in the domain including the defect ("Obstacle"), and (iii) in the domain with the cloaked defect ("Ideal Cloak"). Snapshots of the related displacements fields as obtained from FE harmonic simulations at $\omega^\star = [1, 2]$ are shown in Fig. 2.2$(a) - (f)$. We remark that the propagation of Love waves has a dispersive nature; up to the first cut-off frequency the wave field is dominated by the fundamental Love mode, see Fig. 2.2*a*; conversely, for harmonic simulations at $\omega^\star = 2$, Fig. 2.2*b*, the total field results from the superposition of the first two modes. Regardless of the dispersive and multi-modal nature of Love waves, the triangular pinched cloak smoothly reroutes the waves around the defect (Fig. 2.2$(c) - (d)$). As a result, before and after the cloaked region, the displacement field fully resembles the one of the reference configuration. The performance of the cloak is better appreciated by comparing the cloaked wave fields with those obtained in the uncloaked scenarios (see Fig. 2.2(e) and (f)). In the latter, scattering effects can be seen both before and after the defect.

As a further proof of the broad band capabilities of the proposed carpet cloak, we compare the dispersive properties of Love waves propagating along the pristine double-layered medium and along the cloaked domain. Our aim is to prove that in the cloaked configuration, the geometrical transformation and the related transformed shear modulus in Eq. (2.11) allows to fully replicate the dispersive properties of the pristine layered medium.

For this purpose, we model a portion, namely a unit cell, of the cloak in a finite element environment (COMSOL Multiphysics). The unit cell has dimension $H \times L_c \times d$ (see Fig. 2.2*g*), with $L_c = \lambda^\star/20$. We apply fixed boundary conditions at the bottom surface of the cell, continuity conditions along the x_2 direction, and Bloch boundary conditions along the x_1 direction. As for the harmonic simulations, the domain displacements components $u_2 = u_1 = 0$ are restrained. An equiv-

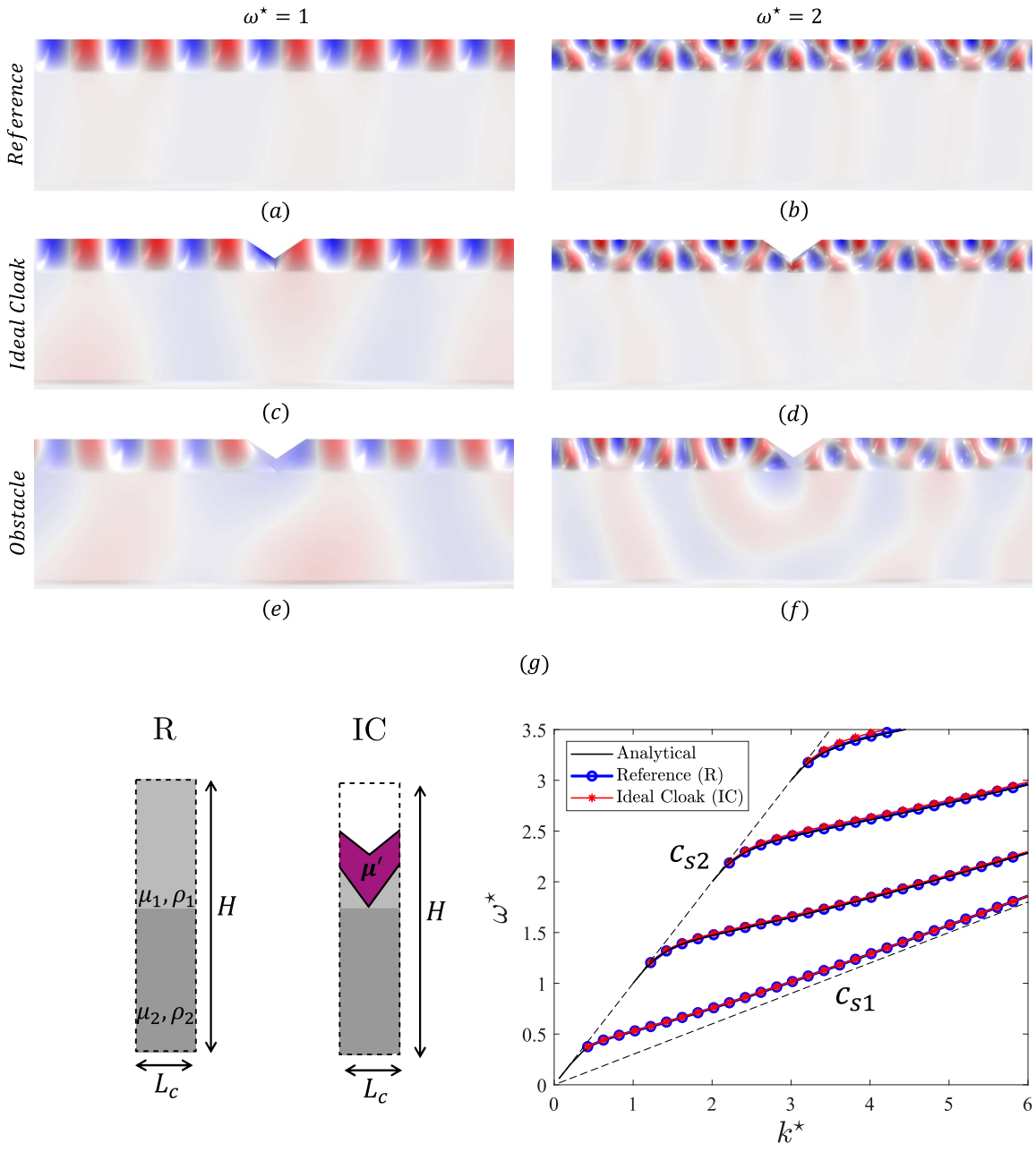

Fig. 2.2: Displacement fields of the Reference $(a)-(b)$, Ideal Cloak $(c)-(d)$ and Obstacle $(e)-(f)$ configurations, for the triangular pinched cloak case of section 3.1 computed at frequencies $\omega^\star = 1$ and $\omega^\star = 2$. (g) Dispersive curves (first 4 modes) for the Reference (blue lines) and the Ideal Cloak (red lines) configurations, as obtained by considering the unit cell in the schematic (R and IC), respectively. The analytical solution for the reference configuration is also presented (black lines). See Table 2.1 for the shear velocity C_{si} and density ρ_i of homogeneous isotropic layer i in R.

alent unit cell is used to model the "Reference" configuration. For all the scenarios, the dispersive properties are obtained by solving an eigenvalue problem by varying the wavenumber inside the first Brillouin zone, $k_{x_1} = [\frac{\pi}{400L_c}; \frac{\pi}{L_c}]$ and extracting the angular frequency ω. The numerical solutions are then sorted to remove spurious plate-like (and leaky) modes with phase velocity $c_p = \omega/k_{x_1} > c_{s2}$ resulting from the finite dimensions of the model.

The dispersive curves of the "Reference" and "Ideal Cloak" configurations are reported in Fig. 2.2*g* as blue and red lines, respectively. Markers indicate the wavenumber-frequency couples obtained from the numerical simulations. The results of the reference configuration are validated against those obtained from the solution of the classical Love wave dispersion law[105] (reported in Fig. 2.2*g* as solid black lines):

$$\tan\left(\frac{\omega}{c_p}h_1\sqrt{\frac{c_p^2}{c_{s1}^2}-1}\right) = \frac{\mu_2\sqrt{1-\frac{c_p^2}{c_{s2}^2}}}{\mu_1\sqrt{\frac{c_p^2}{c_{s1}^2}-1}} \tag{2.12}$$

where $c_p = \frac{\omega}{k}$ the phase velocity of the propagating Love waves, respectively.

The reader can appreciate how the portion of the cloaked defect supports the propagation of Love waves with dispersive properties identical to the pristine scenario. We recognize that the obtained dispersion curves describe a geometrical layout where the portion of the defect is periodically repeated along the direction of the wave propagation. Nonetheless, in our scenario the obtained dispersive properties are invariant w.r.t. the chosen length L_c of the cell, and thus represent the effective dispersive properties of the transformed medium. More information on the dynamics of shear elastic waves across periodically perforated elastic media can be found in the recent work by Meirbekova et al.[108].

Layer	Shear velocity	Density	Depth
1	c_{s1}=300 m/s	1600 kg/m^3	60 m
2	c_{s2}=1000 m/s	1600 kg/m^3	∞

Table 2.1: Mechanical and geometrical properties of the double-layered substrate.

2.3.2 Parabolic pinched cloak

In the second example, we consider a vertically inhomogeneous medium characterized by a constant density ρ and shear velocity profile given by:

$$c_s(X_2) = \begin{cases} c_{s1} + \frac{c_{s2}-c_{s1}}{(h_1)^2}(X_2)^2, & \text{if} \quad |X_2| < |h_1| \\ c_{s2}, & \text{otherwise} \end{cases} \tag{2.13}$$

namely, a parabolic profile varying between the shear velocities c_{s1} and c_{s2} along the depth h_1 supported by a homogeneous half-space with velocity c_{s2}. In this medium, a parabolic-shaped defect is surrounded by a cloak enclosed within the boundaries $z_1(X_1) = \frac{a}{c^2}(X_1)^2 - a$ and $z_2(X_1) = \frac{b}{c^2}(X_1)^2 - b$, see Fig. 2.1$(d)$. The shear velocities c_{s1}, c_{s2} and the geometrical parameters a, b, c are identical to the ones assumed in the previous example.

The distribution of the shear modulus in the cloak region is:

$$\mu(\mathbf{x}) = \rho(c_s(\mathbf{x}))^2 = \rho\left(c_{s1} + \frac{c_{s2}-c_{s1}}{h_1^2}\left(\frac{x_2 - \frac{a}{c^2}x_1^2 + a}{1-\frac{a}{b}}\right)^2\right)^2, \quad \mathbf{x} = \chi(\mathbf{X}) \in \psi \tag{2.14}$$

where the inverse transformation of Eq. (2.7) is used:

$$\begin{cases} X_1 = x_1 \\ X_2 = \frac{x_2 - z_1(x_1)}{1-\frac{\xi}{\xi}} \end{cases} \tag{2.15}$$

The Jacobian of the transformation for the given cloak geometry is:

$$\mathbf{F} = \begin{bmatrix} 1 & 0 \\ \frac{2a}{c^2}x_1 & \frac{b-a}{b} \end{bmatrix}. \tag{2.16}$$

Overall, this leads to an anisotropic inhomogenous effective shear modulus:

$$\mu' = \begin{bmatrix} 1 & \frac{2a}{c^2}x_1 \\ \frac{2a}{c^2}x_1 & \frac{4a^2}{c^4}x_1^2 + \frac{(b-a)^2}{b^2} \end{bmatrix} \mu(\mathbf{x})\frac{b}{b-a}, \quad \rho' = \rho\frac{b}{b-a} \tag{2.17}$$

The reader can fully appreciate the distribution of the effective shear modulus coefficients $\mu'_{11}, \mu'_{12}, \mu'_{22}$ inside the domain of the cloak in the Figure provided in Appendix A (Fig. 2.7$(d)-(f)$)

As for the configuration in Sect. 3.1, we test the performance of the parabolic-shaped cloak with FE harmonic simulations performed in the "Reference", "Obstacle" and "Ideal Cloak" scenarios. The displacements fields, obtained for harmonic sources at $\omega^\star = [1, 2]$, confirm the possibility of smoothly detouring antiplane surface waves propagating in a heterogenous medium around a defect of generic shape, see Fig. 2.3$(a)-(f)$. Similarly, the dispersion analysis, conducted in analogy to what shown for the triangular cloak, corroborate the possibility of replicating the dispersive properties of the pristine scenario using the transformed shear modulus and density obtained according to Eq.(2.17), see Fig. 2.3(g).

Although the implementation of the transformed medium in a FE numerical simulation software is straightforward, the practical realization of such material presents a number of complexities related to its heterogeneity and anisotropicity. Thus, following a consolidated approach developed for both thermal [100] and acoustic [123] cloaking, we utilize a composite medium, structured at a microscale level, to mimic at the macroscale the required mechanical properties of the transformed medium. The design of this composite material is guided by classical results of homogenization theory.

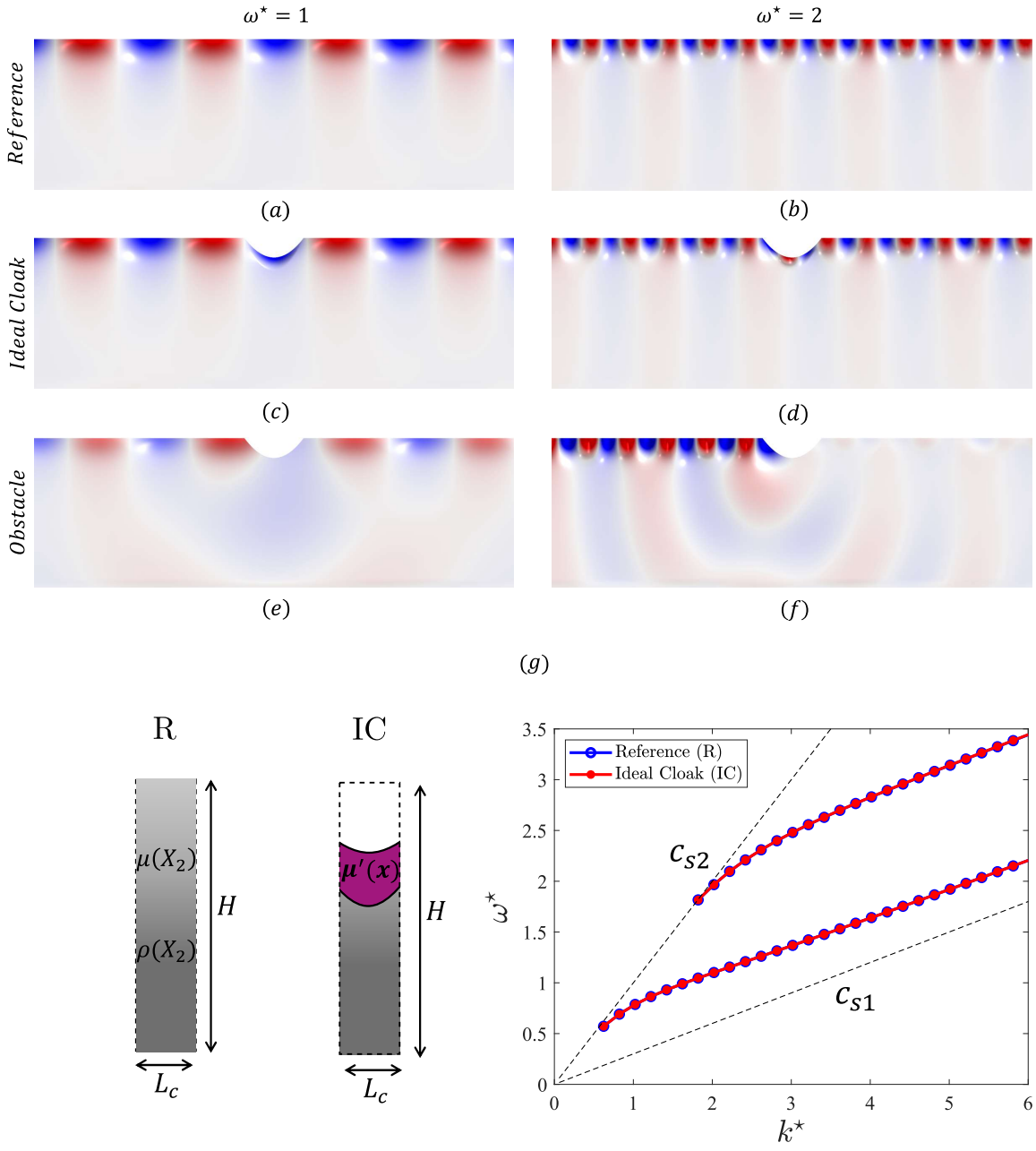

Fig. 2.3: Displacement fields for the Reference $(a) - (b)$, Ideal Cloak $(c) - (d)$ and Obstacle $(e) - (f)$ configurations, considering the parabolic pinched cloak case of section 3.2 computed at frequencies $\omega^\star = 1$ and $\omega^\star = 2$. (g) Dispersive curves (first 2 modes) for the Reference (blue lines) and the Ideal Cloak (red lines) configurations, as obtained by considering the unit cell in the schematic (R and IC), respectively.

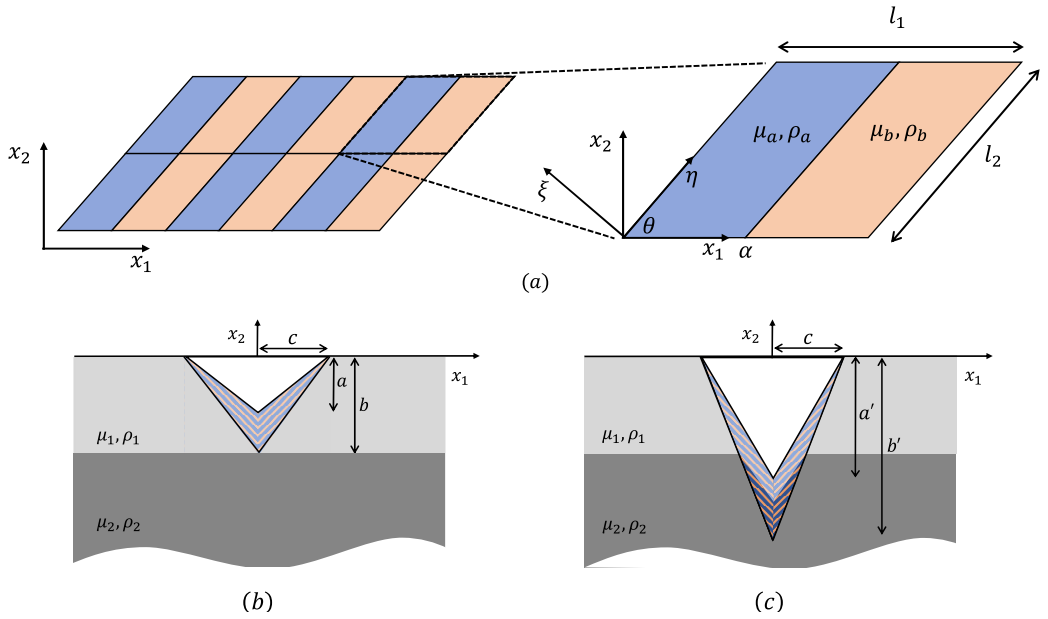

Fig. 2.4: (*a*) Details of the monoclinic unit cell and (*b-c*) schematic representation of the layered cloaks.

2.4 Cloak realization via composite media

We here analyse the possibility of approximating the theoretical anisotropic inhomogeneous materials obtained in the previous section by means of layered composite media.

2.4.1 Effective properties of a monoclinic layered medium

We restrict our interest to the realization of a triangular pinched cloak. As shown in the context of acoustics [126] and electromagnetic waves [131], a layered periodic composite with 2D oblique geometry, i.e., a monoclinic crystal, suffices to achieve this purpose.

Thus, we consider a unit cell made of two isotropic materials, with shear moduli μ_a and μ_b, and density ρ_a and ρ_b, respectively (Fig. 2.4*a*). The lattice unit cell has dimensions $l_1 \times l_2$ along the lattice vectors e_1 and e_2 which enclose the oblique angle θ. The layer a has a thickness $\alpha \cdot l_1$. Our aim is to find the geometrical parameters θ and α and the mechanical parameters $\mu_a, \mu_b, \rho_a, \rho_b$ to mimic, at the

macroscale, the mechanical properties of the cloak. We first recall the expressions of the homogenized density $\rho^{hom} = (1-\alpha)\rho_b + \alpha\rho_a$ and homogenized elastic properties of the layered cell along its principal directions η, ξ[91,109]:

$$\mu^{hom}(\eta,\xi) = \begin{bmatrix} \langle \mu^{-1} \rangle^{-1} & 0 \\ 0 & \langle \mu \rangle \end{bmatrix} = \begin{bmatrix} \frac{\mu_a \mu_b}{(1-\alpha)\mu_a + \alpha\mu_b} & 0 \\ 0 & (1-\alpha)\mu_b + \alpha\mu_a \end{bmatrix} \tag{2.18}$$

where θ is the rotation angle between the principal (η, ξ) and reference (x_1, x_2) axes.

Then, we diagonalize the cloak elastic tensor as:

$$\mu'(\eta,\xi) = \begin{bmatrix} \mu'_I & 0 \\ 0 & \mu'_{II} \end{bmatrix} \tag{2.19}$$

with:

$$\theta' = \frac{1}{2}\arctan\left(\frac{\mu'_{12} + \mu'_{21}}{\mu'_{11} - \mu'_{22}}\right) \tag{2.20}$$

being the related rotation angle. At this stage, we impose $\theta = \theta'$ and find the parameters $\alpha, \mu_a, \mu_b, \rho_a, \rho_b$ which fulfill the expressions:

$$\begin{cases} (1-\alpha)\mu_b + \alpha\mu_a = \mu'_I \\ \frac{\mu_a \mu_b}{(1-\alpha)\mu_a + \alpha\mu_b} = \mu'_{II} \\ (1-\alpha)\rho_b + \alpha\rho_a = \rho' \end{cases} \tag{2.21}$$

The set of parameters which fulfill Eq. (2.21) is not unique. In the examples collected in the next section, we will fix α, select $\rho_a = \rho_b = \rho'$ and obtain μ_a and μ_b from the solution of Eq. (2.21). Finally, we point out that for more complex unit cell geometries, there are no analytical solutions available. Hence, the use of numerical techniques is mandatory for the adequate approximation of the effective properties of the cloak. Such strategy is presented in Appendix B in the form of a genetic

algorithm.

2.4.2 Numerical examples

We here design and show the performance of two triangular pinched cloaks, constructed using the layered medium discussed in the previous section. For the first example, we consider the geometry in Fig. 2.4*b*, where the cloak lies within the boundaries of the first layer. From Eq. (2.11), we factor out the common term $J = \frac{b}{b-a}$ to obtain:

$$\mu' = \begin{bmatrix} 1 & \text{sgn}(x_1)0.6667 \\ \text{sgn}(x_1)0.6667 & 0.6044 \end{bmatrix} \mu_1, \quad \rho' = \rho \tag{2.22}$$

According to Eq. (2.19), the elastic tensor in the principal direction reads:

$$\mu'(\eta, \xi) = \begin{bmatrix} 1.4976 & 0 \\ 0 & 0.1068 \end{bmatrix} \mu_1 \tag{2.23}$$

with $\theta' = \pm 0.6412$ rad. Assuming a value of $\alpha = 0.5$, from Eq. (2.21) we obtain: $\mu_a = 0.0544\mu_1$ and $\mu_b = 2.9409\mu_1$.

Equipped with the mechanical parameters of the layered unit cell, we perform harmonic simulation via FE models to analyse the performance of the layer triangular pinched cloak. The adopted FE model resembles the one used to model the ideal cloak in Sect. 3.1. The layered domain comprises unit cells with dimensions $l_1 = l_2 = 0.1b_1 = 6m$. As for the ideal scenario, we perform harmonic simulations at $\omega^\star = [1, 2]$

The displacement field u_3 extracted along the free surface of the model, $x_2 = 0$, before and after the cloaked region, are shown in Fig. 2.5(a) and (c) and compared with those of an ideal cloak. The reader can appreciate how the displacement fields of the layered cloak (LC) match the ones of the ideal case (IC) obtained from the geometric transformation.

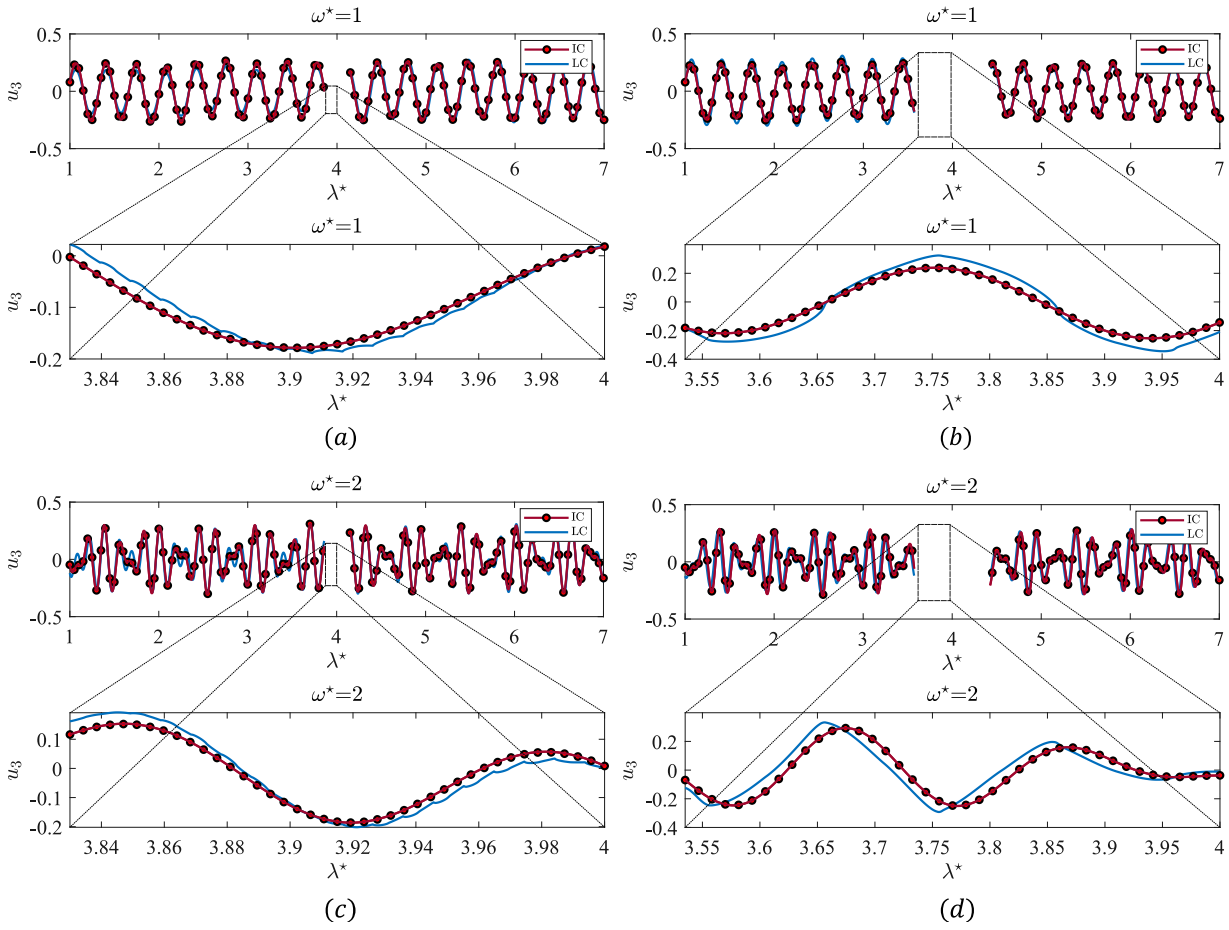

Fig. 2.5: Comparison between the Ideal (IC) and the Layered Cloak (LC) displacement fields, for a cloak fully contained inside the first layer (1^{st} column, panels (a) and (c)) and for a cloak exceeding the first layer (2^{nd} column, panels (b) and (d)). The harmonic simulations are performed at two different normalized frequencies $\omega^\star = [1 - 2]$.

The same occurs inside the cloak, as confirmed by the results collected in the inset of the Fig. 2.5(a) and (c), showing the displacement fields extracted along the boundary $z_1(x)$ of the cloak (2^{nd} row in Fig. 2.5(a) and (c)). The minor discrepancies between layered and ideal cloak in Fig. 2.5 can be attributed to numerical errors due to the FE mesh and the finite dimensions of the unit cell. The latter lead to the presence of several partial cells at the interface between the cloak and the half-space which degrades the overall performance of the cloak. Such boundary layer effects, which characterize a layered medium filled with a non integer number of cells, have been studied in [106] in the context of scalar waves. Thus, we recognize that our effective medium formula (2.18) would benefit from the introduction of some corrective terms depending upon the wave frequency.

Additionally, we remark that even in the absence of such issues, the performance of the layered cloak decreases with an increase in the frequency of the incident waves. A noticeable improvement of the cloaking capabilities is obtained by means of a larger number of cells, namely a smaller unit cell dimension, in accordance with classical error estimates in homogenization theory, as already noticed in the context of thermal layered cloaks [121].

In this regard, the reader can refer to Fig. 2.6 where the wave fields of the layered cloak are evaluated for higher frequencies $\omega^\star = [3, 4]$ and comparing different unit cell dimensions $l_1 = l_2 = 6m$, $l_1 = l_2 = 1.5m$. The wave field of the harmonic analysis shows a significant loss of performance for $\omega^\star = 4$ when the cloak is realized with a bigger unit cell $l_1 = l_2 = 6m$ (Fig. 2.6(d)). At the same frequency, a smaller unit cell, $l_1 = l_2 = 1.5m$, provides adequate cloaking performances (Fig. 2.6(f)). The reader can refer to the supplemental material for further details on the behavior of the cloak against increasing frequency.

To generalize this argument, we performed a parametric study on the dispersion curves by varying the dimension of the unit cell. The results are depicted in Fig. 2.6(g). It is evident that for a unit cell of 6m, significant discrepancy between the layered and the ideal dispersion curves is found for $\omega^\star \geq 4$, which corroborates the results found in the harmonic analysis. Conversely, the layered cloak

dispersion curves converge to the ideal one, as the length of the unit cell decreases. Indeed, this result can be interpreted by evaluating the ratio r between the unit cell dimension and the shortest Love wave wavelength $r = \frac{l_1}{\lambda_{min}}$ at the frequency of interest. When this ratio tends to zero, as for the configuration with the smallest unit cell ($r = 0.05$), the homogenization ensures a proper approximation of the mechanical behaviour of the layered unit cell.

Overall, for practical purpose, the proposed design strategy is a good trade-off between complexity and cloaking efficiency.

Following the same modelling approach, we consider a cloak with dimensions b', c, enclosing a defect that penetrates through the half-space (Fig. 2.4(c)). For this scenario, the layered cloak requires the use of 2 different unit cells, tiling two distinct regions of the cloak. The properties of these unit cells are again given by $\mu_a = 0.5544\mu(x_2)$ and $\mu_b = 2.4004\mu(x_2)$ and $\theta' = \pm 0.5544$ with:

$$\mu(x_2) = \begin{cases} \mu_1, & \text{if} \quad |x_2| < |\chi(h_1)| \\ \mu_2, & \text{otherwise} \end{cases} \tag{2.24}$$

Fig. 2.5(b) and (d) (2^{nd} column) shows a good agreement between the displacements for the ideal (IC) and the layered (LC) cloak along the surface. The reader can refer to the supplemental material for a detailed investigation on the cloaking performance w.r.t. the frequency of the incident Love waves, whose trend resembles the one discussed for the cloak geometry fully contained in the soft layer, Sect. 3.1. Further performance losses are again attributed to boundary layer effects since the two cloak regions are filled with a non integer number of cells. We refer once again to [106] for such issues.

2.5 Conclusion

In this work we proposed a strategy to design carpet cloaks that make surface defects scattering free from the viewpoint of the propagation of shear polarized surface waves. Our approach relies on the invariance of the shear wave equation in 2D setting when subjected to a geometric transformation of coordinates. The change of coordinates, applied to a pinched region embedding the surface defect, is used to mathematically mask the defect. Its application yields a transformed wave equation in the cloaked region which in turn provides the local material properties to be used. Notably, in the proposed cases, the shear modulus of the material turns out to be a point dependent two-by-two fully populated tensor and the mass density a point dependent scalar value. We exploited these formulas to design two ideal cloaks, triangular and parabolic ones. Using finite element simulations, we then demonstrated the capability of the cloaks to render the surface defects transparent to Love waves. As further proof, we showed that a periodically repeated portion of these cloaked defects supports the propagation of classical Love waves, identical to the ones propagating in the pristine substrate.

Finally, we provided a viable strategy to realize the triangular cloak using layered media. To such purpose, we used a monoclinic unit cell with two isotropic materials and exploited results of homogenization theory to devise the dimensions of the two materials over the unit cell, their shear moduli, and the angle of the cell, such that the homogenized properties of the unit cell coincide with those derived from Eq. (2.11) for the ideal cloak. We applied this approach by shaping a second triangular cloak for a defect extending not only within the soft layer but also in the underlying half-space. We verified, via FE simulations, the capabilities of the layered cloaks and found performances in excellent agreement to the ideal ones.

We recognize that the assumption of a 2D geometry (invariant along the out-of-plane direction) restricts the dynamics of the cloak to plane waves with orthogonal incidence w.r.t. the cloak. Nonetheless, we underline that a 2D geometry (invariant along the out-of-plane direction) is the common sce-

nario where cloaking strategies for antiplane waves have been derived and discussed in the past research works. In addition, we investigated the performance of the layered cloaks for increasing frequency. In this regard, the use of homogenization techniques to obtain a monoclinic unit cell limits the operational frequency range of the cloak to those ranges where the characteristic wavelengths of Love waves are larger than the unit cell dimensions. Furthermore, the adopted homogenization technique cannot account for the presence of boundary layer effects, which characterize a layered medium filled with a non integer number of cells. This aspect, introduces some extra deterioration in the performance of the cloak.

In terms of perspectives, experimental realizations of the proposed layered cloak should confirm the possibility of hiding surface defects from Love waves and contribute to advancements of devices for surface waves control. Furthermore, an analogous strategy to design carpet cloaks should be developed for Rayleigh waves. In that case, the transformed elasticity tensor loses its minor symmetry [92]. Thus, the definition of an effective medium for the cloak design requires a specific treatment involving, for example, a symmetrization of the transformed elasticity tensor [96].

2.6 Appendix A. Distribution of the effective shear modulus.

In this appendix we provide the distribution of the effective shear moduli for the triangular and the parabolic cloak, as obtained from Eq. (2.11) and Eq. (2.17), respectively. For the triangular cloak μ'_{11}, μ'_{12} and μ'_{22} are constant inside the cloak and the layer, with μ_{12} being anti-symmetric w.r.t. the cloak vertical axis (Fig. 2.7$(a)-(c)$). The parabolic cloak presents a symmetric distribution for μ'_{11} and μ'_{22}, and an anti-symmetric one for μ'_{12}, respectively (Fig. 2.7$(d)-(f)$).

2.7 Appendix B. Inverse homogenization-Genetic Algorithm

Here we present a more general inverse homogenization approach to approximate the anisotropic effective properties of the pinched triangular cloak by a piece-wise isotropic medium. This can be achieved by adjusting the size, shape and the characteristics of the complex medium whose properties will derive from the homogenization theory. In[90] it was shown that the family of partial differential equation with periodical oscillating coefficients, two-scale converges to the homogenization limit, which is the main result used here. If y is the microscopic variable of the unit cell, the properties of the effective medium are given by:

$$\mu^{hom} = \begin{pmatrix} \langle\mu\rangle - \langle\mu\partial_{y_1} w_1\rangle & -\langle\mu\partial_{y_1} w_2\rangle \\ -\langle\mu\partial_{y_2} w_1\rangle & \langle\mu\rangle - \langle\mu\partial_{y_2} w_2\rangle \end{pmatrix} \tag{2.25}$$

where $\langle\cdot\rangle$ is the mean operator over the unit cell, $\partial_y w_j$ is the partial derivative with respect to the microscopic variable y of w_j, which is the solution of the so-called cell problem and plays the role of a correction factor:

$$\nabla_y \cdot (\mu(\nabla_y w_j(y) + e_j)) = 0 \tag{2.26}$$

for $j = 0, 1$, where $e_1 = (1, 0)$ and $e_2 = (0, 1)$ are the unit vectors. The cell problem is described by a set of 4 parameters $(\mu_a, \mu_b, \alpha, \theta)$, where μ_a and μ_b are the shear modulus of the two isotropic materials a and b, α is a point along the cut line between the two materials and θ is the angle of the cell with respect to the horizontal axis y_2, see Fig. 2.4(a). Our goal is to optimize those 4 parameters to mimic the effective properties of the transformed medium i.e. $\mu^{hom} \approx \mu'$. Taking into account the high accuracy demanded by our problem, the application of a genetic algorithm (GA) is compulsory.

The Genetic Algorithm is a numerical technique that targets to optimize a function over a set of

defined parameters. Some of the main advantages that the (GA) possesses, is that it does not require higher order terms i.e. derivatives and it is well-suited of solving problems of complex nature when the traditional approaches fail miserably. In our case, we define γ as the cost (fitness) function we would like to minimize as:

$$\gamma = \sum_{i,j} \frac{(\mu'_{ij} - \mu^{hom}_{ij})^2}{(\mu'_{ij})^2} \tag{2.27}$$

The smaller the function γ gets, the better the approximation of the effective property μ'. As μ^{hom} derives from the solution of the annex problem, the optimization procedure depends on the set of the geometrical parameters introduced in section 2.3.1. Hence, a MATLAB routine had been prepared to run the (GA). Initially, individual sets of those parameters are generated randomly and defined as the Population Size N. Then, for each set, homogenization theory is being applied, solving the of annex problem using (PDE) module in COMSOL. The results of each individual are being compared, neglecting the ones with poor convergence. Then, a new set of parameters is imported, based on the top performance of the previous iteration. Each iteration can be identified as a *Gene* (G) (from the Biological term). For each particular Gene, we define those best 2 individuals as *Parents* (p_1) and (p_2) and the new set as *Children* (c_1) with the relation:

$$c_1 = \frac{p_1 + p_2}{2} \tag{2.28}$$

Here we demonstrate the efficacy of the generic algorithm for the case of the triangular pinched cloak with the defect inside the layer. For our purpose, we set the population size (N) to 20 and the number of generations (G) to 50. The results obtained through the (GA) (Fig. 2.8) are compared with the analytical solution provided in Section 2.4, as depicted in Table 2.2 (the set solutions is not unique). It is clear that the (GA) is capable of providing an adequate approximation of the effective mechanical properties of the layered cloak. We point out that by constraining the number of unit cell parameters, for instance, by setting $\alpha = 0.5$, the (GA) converges even closer to the theoretical values

of the effective properties.

Parameters	Analytical	Genetic Algorithm
α	0.5	0.8203
$\frac{\mu'_a}{\mu_1}$	0.0544	0.0958
$\frac{\mu'_b}{\mu_1}$	2.9409	7.8180
θ'	± 0.6412	± 0.6424
$\frac{\mu'_{11}}{\mu_1}$	1	0.9926
$\frac{\mu'_{12}}{\mu_1} = \frac{\mu'_{21}}{\mu_1}$	± 0.6667	± 0.6556
$\frac{\mu'_{22}}{\mu_1}$	0.6044	0.6070
γ	0	0.000623

Table 2.2: Mechanical properties obtained from the Analytical solution and the Generic Algorithm for the monoclinic unit cell of the triangular pinched cloak.

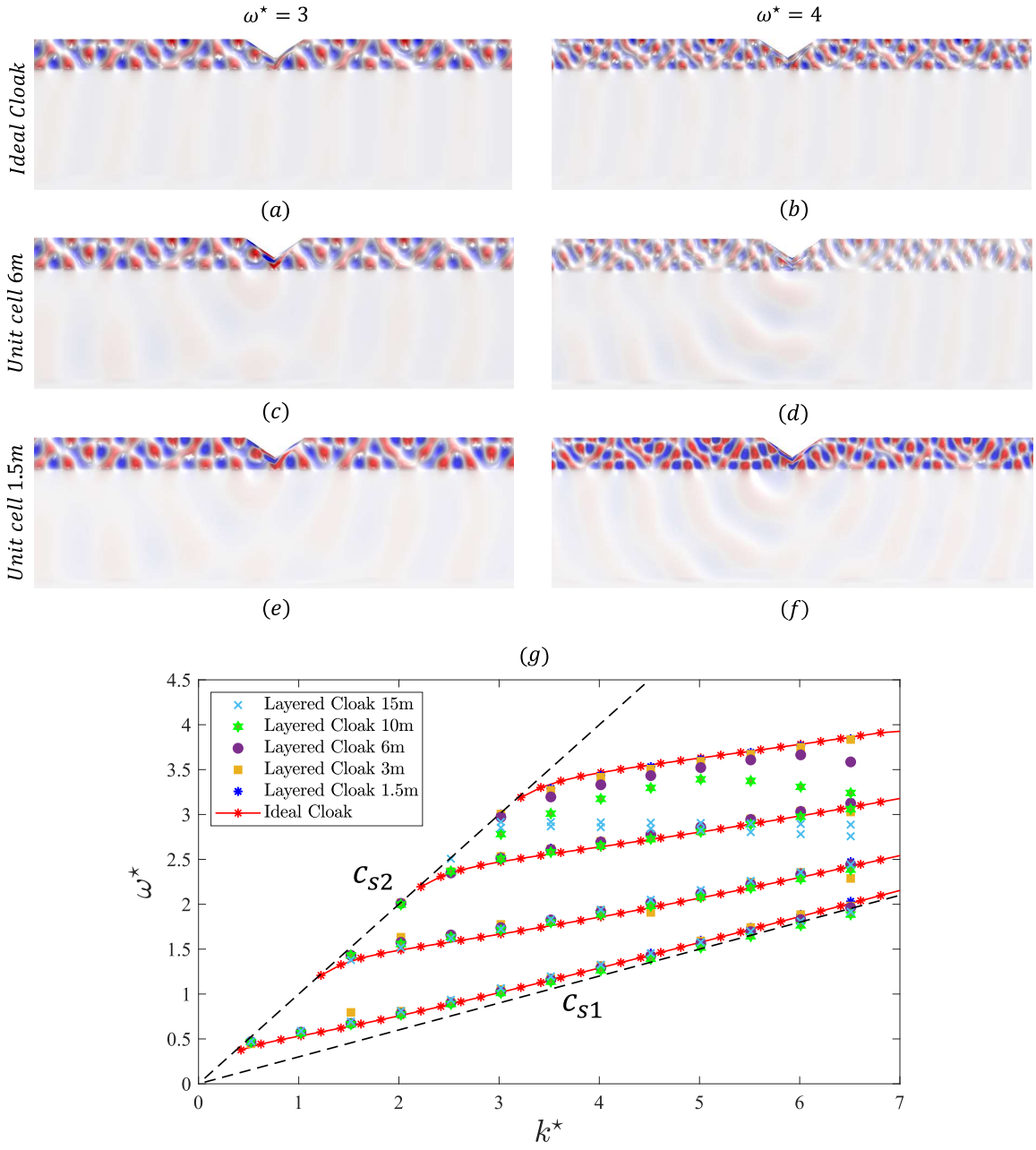

Fig. 2.6: Parametric study on the dispersion curves with respect to the unit cell dimension of the layered cloaks. The dispersion of the Ideal cloak is provided for reference.

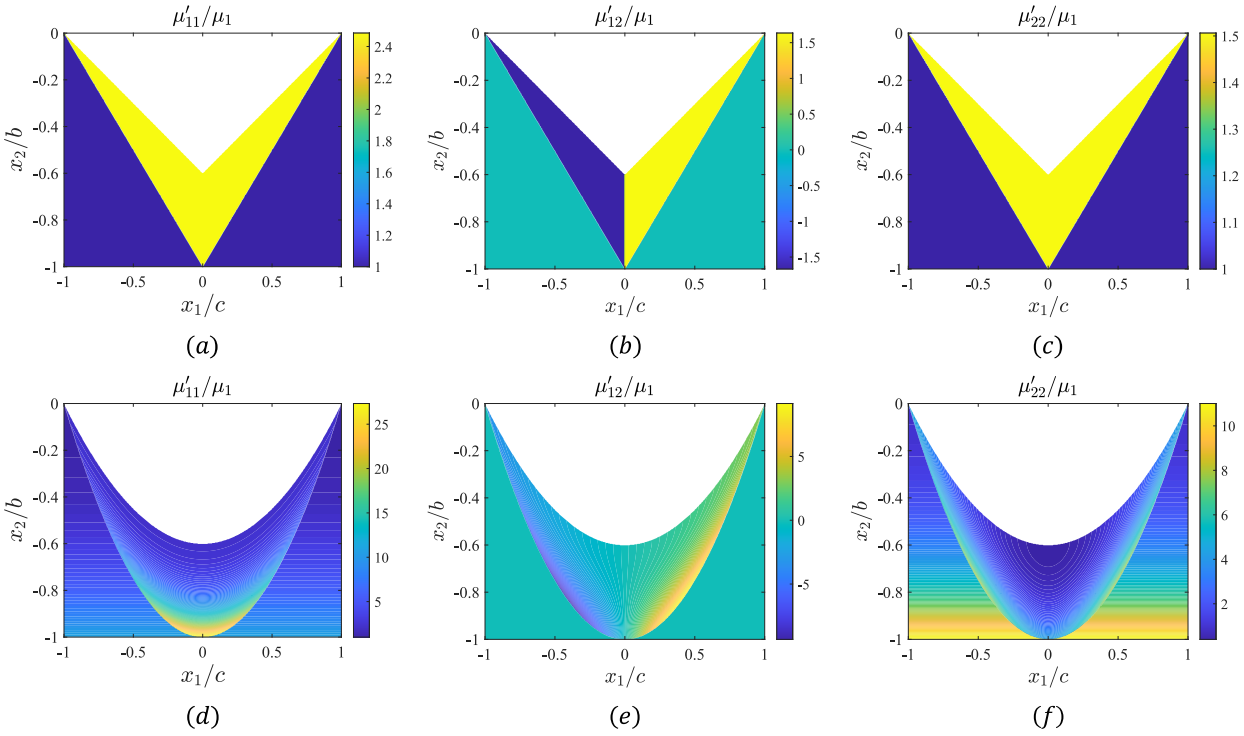

Fig. 2.7: Contour plots of the transformed shear moduli coefficients over a rectangular domain $(-c, c) \times (-b, 0)$, for the triangular $(a) - (c)$ and the parabolic $(d) - (f)$ shaped cloaks, respectively.

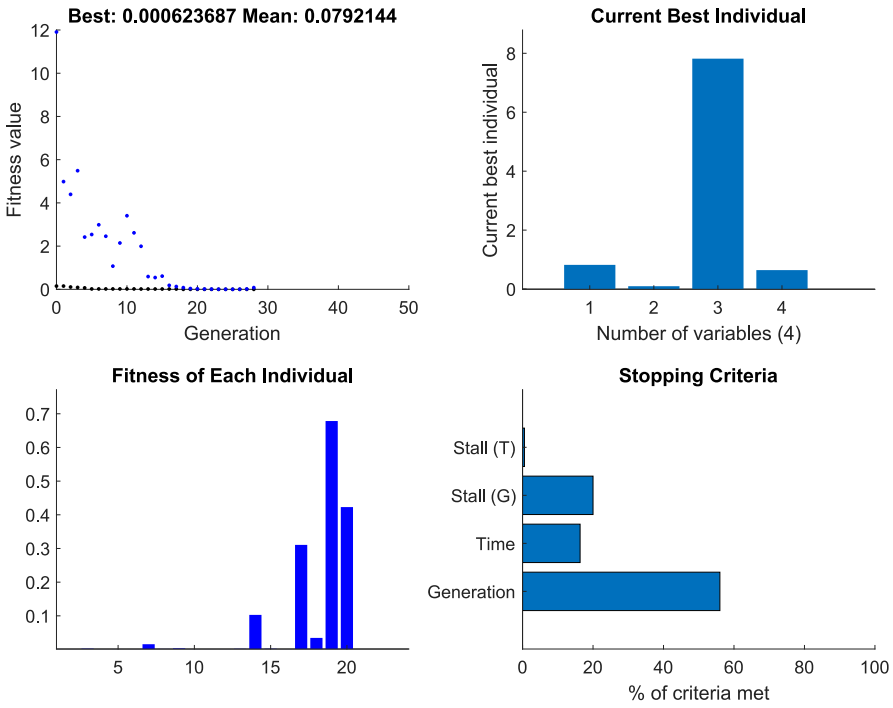

Fig. 2.8: Results of the genetic algorithm, including the fitness value, the value of each parameter, the fitness of each individual and the time of convergence.

References

[89] Achaoui, Y., Diatta, A., Kadic, M., & Guenneau, S. (2020). Cloaking in-plane elastic waves with swiss rolls. *Materials*, 13(2).

[90] Allaire, G. (1992). Homogenization and two-scale convergence. *SIAM Journal on Mathematical Analysis*, 23(6), 1482–1518.

[91] Bensoussan, Lions, P. (1978). *Asymptotic Analysis of Periodic Structures*. North Holland.

[92] Brun, M., Guenneau, S., & Movchan, A. B. (2009). Achieving control of in-plane elastic waves. *Applied Physics Letters*, 94(6), 061903.

[93] Chatzopoulos, Z., Palermo, A., Guenneau, S., & Marzani, A. (2022). Cloaking strategy for love waves. *Extreme Mechanics Letters*, 50, 101564.

[94] Chen, Y., Nassar, H., & Huang, G. (2021). Discrete transformation elasticity: An approach to design lattice-based polar metamaterials. *International Journal of Engineering Science*, 168, 103562.

[95] CHEW, W. & LIU, Q. (1996). Perfectly matched layers for elastodynamics: A new absorbing boundary condition. *Journal of Computational Acoustics*, 04(04), 341–359.

[96] Craster, R., Diatta, A., Guenneau, S., & Hutridurga, H. (2021). On near-cloaking for linear elasticity. *Multiscale Modeling & Simulation*, 19(2), 633–664.

[97] Farhat, M., Guenneau, S., & Enoch, S. (2009). Ultrabroadband elastic cloaking in thin plates. *Phys. Rev. Lett.*, 103, 024301.

[98] Foti, S., Hollender, F., Garofalo, F., Albarello, D., Asten, M., Bard, P.-Y., Comina, C., Cornou, C., Cox, B., Di Giulio, G., et al. (2018). Guidelines for the good practice of surface wave analysis: a product of the interpacific project. *Bulletin of Earthquake Engineering*, 16(6), 2367–2420.

[99] Greenleaf A, L. M. & G, U. (2003). On non-uniqueness for calderón's inverse problem. *Math. Res.Lett.*, 10, 685–93.

[100] Ji, Q., Chen, X., Liang, J., Laude, V., Guenneau, S., Fang, G., & Kadic, M. (2021). Designing thermal energy harvesting devices with natural materials through optimized microstructures. *International Journal of Heat and Mass Transfer*, 169, 120948.

[101] Kadic, M., Bückmann, T., Schittny, R., & Wegener, M. (2013). Metamaterials beyond electromagnetism. *Reports on Progress in Physics*, 76(12), 126501.

[102] Kadic, M., Bückmann, T., Stenger, N., Thiel, M., & Wegener, M. (2012). On the practicability of pentamode mechanical metamaterials. *Applied Physics Letters*, 100(19), 191901.

[103] Khlopotin, A., Olsson, P., & Larsson, F. (2015). Transformational cloaking from seismic surface waves by micropolar metamaterials with finite couple stiffness. *Wave Motion*, 58, 53–67.

[104] Li, J. & Pendry, J. B. (2008). Hiding under the carpet: a new strategy for cloaking. *Physical review letters*, 101(20), 203901.

[105] Love, A. E. H. (1911). *Some Problems of Geodynamics*. SAO/NASA Astrophysics Data System.

[106] Maurel, A. & Marigo, J.-J. (2018). Sensitivity of a dielectric layered structure on a scale below the periodicity: A fully local homogenized model. *Physical Review B*, 98(2), 024306.

[107] Maurel, A., Marigo, J.-J., Pham, K., & Guenneau, S. (2018). Conversion of love waves in a forest of trees. *Physical Review B*, 98(13), 134311.

[108] Meirbekova, B. & Brun, M. (2020). Control of elastic shear waves by periodic geometric transformation: cloaking, high reflectivity and anomalous resonances. *Journal of the Mechanics and Physics of Solids*, 137, 103816.

[109] Milton, G. W. (2002). *The theory of composites*. Cambridge university press.

[110] Milton, G. W., Briane, M., & Willis, J. R. (2006). On cloaking for elasticity and physical equations with a transformation invariant form. *New Journal of Physics*, 8(10), 248–248.

[111] Misseroni, D., Colquitt, D. J., Movchan, A. B., Movchan, N. V., & Jones, I. S. (2016). Cymatics for the cloaking of flexural vibrations in a structured plate. *Scientific reports*, 6(1), 1–11.

[112] Misseroni, D., Movchan, A., & Bigoni, D. (2019). Omnidirectional flexural invisibility of multiple interacting voids in vibrating elastic plates. *Proceedings of the Royal Society A*, 475(2229), 20190283.

[113] Nassar, H., Chen, Y., & Huang, G. (2019). Isotropic polar solids for conformal transformation elasticity and cloaking. *Journal of the Mechanics and Physics of Solids*, 129, 229–243.

[114] Nassar, H., Chen, Y. Y., & Huang, G. L. (2020). Polar metamaterials: A new outlook on resonance for cloaking applications. *Phys. Rev. Lett.*, 124, 084301.

[115] Norris, A. & Shuvalov, A. (2011). Elastic cloaking theory. *Wave Motion*, 48(6), 525–538. Special Issue on Cloaking of Wave Motion.

[116] Norris, A. N. (2008). Acoustic cloaking theory. *Proceedings of the Royal Society A: Mathematical, Physical and Engineering Sciences*, 464(2097), 2411–2434.

[117] O'Neill, J., Selsil, Ö., McPhedran, R., Movchan, A., Movchan, N., & Henderson Moggach, C. (2016). Active cloaking of resonant coated inclusions for waves in membranes and kirchhoff plates. *The Quarterly Journal of Mechanics and Applied Mathematics*, 69(2), 115–159.

[118] Palermo, A. & Marzani, A. (2018). Control of love waves by resonant metasurfaces. *Scientific reports*, 8(1), 1–8.

[119] Parnell, W. J. (2012). Nonlinear pre-stress for cloaking from antiplane elastic waves. *Proceedings of the Royal Society A: Mathematical, Physical and Engineering Sciences*, 468(2138), 563–580.

[120] Parnell, W. J. & Shearer, T. (2013). Antiplane elastic wave cloaking using metamaterials, homogenization and hyperelasticity. *Wave Motion*, 50(7), 1140–1152. Advanced Modelling of Wave Propagation in Solids.

[121] Petiteau, D., Guenneau, S., Bellieud, M., Zerrad, M., & Amra, C. (2014). Spectral effectiveness of engineered thermal cloaks in the frequency regime. *Scientific reports*, 4(1), 1–9.

[122] Pomot, L., Bourgeois, S., Payan, C., Remillieux, M., & Guenneau, S. (2019). On form invariance of the kirchhoff-love plate equation. *arXiv preprint arXiv:1901.00067*.

[123] Pomot, L., Payan, C., Remillieux, M., & Guenneau, S. (2020). Acoustic cloaking: Geometric transform, homogenization and a genetic algorithm. *Wave Motion*, 92, 102413.

[124] Quadrelli, D. E., Craster, R., Kadic, M., & Braghin, F. (2021). Elastic wave near-cloaking. *Extreme Mechanics Letters*, 44, 101262.

[125] Stenger, N., Wilhelm, M., & Wegener, M. (2012). Experiments on elastic cloaking in thin plates. *Phys. Rev. Lett.*, 108, 014301.

[126] Sun, Z., Sun, X., Jia, H., Bi, Y., & Yang, J. (2019). Quasi-isotropic underwater acoustic carpet cloak based on latticed pentamode metafluid. *Applied Physics Letters*, 114(9), 094101.

[127] Tang, K., Xu, C., Guenneau, S., & Sebbah, P. (2021). Pulse dynamics of flexural waves in transformed plates. *Advanced Functional Materials*, 31(15), 2009266.

[128] Tuttipongsawat, P., Wijeyewickrema, A. C., & Leungvichcharoen, S. (2020). Cloaking of a circular cylindrical elastic inclusion from antiplane elastic waves and resonance effects. *Wave Motion*, 94, 102491.

[129] Vasquez, F. G., Milton, G. W., & Onofrei, D. (2009). Active exterior cloaking for the 2d laplace and helmholtz equations. *Physical Review Letters*, 103(7), 073901.

[130] Vasquez, F. G., Milton, G. W., Onofrei, D., & Seppecher, P. (2013). Transformation elastodynamics and active exterior acoustic cloaking. In *Acoustic metamaterials* (pp. 289–318). Springer.

[131] Wang, R., Lei Mei, Z., & Jun Cui, T. (2013). A carpet cloak for static magnetic field. *Applied Physics Letters*, 102(21), 213501.

[132] Xu, X., Wang, C., Shou, W., Du, Z., Chen, Y., Li, B., Matusik, W., Hussein, N., & Huang, G. (2020). Physical realization of elastic cloaking with a polar material. *Phys. Rev. Lett.*, 124, 114301.

[133] Zhang, H., Chen, Y., Liu, X., & Hu, G. (2020). An asymmetric elastic metamaterial model for elastic wave cloaking. *Journal of the Mechanics and Physics of Solids*, 135, 103796.

[134] Zhang, P. & Parnell, W. J. (2018). Hyperelastic antiplane ground cloaking. *The Journal of the Acoustical Society of America*, 143(5), 2878–2885.

3

Cloaking of Rayleigh waves

In this chapter we propose a strategy based on coordinate transformation to cloak Rayleigh waves. Rayleigh waves are in-plane elastic waves which propagate along the free surface of semi-infinite media. They are governed by Navier equations that retain their form for an in-plane arbitrary coordinate transformation $\mathbf{x} = \Xi(\mathbf{X})$, upon choosing the specific kinematic relation $\mathbf{U}(\Xi(\mathbf{X})) = \mathbf{u}(\mathbf{x})$ be-

tween displacement fields in virtual, i.e. reference, (**U**) and transformed, i.e. cloaked, (**u**) domains. However, the elasticity tensor of the transformed domain is no longer fully symmetric, and thus, it is difficult to design with common materials. Motivated by this issue, we propose a symmetrization technique, based on the arithmetic mean, to obtain anisotropic, yet symmetric, elastic tensors for Rayleigh wave near-cloaking. In particular, by means of time-harmonic numerical simulations and dispersion analyses, we compare the efficiency of triangular and semi-circular cloaks designed with the original non-symmetric tensors and the related symmetrized versions. In addition, different coordinate transformations, e.g. linear, quadratic and cubic, are adopted for the semi-circular cloaks. Through the analyses, we show that a symmetrized semi-circular cloak, obtained upon the use of a quadratic transformation, performs better than the other investigated designs. Our study provides a step toward the design of feasible and efficient broadband elastic metamaterial cloaks for surface waves.

3.1 Introduction

Controlling surface waves with architected materials is an open challenge in several engineering applications, ranging from microdevices for electronic components [153], namely SAW devices, to meter-sized barriers [175,159,167,157,152,179,180,162] and seismic cloaks [182] for ground-borne vibrations. In the latter context, two large-scale experiments recently demonstrated that one can reflect [136] or even focus [137] surface Rayleigh waves in structured sedimentary soils. These experiments were the result of collaborative work between geotechnical engineers and wave physicists that explored analogies between models of electromagnetic and elastodynamic waves in metamaterials [148,150,183,145,191,158,184].

Based on those experiments, it was argued that one might build a cloak for Rayleigh waves with concentric layers of structured soil around a building one may wish to protect. Such an approach amounts to considering a physical setup in a plane parallel to the surface. Many numerical works followed, mostly considering the same approach, notably a proposal to reroute Love waves [176] in the

transverse plane thanks to a graded metasurface, and some conversion of Love waves into downward propagating anti-plane shear bulk waves via a wedge effect in the vertical plane [160]. In parallel, small-scale experiments on the control of surface seismic waves [143,174,144] have shown that one can also act upon the deflection of Rayleigh waves in the vertical plane with an array of resonators atop, or buried, in the soil. The corresponding physical setups consider devices acting on a plane orthogonal to the surface.

Following this approach, some authors of this manuscript investigated the cloaking of surface Love waves by transforming the elastic medium along the vertical plane [141]. At first sight, this strategy for cloaking of Love waves should equally work for Rayleigh waves. However, unlike Love waves, which are polarized out-of-plane and can thus be modelled by a scalar Helmholtz equation in the vertical plane, Rayleigh waves are governed by the Navier equations, where the coupling between in-plane pressure and shear waves cannot be avoided.

In this regard, we stress that a major hurdle in Rayleigh wave cloaking is that the Navier equations are not form invariant under an arbitrary geometric transformation [165], leading to non-scalar density and additional third-order elastic tensors in the transformed medium. Notably, Norris et al. [172] investigated the relation, e.g. the gauge, between the displacement field of the reference domain and the transformed one and showed that it directly affects the symmetry of the elastic tensor. Recently, 2D elastodynamic cloaking has been approached either by direct design and homogenization of the so-called micropolar metamaterials [170,171,169,194,187], which can achieve the required non-symmetric elastic tensor, or by utilizing symmetrization techniques to restore the symmetries of the elastic tensor [182,147]. An alternative route to achieve cloaking exploits the use of non-linear elastic pre-stress in hyperelastic material models to relax the constraints on material properties [177,178,173,135,193].

Relevant studies in the context of Rayleigh waves cloaking include the use of micropolar materials to hide a cylinder embedded in the medium [155] and near-cloaking techniques to decouple P and S waves [181]. Here, we focus, instead, on the use of symmetrized tensors, since micropolar materials can

exhibit zero-modes and mechanical instabilities, making them complex to manufacture[154]. Specifically, our scope is to delve into the effects of symmetrization on the cloaking performance of Rayleigh waves, considering different transformation and cloaking geometries.

To this aim, we organize our manuscript as follows: we first recall the Navier equations for the reference and transformed semi-infinite media. We stress that depending on the choice of the gauge, one can either assume a modified Willis medium, or a Cosserat medium with a non-symmetric elastic tensor.

After adopting the latter, we manipulate its non-symmetric components using the arithmetic mean and assess the effect of symmetrization on the cloaking of Rayleigh waves. Our analysis considers a triangular pinched cloak and 3 types of semi-circular cloaks, distinguished by the adopted radial transformation C_i (linear C_1, quadratic C_2, cubic C_3). The cloaking performance is analyzed by comparing the harmonic wave fields and dispersion relations of ideal, e.g. non-symmetric, and symmetrized cloaks. In particular, the dispersive analysis exploits the inverse participation ratio (IPR), which addresses the localization level of the displacement fields, to identify and count the surface modes (of interest).

Next, the performance analysis is continued by means of harmonic simulations and by comparing the transmitted displacement fields after the cloak of symmetrized and ideal cases. We conclude the investigation with a focus on the circular cloaks by examining the requirements for a symmetric elastic tensor for each C_i type of transformation.

3.2 Governing Equations for 2-D Elasticity

We consider a homogeneous isotropic semi-infinite half-space with material properties (λ, μ, ρ), where λ and μ are the Lamé coefficients and ρ the mass density, respectively, and the spatial coordinates for the reference domain are $\mathbf{X} = (X_1, X_2)$. For in-plane surface waves, i.e. Rayleigh waves, propagating

along the horizontal X_1 direction, the governing Navier elastodynamic equation reads:

$$\nabla_X \cdot (\mathbf{C} : \nabla_X \mathbf{U}) = \rho \mathbf{U}_{tt} \tag{3.1}$$

where $\mathbf{C}$ is the isotropic 4th order elasticity tensor, $\mathbf{U} = (U_1, U_2)$ is the displacement and $\mathbf{U}_{tt}$ denotes the second order derivative in time of $\mathbf{U}$. Under the assumption of plane-strain elasticity, the elastic tensor can be written in Voigt's notation $\{1, 2, 6\} = \{11, 22, 12\}$ as:

$$\mathbf{C}_{IJ} = \begin{bmatrix} \lambda + 2\mu & \lambda & 0 \\ \lambda & \lambda + 2\mu & 0 \\ 0 & 0 & \mu \end{bmatrix}, \tag{3.2}$$

where $I, J = 1, 2, 6$.

We apply a point-wise invertible transformation that maps the reference configuration (virtual domain) $\mathbf{X} \in \Upsilon$ to the deformed region (physical domain) as $\mathbf{x} = (\mathbf{X}) \in \psi$ and the remaining domain to itself ($\mathbf{X} \notin \Upsilon$). As a result, we derive the transformed elasticity tensor in the cloaked region. In Figs. 3.1$(a) - (d)$, we show two examples of carpet cloaks, a triangular and a semi-circular one, with the related virtual and deformed domains. The transformation gradients for the deformed and the reference domains are $\mathbf{F} = \nabla_X x$ and $\mathbf{F}^{-1} = \nabla_x X$, respectively. Also, $J = det(\mathbf{F})$ is the determinant of the transformation gradient. Given $\mathbf{x} = \{x_1, x_2\}$ the coordinates for the physical domain, the transformation gradient $\mathbf{F}$ reads:

$$\mathbf{F} = \nabla_X x = \begin{pmatrix} \frac{\partial x_1}{\partial X_1} & \frac{\partial x_1}{\partial X_2} \\ \frac{\partial x_2}{\partial X_1} & \frac{\partial x_2}{\partial X_2} \end{pmatrix} \tag{3.3}$$

As discussed in the literature, see for example [165], Eq. (4.1) is not form invariant upon an arbitrary coordinate transformation and it depends on the choice of the gauge $\mathbf{U}((\mathbf{X})) = \mathbf{A}\mathbf{u}(\mathbf{x})$, where $\mathbf{A}$ is

a non-singular matrix. In particular, the choice $\mathbf{A} = \mathbf{F}$ leads to the so-called Willis setting that guarantees symmetric stress tensor [165,172]. Despite possessing such a symmetry, a medium that is governed by the Willis equation is difficult to design due to the presence of two additional 3rd order symmetric tensors, which may require the introduction of pre-stresses [146,188]. Additionally, in the Willis setting the material density is a 2nd order symmetric tensor, a requirement which can be physically replicated only within narrow frequency bands using resonant microstructures.

For this reason, in the present work, we refrain from using Willis materials and we employ a Cosserat setting. In particular, following the idea by Norris et al. [172], by assuming the gauge $\mathbf{U}((\mathbf{X})) = \mathbf{u}(\mathbf{x})$ $(\mathbf{A} = \mathbf{I})$ for the displacements [139,138], we derive the governing equation in the physical domain $\mathbf{x} = (x_1, x_2)$ as:

$$\nabla_x \cdot (\mathbf{C}^{eff} : \nabla_x \mathbf{u}) = \rho^{eff} \mathbf{u}_{tt} \tag{3.4}$$

where

$$\begin{aligned} C^{eff}_{ijkl} &= J^{-1} C_{IjKl} F_{iI} F_{kK} \\ \rho^{eff} &= \rho J^{-1} \end{aligned} \tag{3.5}$$

are the transformed mechanical parameters of the cloaked region (purple region in Fig.3.1b and blue region in Fig.3.1d) in Einstein summation. As a result, the transformed elasticity tensor C^{eff} preserves the major symmetries ($C^{eff}_{ijkl} = C^{eff}_{klij}$, etc.), but does not possess the minor ones as:

$$C^{eff}_{ijkl} \neq C^{eff}_{jikl} \neq C^{eff}_{ijlk} \neq C^{eff}_{jilk} \tag{3.6}$$

except for very special cases such as in the framework of conformal transformations. Nonetheless, the medium can still be described by a single 4th-order non-symmetric and, eventually, inhomogeneous elastic tensor.

3.3 Carpet cloaking for Rayleigh waves: Transformation

Due to the vectorial nature of Rayleigh waves, cloaking has been hindered by the requirement of a material with non-symmetric elasticity tensor. Indeed, several researchers [142,192,151,194] have presented metamaterials that can obtain the non-symmetric behaviour required for cloaking. Here, however, we focus our investigation on a different aspect, aiming at analysing and comparing different linear and non-linear transformations, as well as symmetrization strategies, to obtain an easy-to-realize, well-performing, symmetric cloaks for Rayleigh waves. Specifically, we delve into the behaviour of carpet cloaks with boundaries described by either linear functions (triangular shape) or semi-circular ones.

3.3.1 Triangular carpet cloak

We first consider a two-dimensional carpet cloak of triangular shape. Given a set of cartesian coordinates centred along the cloak symmetry axis ($\mathbf{X} = \{X_1, X_2\}$, $\mathbf{x} = \{x_1, x_2\}$), we denote with $z_1(x_1)$ and $z_2(x_1)$ the interior and exterior boundaries of the cloak, respectively. The transformation Ξ^T that maps the region enclosed between two curves $(X_1; 0)$ and $(X_1; z_2(X_1))$ of the virtual domain, Fig. 3.1a, to the one comprised between $(x_1; z_1(x_1))$ and $(x_1; z_2(x_1))$ of the real domain, Fig. 3.1b, is:

$$\Xi^T : \begin{cases} x_1 = X_1 \\ x_2 = (\frac{z_2(X_1) - z_1(X_1)}{z_2(X_1)})X_2 + z_1(X_1) \end{cases} \tag{3.7}$$

Note that $(X_1; 0)$ is mapped on $(x_1; z_1(x_1))$ while $(X_1; z_2(X_1))$ is point-wise fixed. Let $z_1(x_1) = \frac{a}{c}|x_1| - a$ and $z_2(x_1) = \frac{b}{c}|x_1| - b$ be piece-wise linear curves, where a, b, c are the geometric parameters of the cloak, as illustrated in Fig. 3.1b. Then, using Cartesian $\mathbf{X} = \{X_1, X_2\}$, $\mathbf{x} = \{x_1, x_2\}$

coordinates the Jacobian of the transformation reads:

$$\mathbf{F}^T = \begin{bmatrix} \frac{\partial x_1}{\partial X_1} & \frac{\partial x_1}{\partial X_2} \\ \frac{\partial x_2}{\partial X_1} & \frac{\partial x_2}{\partial X_2} \end{bmatrix} = \begin{bmatrix} 1 & 0 \\ F_{21}(x_1) & F_{22} \end{bmatrix} \tag{3.8}$$

where $F_{21}(x_1) = sign(x_1)\frac{a}{c}$ and $F_{22} = det(\mathbf{F}^T) = \frac{b-a}{b}$. According to Eq. (3.5) and adopting the augmented Voigt notation for the plane problem as $\{1,2,6,\overline{6}\} = \{11,22,12,21\}$, we obtain the following transformed elastic tensor and material density properties within the cloak domain:

$$\mathbf{C}_{IJ}^{effT} = \begin{bmatrix} \frac{\lambda+2\mu}{F_{22}} & \lambda & 0 & \frac{F_{21}(x_1)}{F_{22}}(\lambda+2\mu) \\ \lambda & \frac{F_{21}(x_1)^2\mu+F_{22}^2(\lambda+2\mu)}{F_{22}} & \frac{F_{21}(x_1)}{F_{22}}\mu & F_{21}(x_1)(\lambda+\mu) \\ 0 & \frac{F_{21}(x_1)}{F_{22}}\mu & \frac{\mu}{F_{22}} & \mu \\ \frac{F_{21}(x_1)}{F_{22}}(\lambda+2\mu) & F_{21}(x_1)(\lambda+\mu) & \mu & \frac{F_{21}(x_1)^2(\lambda+2\mu)+F_{22}^2\mu}{F_{22}} \end{bmatrix}, \quad \rho^{effT} = \rho F_{22}^{-1} \tag{3.9}$$

for $I,J = 1,2,6,\overline{6}$. Note that the effective density is constant. As anticipated in the previous section, the elastic tensor of Eq. (3.9) is non-symmetric. In particular, it has 3 non-symmetric entries, which in the augmented Voigt notation read:

$$\begin{cases} C_{16}^{effT} \neq C_{1\overline{6}}^{effT} \\ C_{26}^{effT} \neq C_{2\overline{6}}^{effT} \\ C_{66}^{effT} \neq C_{6\overline{6}}^{effT} \neq C_{\overline{66}}^{effT} \end{cases} \tag{3.10}$$

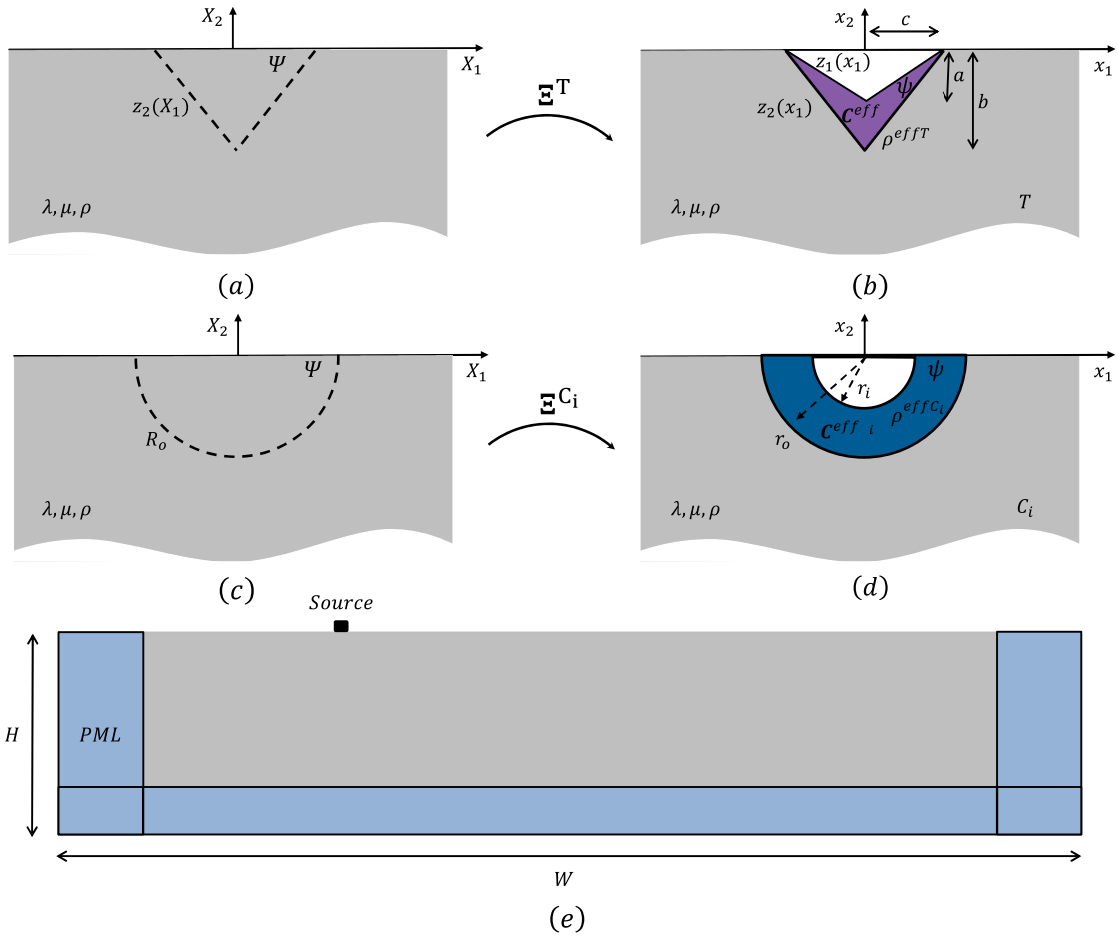

Fig. 3.1: (*a*) Reference configuration (virtual domain) of the triangular cloak. (*b*) Deformed configuration (physical domain) obtained by the action of (Ξ^T) that maps the (virtual domain) into a defect (white region) surrounded by the cloak (purple region). (*c*) Reference configuration (virtual domain) of the semi-circular cloak. (*d*) Deformed configuration (physical domain) obtained by the action of (Ξ^{C_i}) that maps the (virtual domain) into a defect (white region) surrounded by the cloak (blue region). (*e*) Schematic representation of the FEM model.

3.3.2 Circular carpet cloak

We now consider the case of annulus shaped semi-circular cloaks located at the free-surface of the semi-infinite domain (Fig. 3.1d). To simplify the definition of the transformed mechanical properties, we introduce a set of polar coordinates $\mathbf{X} = \{R, \Theta\}$ centered within the cloaked domain, where $R = \sqrt{{X_1}^2 + {X_2}^2}$ and $\Theta = \arctan \frac{X_2}{X_1}[\pi]$, where $[\pi]$ specifies the branch cut taken for arctan.

For such a configuration, we consider and compare 3 different types of radial transformations $\Xi^{C_i} : (R, \Theta) \rightarrow (r, \theta)$ that map the origin (0,0) of the reference system, Fig. 3.1c, onto an inner circle of radius $r_i = a$ in the physical one, and the outer circle $R_o = r_o = b$ to itself (see Fig. 3.1d):

$$\Xi^{C_1} : \begin{cases} r = \frac{b-a}{b} R + a \quad 0 \leq R \leq R_o \\ \theta = \Theta \end{cases} \tag{3.11}$$

$$\Xi^{C_2} : \begin{cases} r = A_2 R^2 + A_1 R + A_0 \quad 0 \leq R \leq R_o \\ \theta = \Theta \end{cases} \tag{3.12}$$

where:

$$A_2 = \frac{a}{b^2}, \quad A_1 = \frac{b - 2a}{b}, \quad A_0 = a. \tag{3.13}$$

$$\Xi^{C_3} : \begin{cases} r = B_3 R^3 + B_2 R^2 + B_1 R + B_0 \quad 0 \leq R \leq R_o \\ \theta = \Theta \end{cases} \tag{3.14}$$

where:

$$B_3 = \frac{2a}{b^3}, \quad B_2 = \frac{-3a}{b^2}, \quad B_1 = 1, \quad B_0 = a. \tag{3.15}$$

The general form of the Jacobian of such transformation in polar basis reads:

$$\mathbf{F}^{C} = \begin{bmatrix} \frac{\partial r}{\partial R} & \frac{\partial r}{R\partial\Theta} \\ \frac{r\partial\theta}{\partial R} & \frac{r\partial\theta}{R\partial\Theta} \end{bmatrix} \tag{3.16}$$

Specifically, for each transformation C_i in Eqs. (3.11), (3.12), (3.14) we obtain:

$$\mathbf{F}^{C_1} = \begin{bmatrix} F_{11}^{C_1} & 0 \\ 0 & F_{22}^{C_1} \end{bmatrix} = \begin{bmatrix} \frac{(b-a)}{b} & 0 \\ 0 & \frac{(b-a)}{(r-a)}\frac{r}{b} \end{bmatrix} \tag{3.17}$$

$$\mathbf{F}^{C_2} = \begin{bmatrix} F_{11}^{C_2} & 0 \\ 0 & F_{22}^{C_2} \end{bmatrix} = \begin{bmatrix} \frac{\sqrt{b^2-4ab+4ar}}{b} & 0 \\ 0 & \frac{2ar}{2ab-b^2+b\sqrt{b^2-4ab+4ar}} \end{bmatrix} \tag{3.18}$$

$$\mathbf{F}^{C_3} = \begin{bmatrix} F_{11}^{C_3} & 0 \\ 0 & F_{22}^{C_3} \end{bmatrix} = \begin{bmatrix} \frac{6aR^2(r)}{b^3} - \frac{6aR(r)}{b^2} + 1 & 0 \\ 0 & \frac{r}{R(r)} \end{bmatrix} \tag{3.19}$$

where:

$$R(r) = \frac{b}{2} + \frac{\frac{b^2}{4} - \frac{b^3}{6a}}{\left(\sqrt{\left(\frac{ab^3-b^3r}{4a} - \frac{b^3}{8} + \frac{b^4}{8a}\right)^2 - \left(\frac{b^2}{4} - \frac{b^3}{6a}\right)^3} - \frac{ab^3-b^3r}{4a} + \frac{b^3}{8} - \frac{b^4}{8a}\right)^{1/3}} + \left(\sqrt{\left(\frac{ab^3-b^3r}{4a} - \frac{b^3}{8} + \frac{b^4}{8a}\right)^2 - \left(\frac{b^2}{4} - \frac{b^3}{6a}\right)^3} - \frac{ab^3-b^3r}{4a} + \frac{b^3}{8} - \frac{b^4}{8a}\right)^{1/3}. \tag{3.20}$$

We remark that the above transformations are singular, since they map the origin (a point) into a circle of radius r_i. The proper approach to avoid such singularities requires considering a very small circle of radius ε instead of the origin [156]. The reader can find a more detailed discussion concerning the offset parameter ε in the Appendix A.

Additionally, we underline that the parameters A_i, B_i in C_2 and C_3 types of transformations, respectively, are obtained from the traction continuity requirement on the outer boundary i.e. $\frac{\partial r}{\partial R}(R_o) = 1$, since the surrounding space of Υ is mapped onto itself. In contrast, this requirement is not satisfied in the C_1 transformation.

At this stage, using the augmented Voigt notation for the plane strain problem in polar coordinates: $\{1, 2, 6, \overline{6}\} = \{rr, \theta\theta, r\theta, \theta r\} = \{11, 22, 12, 21\}$, we obtain the following effective properties for any type of transformation ($i = 1, 2, 3$):

$$\mathbf{C}_{IJ}^{effC_i} = \begin{bmatrix} \frac{F_{11}^{C_i}}{F_{22}^{C_i}}(\lambda + 2\mu) & \lambda & 0 & 0 \\ \lambda & \frac{F_{22}^{C_i}}{F_{11}^{C_i}}(\lambda + 2\mu) & 0 & 0 \\ 0 & 0 & \frac{F_{11}^{C_i}}{F_{22}^{C_i}}\mu & \mu \\ 0 & 0 & \mu & \frac{F_{22}^{C_i}}{F_{11}^{C_i}}\mu \end{bmatrix}, \rho^{effC_i} = \frac{\rho}{det(\mathbf{F}^{C_i})} \tag{3.21}$$

for $I,J = 1, 2, 6, \bar{6}$. Again, the elastic tensor presents non-symmetric components:

$$C_{66}^{effC_i} \neq C_{6\overline{6}}^{effC_i} \neq C_{\overline{66}}^{effC_i} \tag{3.22}$$

Hence, compared to the triangular-shaped cloak, the circular one presents a reduced number of non-symmetric elastic tensor components. In what follows, we discuss and show how this feature impacts the performance of symmetrized cloaks.

3.4 Carpet cloaking for Rayleigh waves: Symmetrization

The symmetrization of an elastic tensor is a simple, yet effective, strategy to approximate the non-symmetric constitutive behavior of an "ideal" cloak with a standard Cauchy-type material, easily realiz-

able with common media. Different symmetrization strategies, such as geometric [182] or arithmetic [147] means have already been explored to realize feasible cloaks for bulk and flexural waves. In this study, we build upon a recent work proposed by Craster et al. [146], where it is shown that a symmetric tensor $\mathbf{C}^{Sym}$ obtained from the arithmetic mean nullifies the variational problem:

$$min_{\mathbf{A}\in M}|((\mathbf{C}^{eff}-\mathbf{C}^{Sym}):\mathbf{A}):\mathbf{A}|=0 \tag{3.23}$$

where M stands for the space of symmetric square matrices. In other words, the elastic energy per unit volume due to strain remains unchanged upon replacing the transformed Cosserat material (C^{eff},ρ) by the corresponding approximated Cauchy material (C^{Sym},ρ).

Our strategy is to choose the tensor components in such a way that the constraints above are satisfied, whilst keeping the remaining entries unaltered. For the triangular cloak, the requirements for a symmetric elastic tensor are:

$$\begin{cases} C^{Sym}_{16}=C^{Sym}_{1\bar{6}} \\ C^{Sym}_{26}=C^{Sym}_{2\bar{6}} \\ C^{Sym}_{66}=C^{Sym}_{6\bar{6}}=C^{Sym}_{\bar{6}\bar{6}} \end{cases} \tag{3.24}$$

Then, from Eqs. (3.23)-(3.24) we have:

$$\begin{aligned} |((\mathbf{C}^{effT}-\mathbf{C}^{Sym}):\mathbf{A}):\mathbf{A}| = |(C^{eff}_{16}+C^{eff}_{1\bar{6}}+C^{eff}_{\bar{6}1}+C^{eff}_{\bar{6}\bar{1}}-4C^{Sym}_{16})A_{11}A_{12} \\ +(C^{eff}_{26}+C^{eff}_{2\bar{6}}+C^{eff}_{\bar{6}2}+C^{eff}_{\bar{6}\bar{2}}-4C^{Sym}_{26})A_{22}A_{12}+(C^{eff}_{66}+C^{eff}_{6\bar{6}}+C^{eff}_{\bar{6}6}+C^{eff}_{\bar{6}\bar{6}}-4C^{Sym}_{66})A^2_{12}| \end{aligned} \tag{3.25}$$

Conversely, for the circular cloaks C_i $(i=1,2,3)$ we get the condition:

$$C^{Sym}_{66}=C^{Sym}_{6\bar{6}}=C^{Sym}_{\bar{6}\bar{6}} \tag{3.26}$$

In similar fashion, using Eq. (3.26) we obtain:

$$|((\mathbf{C}^{eff C_i} - \mathbf{C}^{Sym}) : \mathbf{A}) : \mathbf{A}| = (C^{eff}_{66} + C^{eff}_{\overline{66}} + C^{eff}_{\overline{66}} + C^{eff}_{\overline{66}} - 4C^{Sym}_{66})A^2_{12}| \tag{3.27}$$

i.e. the variational problem is equal to zero if we choose the function $C^{Sym}_{IJ} = \frac{C^{eff}_{IJ}+C^{eff}_{I\overline{J}}+C^{eff}_{\overline{I}J}+C^{eff}_{\overline{I}\overline{J}}}{4}$ for $I,J = 1,2,6$, where: $\{1,2,6,\overline{6}\} = \{11,22,12,21\}$.

Regarding the symmetrization approach and the related design of composite materials matching the symmetrized effective properties, we remark that the set of possible (symmetric) effective elasticity tensors of composites built from two materials with isotropic elasticity tensors has been studied in a number of papers, see e.g.[163] for a review. Additionally, if one restricts the analysis to mechanical metamaterials consisting of two phases, one of which being void, then microgeometries within the elementary cells can be found in [164]; these would be good candidates to design the metamaterial cloak. Conversely, it is possible to follow a different route avoiding the symmetrization and approximating the elasticity tensor without the minor-symmetries with chiral elastic metamaterials. However, the latter approach cannot achieve the required effective elasticity tensor over a finite bandwidth.

3.5 Numerical results and comparisons

We analyse the propagation of Rayleigh waves in a homogeneous half-space hosting a triangular or semi-circular shaped defect. For both configurations, the cloak mechanical parameters are obtained according to the geometrical transformation in Eq. (3.7) and Eqs. (3.11)-(3.14). For the numerical example, we consider a material density $\rho = 1600 kg/m^3$, shear and pressure velocities equal to $c_s = 300 m/s$ and $c_p = \sqrt{3}c_s$, respectively.

We introduce the following normalized quantities to ease and generalize the discussion of the

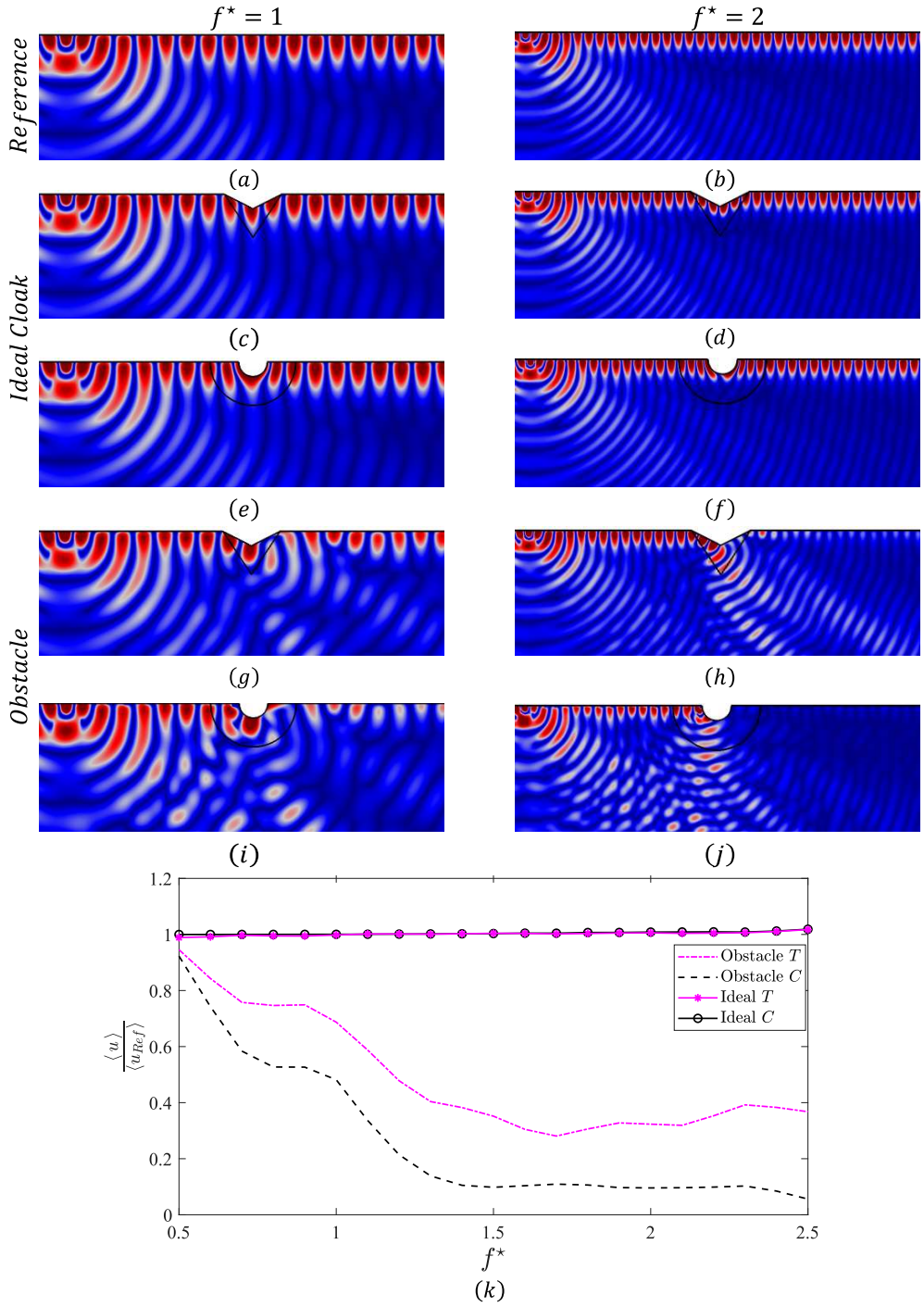

Fig. 3.2: Displacement fields for the Reference $(a)-(b)$, Ideal Cloak $(c)-(f)$ and Obstacle $(g)-(j)$ configurations, of the triangular T and the circular C_i type of cloaks, computed at frequencies $f^\star = [1, 2]$, respectively. (k) Performance of the ideal cloaks and the obstacle cases, computed by using the average of the total displacement of the transmitted field along the surface beyond the cloaked region.

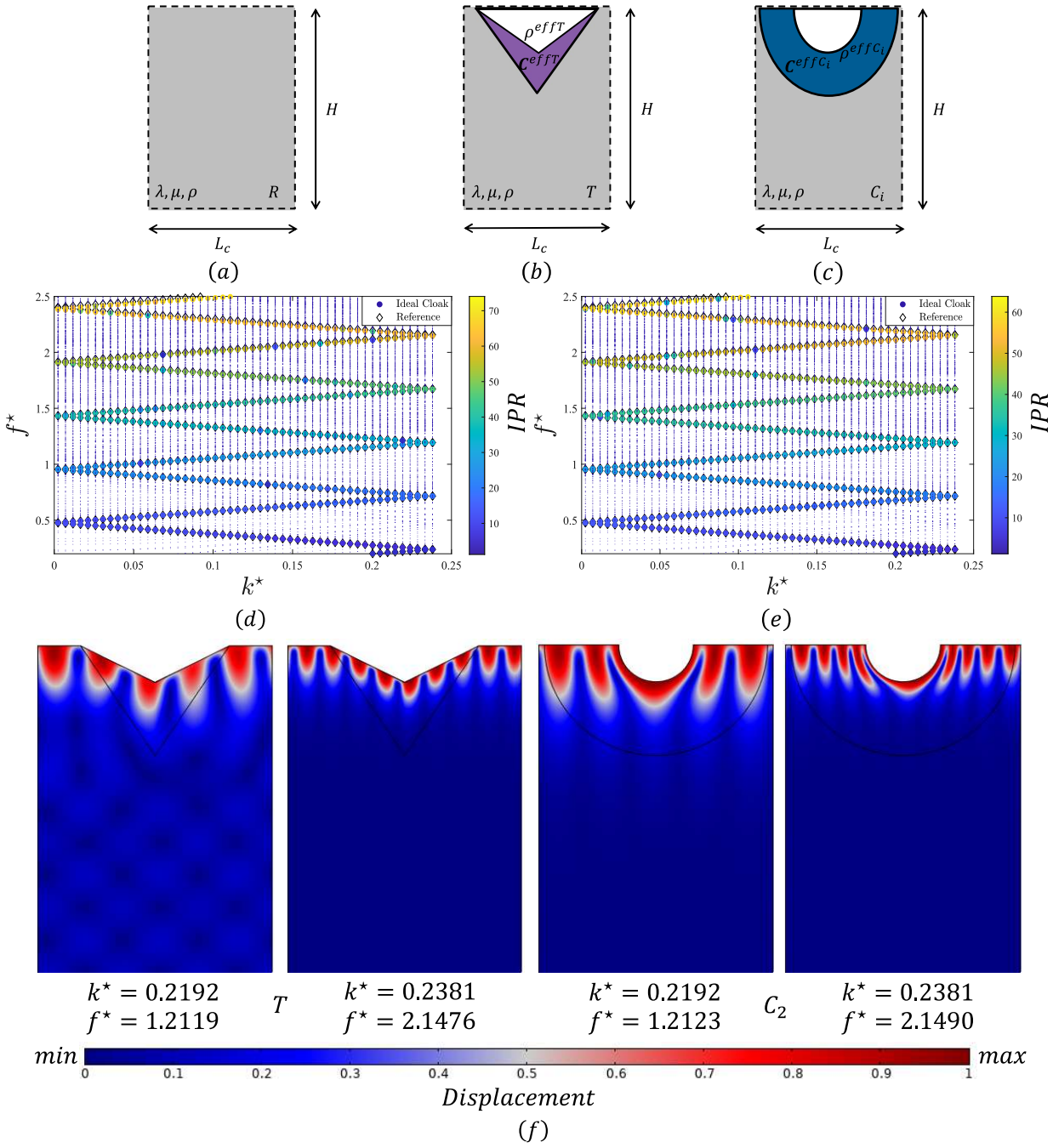

Fig. 3.3: Schematics of the unit cells for the reference R (*a*), triangular T (*b*) and circular C_i (*c*) cloak configurations, respectively. (*d*)-(*e*) Dispersion curves for the reference (diamond dots) and the ideal cloaks (contour circle dots) configurations, respectively. (*f*) Snapshots of surface modes displacement field, as obtained for the triangular T (left) and the circular C_2 (right) ideal cloaks, respectively.

results:

- Normalized wavelength $\lambda^\star = b$, so that $k^\star = \frac{2\pi}{\lambda^\star}$, i.e. we normalize with respect to a wavelength which is equal to the depth of the cloak.
- Normalized frequency $f^\star = \frac{c_R}{\lambda^\star}$, where c_R is Rayleigh wave velocity, which can be approximated by the following formula: $c_R = c_s \frac{0.826+1.14\nu}{1+\nu}$ where ν is the Poisson's ratio.

To assess the cloaking abilities, we perform time-harmonic simulation using the finite element software COMSOL Multiphysics. We begin by modeling a 2D domain of dimensions $W \times H$ (Fig. 3.1e). The dimensions of the model are chosen as $W = 12.5\lambda^\star$ and $H \approx 4.305\lambda^\star$.

The bottom of the half-space model is fixed, the surface is stress-free, and Perfectly Matched Layers are used to diminish reflections from the model boundaries. Rayleigh waves are generated by a surface point source located at $0.35W$ from the left edge of the model. The triangular-shaped inclusion has length $a = 0.0774H$ and width $2c = 0.309H$, and is surrounded by a cloak of related shape that extends along the depth of $b = 3a = 0.232H$. The semicircular defect has radius a and its adjoined cloak has radius b.

3.5.1 Ideal cloaks

We begin our investigation by analyzing the performance of the "Ideal Cloaks", namely domains with mechanical parameters defined according to the transformation in Eq. (3.5). Our aim is to verify that such Cosserat (non-symmetric) cloak can perfectly hide a surface defect from the propagation of Rayleigh waves in a broadband frequency range.

To this purpose, time-harmonic simulations are performed in order to compare the surface displacement field of the system in (i) the pristine configuration, i.e., the domain with no defect ("Reference"), (ii) the domain with the defect ("Obstacle"), and (iii) the domain with the cloaked defect

("Ideal Cloak"). In particular, we display the fields as computed for harmonic excitation at $f^* = [1, 2]$ in Fig. 3.2. The results for the pinched triangular T and semi-circular cloaks C_i at both selected frequencies verify that the displacement field of the reference configuration (Fig. 3.2(a) and (b)) is almost perfectly approximated by the case with the ideal (non-symmetric) cloak (Figs. 3.2(c) $-$ (f)), as the waves are smoothly detoured around the obstacle. The performance of the cloaks is better understood by comparing the cloaked wave fields with those obtained in the uncloaked scenarios (see Figs. 3.2(g) $-$ (j)). In the latter, scattering effects dominate the field around the cloak and lead to bulk mode conversion. To generalize these results, we calculate the normalized transmitted displacement field $\frac{\langle u \rangle}{\langle u_{Ref} \rangle}$, namely the ratio between the average surface displacement $\langle u \rangle$ computed beyond the obstacle for the ideal cloaks and the obstacle cases, and the same average displacement computed for the reference configuration $\langle u_{Ref} \rangle$. The results depicted in Fig. 3.2k indicate perfect performance of the ideal cloaks ($\frac{\langle u \rangle}{\langle u_{Ref} \rangle} \approx 1$), whereas the cases of a defect without the cloaking device are unable to provide adequate efficiency since the transmitted surface field is highly reduced compared to the reference.

For a more complete description of the capabilities of the cloak, we compare the dispersive properties of Rayleigh waves propagating along a homogeneous reference medium and along the cloaked setting. Here, our scope is to prove that a cloak with effective properties given by Eqs. (3.9) or (3.21) is able to fully duplicate the properties of the pristine homogeneous medium in a broadband range of frequencies. Thus, for both the triangular and semi-circular defects, we investigate a small portion (unit cell) of the 2D medium enclosing the analyzed cloaks. The unit cells have dimension $H \times L_c$ (see top of Figs. 3.3(a) $-$ (b)) and are modeled with FE using COMSOL Multiphysics. To obtain the dispersive properties of surface elastic waves propagating in such media, we impose fixed boundary conditions at the bottom surface of the cell, and Bloch boundary conditions along the x_1 direction. Note that, as in Ref.[141], the transformation for the triangular carpet cloak is invariant along the x_1 direction and thus the unit cell could be chosen accordingly by varying the wavenumber inside the

first Brillouin zone of interest, $k_{x_1} = [\frac{\pi}{100L_c}; \frac{\pi}{L_c}]$. In contrast, for radial transformations discussed in this work, a unit cell of dimension smaller than the dimension of the cloak ($L_c < r_o = b$) subjected to Bloch boundary conditions along the x_1 direction leads to overlapping transformation, In this regard, Meirbekova et. al.[161] recently showed that in such scenario discrepancies arise in the dispersive properties due to the intersection of the cloak with the boundary of the unit cell. Hence, to avoid this phenomenon, the unit cell must be at least the size of the cloak (we choose $L_c = 2.1r_o$). However, the above restriction on the dimension of the unit cell narrows the size of the first Brillouin zone (which is inversely proportional to the unit cell length) and forces the calculation of multiple modes (> 500) for each wavenumber to compute frequencies up to $f^\star = 2.5$. Among these, only a small portion of them represent waves confined at the surface (in particular, in a homogeneous medium, there exists only a Rayleigh mode). The problem is thus shifted into the collection/recognition of such surface modes among the plethora of wave solutions computed with a finite cell. For this purpose, we utilize the inverse participation ratio (IPR)[186,149,168,185,166], computed in terms of the displacements, according to the relation:

$$IPR = \frac{\iint_{\psi^\star} \|\mathbf{u}\|^4 \, dx_1 \, dx_2}{(\iint_{\psi^\star} \|\mathbf{u}\|^2 \, dx_1 \, dx_2)^2} |\psi^\star| \tag{3.28}$$

where we normalize the ratio by multiplying it with the area of the model $|\psi^\star|$ and $\|\mathbf{u}\| = \sqrt{u_1^2 + u_2^2}$ is the total displacement. The IPR has been used extensively in solid state physics to measure the localization of particles-atoms over a domain. In our context, the IPR measures the localization of the displacement field which will occur at the free-surface for the domain of interest; in practice, the larger the IPR the higher is the localization of the displacement field.

In particular, for our example, an IPR> 3.5 allows us to clearly distinguish surface modes from bulk ones. In Figs. $3.3(d) - (e)$ we display with colored dots (based on the IPR values) the surface wave modes traveling within the triangular and semicircular cloak, respectively. The remaining bulk

modes (IPR$<$ 3.5) are marked in the background by smaller gradually sized dots. The reader can appreciate the matching between Rayleigh modes within the cloaked domains and the Rayleigh solution within the reference field, which demonstrate the broadband cloaking capabilities of the analyzed non-symmetric cloaks. As an example, surface modes pertaining to two wavenumber solutions ($k^\star = [0.2192, 0.2381]$) for each of the T and C_2 cloaks are portrayed in Fig. 3.3*f*.

3.5.2 Symmetrized cloaks

In what follows, we delve into the behavior of symmetrized cloaks with triangular T and semi-circular C_i transformations. Our scope is to find which combination of symmetrization/cloak geometry provides the best cloaking performance. The displacement field of harmonic solutions for the symmetrized cloaks at frequencies $f^\star = [1, 2]$ are displayed in Figs. 3.4$(a)-(h)$. For $f^\star = 1$, all the investigated symmetric cloaks are unable to efficiently reroute the wavefield around the defect (see Figs. 3.4(a), (c), (e), (g)) and have a similar response with the "Obstacle" case (Figs. 3.2(g) and (i)). Conversely, at frequency $f^\star = 2$ the symmetric cloaks are able to better reroute the wavefield around the obstacle (see Figs. 3.4(b), (d), (f) and (h)). To quantify the performance of the cloak over a broader frequency range, we compute again the normalized average transmitted field $\frac{\langle u_{Sym} \rangle}{\langle u_{Ideal} \rangle}$ along the domain's surface after the cloak. Here, the surface displacement field is normalized by the field of the ideal case. The ratio $\frac{\langle u_{Sym} \rangle}{\langle u_{Ideal} \rangle}$ versus the frequency of excitation is reported in Fig. 3.4*i* for all the considered symmetric cloaks. For $f^\star = 0.5$, all cases have similar behavior, since the wavelength is too long compared to the dimension of the cloak. Furthermore, all the cloaks show a performance drop at around $f^\star = 1$, where the wavelength is equal to the size of the cloak. In particular, for the triangular inclusion, the uncloaked obstacle transmits more energy than symmetrized cloak until frequencies at around $f^\star = 1.4$. The poorer performance of the triangular-shaped cloak w.r.t. the circular ones, can be possibly attributed to the larger number of conditions (3) required for its symmetrization, as compared to the circular one (1), as shown in Eqs. (3.24) and (3.26). Better cloak efficacy is obtained in the higher frequency regime, i.e. when

$f^* > 1.5$, with a peak performance around $f^* = 2$. Overall, from Fig. 3.4*i*, it is clear that the C_2 transformation provides the best performance compared to C_1 and C_3. To better appreciate the above results, we replicate the dispersive analysis with unit cells consisting of symmetrized cloaks. The results are depicted in Fig. 3.5. It is evident that up to $f^* = 0.75$, the dispersive properties of the symmetrized cloak match the ones of the reference, since at those frequencies the wavelength is small compared to the dimension of the cloak. In addition, the C_2 transformation (Fig. 3.5*c*) shows the highest number of surface modes, 417 out of the 520 of the ideal case in Figs. 3.3(*d*) and (*e*), followed by 388 modes in the triangular pinched cloak T(Fig. 3.5*a*), 370 modes in C_1 (Fig. 3.5*b*) and 296 modes in C_3 (Fig. 3.5*d*) upon the same IPR value. This is a further indication of the better performance of the C_2 cloak. The reader can find examples of such localized surface modes obtained for symmetrized T and C_2 cloaks in Fig. 3.5*e*.

To further support the premise that the C_2 transformation presents better performance w.r.t. other ones, we notice that from Eqs. (3.21) and (3.26) the approximation of the symmetrized circular cloak depends on the ratio $D^{C_i} = \frac{F_{11}^{C_i}}{F_{22}^{C_i}}$. A value of $D^{C_i} = 1$ represents a scenario where the ideal tensor is symmetric, namely a scenario where symmetrization is not required. Note that, according to Milton et al[165] this cannot be achieved with our choice of gauge. Nonetheless we can rank the level of minor symmetry breaking introduced by the different transformation by using the ratio D^{C_i}.

Since D^{C_i} varies along the radial coordinate, we compute its mean value along the radial direction of the cloak as:

$$\langle D^{C_i} \rangle = \frac{1}{r_{cloak}} \int_{r_{cloak}} D^{C_i} dr \tag{3.29}$$

where $r_{cloak} = r_o - r_i = b - a$ is the radial length of the cloak. The results obtained for the 3 types of transformations C_i are collected in Table 3.1:

As expected, the D^{C_2} is higher than the analogous ratio computed for the linear C_1 and cubic transformation C_3, thus indicating a lower deterioration of the performance upon symmetrization.

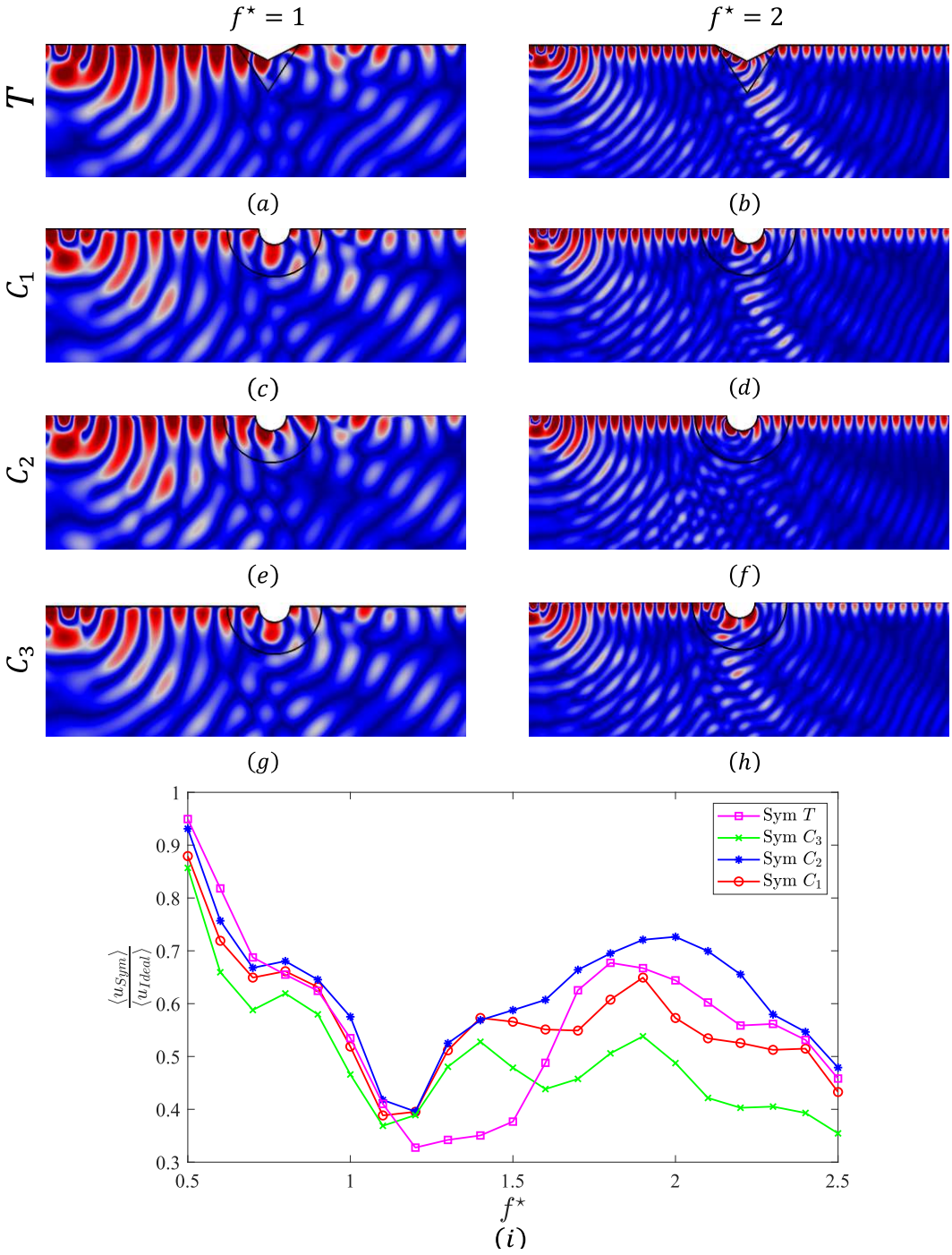

Fig. 3.4: Displacement field of the symmetrized cloaks for the T (a)-(b), C_1 (c)-(d), C_2 (e)-(f) and C_3 (g)-(h) class of transformations, computed at frequencies $f^\star = 1.5$ and $f^\star = 2$, respectively. (i) Performance of the cloaks using the ratio of the transmitted field of the symmetrized cloak over the ideal one, calculated at normalized frequencies $f^\star = [0.5 - 2.5]$.

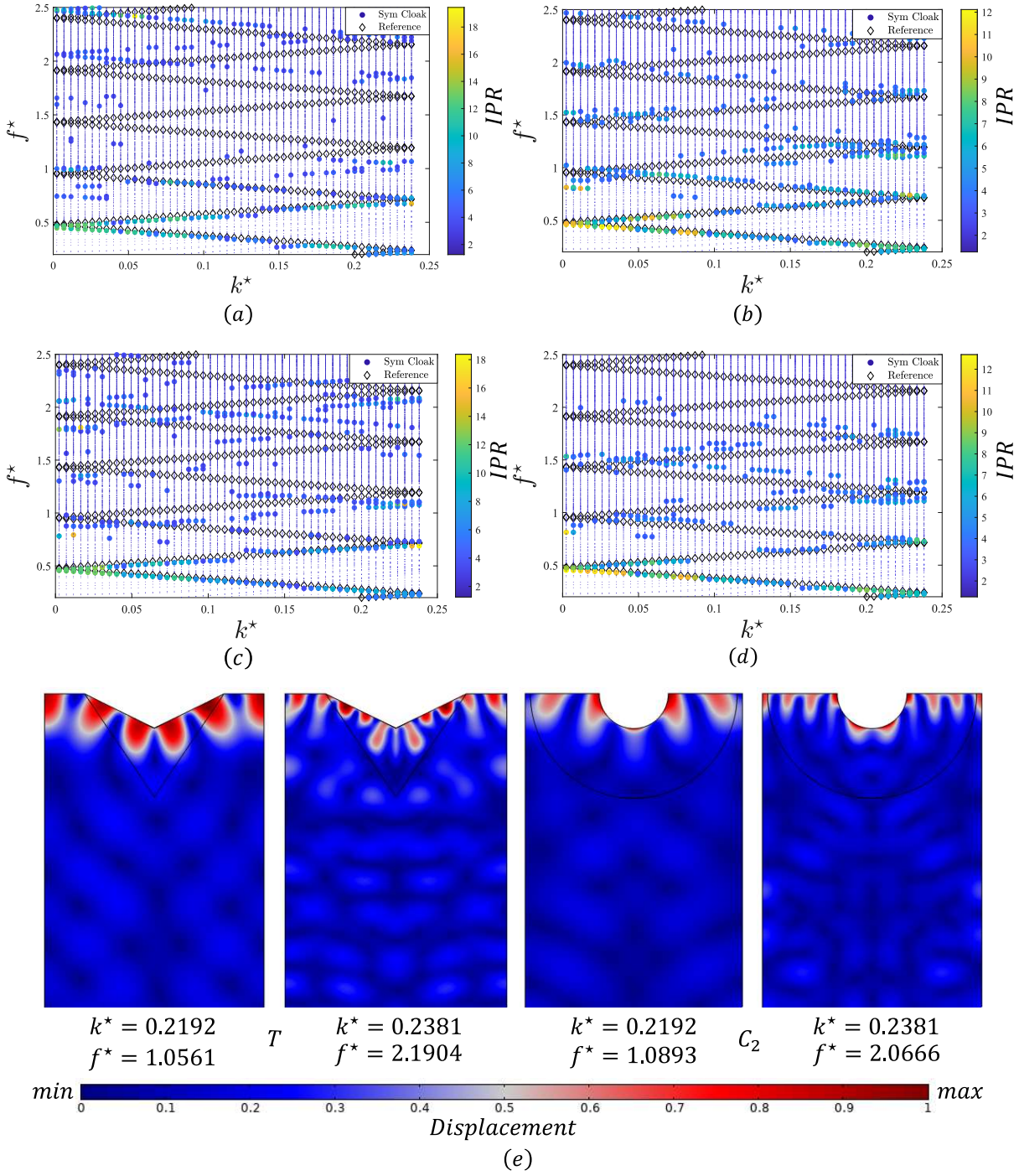

Fig. 3.5: Dispersion curves for the Triangular T (a) and Circular Symmetrized cloaks of C_1 (b), C_2 (c) and C_3 (d) type of transformation, respectively, as obtained from the IPR method. (e) Snapshots of particular surface modes of the displacement fields, as obtained for the triangular T (Left) and the Circular C_2 (Right) symmetrized cloaks, respectively.

Transformation	$\langle D^{C_i} \rangle$
C_1	0.45069
C_2	0.63
C_3	0.4527

Table 3.1: Average value of the ratio $\frac{F_{11}^{C_i}}{F_{22}^{C_i}}$ of each symmetrized circular cloak.

3.6 Conclusion

In this study, we investigated the cloaking of Rayleigh waves by means of cloaks with symmetrized elastic tensors. Since the Navier elastodynamic equation is not form-invariant for in-plane surface waves, we assumed a Cosserat gauge for the displacements to recover the form invariance of the governing equation. However, this step comes at the cost of demanding a material with effective properties that do not satisfy the minor symmetries of the elasticity tensor. For this reason, our strategy relied on the symmetrization of the elasticity tensor using the arithmetic mean. In particular, we examined the performance of cloaks with pinched triangular and semi-circular shapes, respectively. For the latter, we delved into 3 types of transformations: linear (C_1), quadratic (C_2) and cubic (C_3) and we compared their cloaking performance via FE harmonic simulations computing the normalized transmitted displacement field in each case. We found that a symmetrized semi-circular cloak obtained from a quadratic (C_2) transformation provided the best approximation of the ideal one. Additionally, we conducted dispersive analyses and employed the inverse participation ratio (IPR) as a tool to identify the surface modes among all the wave solutions. Again, we compared the results obtained for the ideal and the symmetrized scenarios and found that the C_2 transformation was able to support the propagation of the highest number of surface modes in comparison with all the other types of transformations. As a further proof, we discussed the value of the ratio D^{C_i} and addressed its connection with the performance of the symmetrized cloak by computing its mean value with respect to the pa-

rameter r. The results converged with the findings of the time-harmonic numerical simulations and the dispersive properties of the cloaks, concluding that the quadratic C_2 transformation displayed the best overall cloaking protection.

We stress that a classical homogenization procedure could be implemented to mimic the now symmetric, yet anisotropic behaviour of the cloaks via isotropic layered media, providing a feasible protection from incident Rayleigh waves. Finally, since experiments on elastodynamic cloaking are scarce and only recently Xianchen, et al.[189] made the first physical realization of a polar cloak that provided shielding from static loads, we hope this study could pave the way towards more experimental validation for cloaking from surface elastic waves.

3.7 Appendix A. Transformations with offset parameter ε.

In this section we present the so-called Kohn's transformation [156], which amounts to transforming the region $\varepsilon \leq R \leq R_o$ to the cloaking region $r_i \leq r \leq r_o$, where ε is a small positive number introduced to remove the singularity at the origin. In addition, for the C_1^{ε} type transformation we provide the more general scenario, which is parametric with respect to N:

$$\Xi^{C_1^{\varepsilon}(N)} : \begin{cases} r = \sqrt[N]{\frac{b^N - a^N}{b^N - \varepsilon^N} R^N + a^N - \varepsilon^N \frac{b^N - a^N}{b^N - \varepsilon^N}} & 0 \leq R \leq R_o \\ \theta = \Theta \end{cases} \tag{3.30}$$

Note that when $\varepsilon = 0$, for $N = 1$ in Eq. (3.30) we obtain the classical "Pendry" transformation of Eq. (3.11). The case of $N = 2$ has been used in [191,158] for cloaking of elastic plates and in [190] for cloaking of shallow water waves, and has the special property that its determinant $det(\mathbf{F}^{C_1})$ is constant.

In a similar fashion, the general C_2^ε type of transformation is given by:

$$\Xi^{C_2^\varepsilon}: \begin{cases} r = A_2^\varepsilon R^2 + A_1^\varepsilon R + A_0^\varepsilon \quad 0 \le R \le R_o \\ \theta = \Theta \end{cases} \tag{3.31}$$

where

$$A_2^\varepsilon = \frac{a-e}{(b-e)^2}, \quad A_1^\varepsilon = -\frac{2\,b\,(a-e)-(b-e)^2}{(b-e)^2}, \quad A_0^\varepsilon = \frac{b^2\,(a-e)}{(b-e)^2} \tag{3.32}$$

Finally the C_3^ε reads:

$$\Xi^{C_3^\varepsilon}: \begin{cases} r = B_3^\varepsilon R^3 + B_2^\varepsilon R^2 + B_1^\varepsilon R + B_0^\varepsilon \quad 0 \le R \le R_o \\ \theta = \Theta \end{cases} \tag{3.33}$$

where

$$B_3^\varepsilon = 2\frac{(a-\varepsilon)}{(b-e)^3}, \quad B_2^\varepsilon = \frac{3\,(b+\varepsilon)\,(\varepsilon-a)}{(b-\varepsilon)^3}, \quad B_1^\varepsilon = \frac{b^3-3\,b^2\,\varepsilon-3\,b\,\varepsilon^2+6\,a\,b\,\varepsilon-\varepsilon^3}{(b-\varepsilon)^3},$$
$$B_0^\varepsilon = \frac{b^2\,(a-\varepsilon)\,(b-3\,\varepsilon)}{(b-\varepsilon)^3}, \tag{3.34}$$

Note that when $\varepsilon = 0$, Eqs. (3.31)-(3.34) reduce to Eqs. (3.11)-(3.15).

References

[135] Barnwell, E. G., Parnell, W. J., & David Abrahams, I. (2016). Antiplane elastic wave propagation in pre-stressed periodic structures; tuning, band gap switching and invariance. *Wave Motion*, 63, 98–110.

[136] Brûlé, S., Javelaud, E. H., Enoch, S., & Guenneau, S. (2014). Experiments on seismic metamaterials: Molding surface waves. *Phys. Rev. Lett.*, 112, 133901.

[137] Brûlé, S., Javelaud, E. H., Enoch, S., & Guenneau, S. (2017). Flat lens effect on seismic waves propagation in the subsoil. *Scientific Reports*, 7, 2045–2322.

[138] Brun, M. & Guenneau, S. (2023). Transformation design of in-plane elastic cylindrical cloaks, concentrators and lenses. *Wave Motion*, (pp. 103124).

[139] Brun, M., Guenneau, S., & Movchan, A. B. (2009). Achieving control of in-plane elastic waves. *Applied Physics Letters*, 94(6), 061903.

[140] Chatzopoulos, Z., Palermo, A., Diatta, A., Guenneau, S., & Marzani, A. (2023). Cloaking rayleigh waves via symmetrized elastic tensors. *International Journal of Engineering Science*, 191, 103899.

[141] Chatzopoulos, Z., Palermo, A., Guenneau, S., & Marzani, A. (2022). Cloaking strategy for love waves. *Extreme Mechanics Letters*, 50, 101564.

[142] Chen, Y., Nassar, H., & Huang, G. (2021). Discrete transformation elasticity: An approach to design lattice-based polar metamaterials. *International Journal of Engineering Science*, 168, 103562.

[143] Colombi, A., Roux, P., Guenneau, S., Gueguen, P., & Craster, R. V. (2016). Forests as a natural seismic metamaterial: Rayleigh wave bandgaps induced by local resonances. *Scientific Reports*, 6, 2045–2322.

[144] Colombi, A., Zaccherini, R., Aguzzi, G., Palermo, A., & Chatzi, E. (2020). Mitigation of seismic waves: Metabarriers and metafoundations bench tested. *Journal of Sound and Vibration*, 485, 115537.

[145] Colquitt, D., Brun, M., Gei, M., Movchan, A., Movchan, N., & Jones, I. (2014). Transformation elastodynamics and cloaking for flexural waves. *Journal of the Mechanics and Physics of Solids*, 72, 131–143.

[146] Craster, R., Diatta, A., Guenneau, S., & Hutridurga, H. (2021). On near-cloaking for linear elasticity. *Multiscale Modeling and Simulation*, 19(2), 633–664.

[147] Diatta, A., Kadic, M., Wegener, M., & Guenneau, S. (2016). Scattering problems in elastodynamics. *Phys. Rev. B*, 94, 100105.

[148] Dubois, M., Etaix, N., Farhat, M., Enoch, S., Guenneau, S., Ing, R.-K., & Sebbah, P. (2012). Flat lens for Lamb waves focusing. In S. F. d'Acoustique (Ed.), *Acoustics 2012* Nantes, France.

[149] Evers, F. & Mirlin, A. D. (2000). Fluctuations of the inverse participation ratio at the anderson transition. *Phys. Rev. Lett.*, 84, 3690–3693.

[150] Farhat, M., Guenneau, S., & Enoch, S. (2009). Ultrabroadband elastic cloaking in thin plates. *Phys. Rev. Lett.*, 103, 024301.

[151] Frenzel, T., Kadic, M., & Wegener, M. (2017). Three-dimensional mechanical metamaterials with a twist. *Science*, 358(6366), 1072–1074.

[152] Huang, J. & Shi, Z. (2013). Attenuation zones of periodic pile barriers and its application in vibration reduction for plane waves. *Journal of Sound and Vibration*, 332(19), 4423–4439.

[153] Jin, Y., Pennec, Y., Bonello, B., Honarvar, H., Dobrzynski, L., Djafari-Rouhani, B., & Hussein, M. I. (2021). Physics of surface vibrational resonances: Pillared phononic crystals, metamaterials, and metasurfaces. *Reports on progress in physics*, 84(8), 086502.

[154] Kadic, M., Bückmann, T., Stenger, N., Thiel, M., & Wegener, M. (2012). On the practicability of pentamode mechanical metamaterials. *Applied Physics Letters*, 100(19), 191901.

[155] Khlopotin, A., Olsson, P., & Larsson, F. (2015). Transformational cloaking from seismic surface waves by micropolar metamaterials with finite couple stiffness. *Wave Motion*, 58, 53–67.

[156] Kohn, R. V., Lu, J., Schweizer, B., & Weinstein, M. I. (2014). A variational perspective on cloaking by anomalous localized resonance. *Communications in Mathematical Physics*, 328, 1432–0916.

[157] Liu, C.-X. & Yu, G.-L. (2022). Inverse design of locally resonant metabarrier by deep learning with a rule-based topology dataset. *Computer Methods in Applied Mechanics and Engineering*, 394, 114925.

[158] Liu, M. & Zhu, W. (2019). Nonlinear transformation-based broadband cloaking for flexural waves in elastic thin plates. *Journal of Sound and Vibration*, 445, 270–287.

[159] Liu, Z., Qin, K.-Q., & Yu, G.-L. (2020). Partially embedded gradient metabarrier: Broadband shielding from seismic rayleigh waves at ultralow frequencies. *Journal of Engineering Mechanics*, 146(5), 04020032.

[160] Maurel, A., Marigo, J.-J., Pham, K., & Guenneau, S. (2018). Conversion of love waves in a forest of trees. *Phys. Rev. B*, 98, 134311.

[161] Meirbekova, B. & Brun, M. (2020). Control of elastic shear waves by periodic geometric transformation: cloaking, high reflectivity and anomalous resonances. *Journal of the Mechanics and Physics of Solids*, 137, 103816.

[162] Meng, L., Cheng, Z., & Shi, Z. (2020). Vibration mitigation in saturated soil by periodic pile barriers. *Computers and Geotechnics*, 117, 103251.

[163] Milton, G. W. (2002). *The theory of composites*. Cambridge university press.

[164] Milton, G. W., Briane, M., & Harutyunyan, D. (2017). On the possible effective elasticity tensors of 2-dimensional and 3-dimensional printed materials. *Mathematics and Mechanics of Complex Systems*, 5, 4194.

[165] Milton, G. W., Briane, M., & Willis, J. R. (2006). On cloaking for elasticity and physical equations with a transformation invariant form. *New Journal of Physics*, 8(10), 248–248.

[166] Monthus, C. & Garel, T. (2010). Anderson localization of phonons in dimension $d = 1, 2, 3$: Finite-size properties of the inverse participation ratios of eigenstates. *Phys. Rev. B*, 81, 224208.

[167] Muhammad, Lim, C., & Kamil Żur, K. (2021). Wide rayleigh waves bandgap engineered metabarriers for ground born vibration attenuation. *Engineering Structures*, 246, 113019.

[168] Murphy, N. C., Wortis, R., & Atkinson, W. A. (2011). Generalized inverse participation ratio as a possible measure of localization for interacting systems. *Phys. Rev. B*, 83, 184206.

[169] Nassar, H., Chen, Y., & Huang, G. (2019). Isotropic polar solids for conformal transformation elasticity and cloaking. *Journal of the Mechanics and Physics of Solids*, 129, 229–243.

[170] Nassar, H., Chen, Y. Y., & Huang, G. L. (2018). A degenerate polar lattice for cloaking in full two-dimensional elastodynamics and statics. *Proceedings of the Royal Society A: Mathematical, Physical and Engineering Sciences*, 474(2219), 20180523.

[171] Nassar, H., Chen, Y. Y., & Huang, G. L. (2020). Polar metamaterials: A new outlook on resonance for cloaking applications. *Phys. Rev. Lett.*, 124, 084301.

[172] Norris, A. & Shuvalov, A. (2011). Elastic cloaking theory. *Wave Motion*, 48(6), 525–538. Special Issue on Cloaking of Wave Motion.

[173] Norris, A. N. & Parnell, W. J. (2012). Hyperelastic cloaking theory: transformation elasticity with pre-stressed solids. *Proceedings of the Royal Society A: Mathematical, Physical and Engineering Sciences*, 468(2146), 2881–2903.

[174] Palermo, A., Krödel, S., Matlack, K. H., Zaccherini, R., Dertimanis, V. K., Chatzi, E. N., Marzani, A., & Daraio, C. (2018). Hybridization of guided surface acoustic modes in unconsolidated granular media by a resonant metasurface. *Physical Review Applied*, 9(5), 054026.

[175] Palermo, A., Krödel, S., Marzani, A., & Daraio, C. (2016). Engineered metabarrier as shield from seismic surface waves. *Scientific Reports*, 6, 2045–2322.

[176] Palermo, Antonio Marzani, A. (2018). Control of love waves by resonant metasurfaces. *Scientific Reports*, 8, 7234.

[177] Parnell, W. J. (2012). Nonlinear pre-stress for cloaking from antiplane elastic waves. *Proceedings of the Royal Society A: Mathematical, Physical and Engineering Sciences*, 468(2138), 563–580.

[178] Parnell, W. J. & Shearer, T. (2013). Antiplane elastic wave cloaking using metamaterials, homogenization and hyperelasticity. *Wave Motion*, 50(7), 1140–1152. Advanced Modelling of Wave Propagation in Solids.

[179] Pu, X. & Shi, Z. (2018). Surface-wave attenuation by periodic pile barriers in layered soils. *Construction and Building Materials*, 180, 177–187.

[180] Pu, X. & Shi, Z. (2019). Periodic pile barriers for rayleigh wave isolation in a poroelastic half-space. *Soil Dynamics and Earthquake Engineering*, 121, 75–86.

[181] Quadrelli, D. E., Craster, R., Kadic, M., & Braghin, F. (2021). Elastic wave near-cloaking. *Extreme Mechanics Letters*, 44, 101262.

[182] Sklan, S. R., Pak, R. Y. S., & Li, B. (2018). Seismic invisibility: elastic wave cloaking via symmetrized transformation media. *New Journal of Physics*, 20(6), 063013.

[183] Stenger, N., Wilhelm, M., & Wegener, M. (2012). Experiments on elastic cloaking in thin plates. *Phys. Rev. Lett.*, 108, 014301.

[184] Tang, K., Luz, E., Amram, D., Kadysz, L., Guenneau, S., & Sebbah, P. (2023). Dynamic cloaking of a diamond-shaped hole in elastic plate. *Applied Physics Letters*, 122(1), 011701.

[185] Tsukerman, E. (2017). Inverse participation ratios in the xx spin chain. *Phys. Rev. B*, 95, 115121.

[186] Wegner, F. (1980). Inverse participation ratio in $2+\varepsilon$ dimensions. *Zeitschrift für Physik B Condensed Matter*, 36, 270–287.

[187] Wu, Q. & Huang, G. (2022). Omnidirectional wave polarization manipulation in isotropic polar solids. *International Journal of Solids and Structures*, 241, 111481.

[188] Xiang, Z. & Yao, R. (2016). Realizing the willis equations with pre-stresses. *Journal of the Mechanics and Physics of Solids*, 87, 1–6.

[189] Xu, X., Wang, C., Shou, W., Du, Z., Chen, Y., Li, B., Matusik, W., Hussein, N., & Huang, G. (2020). Physical realization of elastic cloaking with a polar material. *Phys. Rev. Lett.*, 124, 114301.

[190] Zareei, A. & Alam, M.-R. (2015). Cloaking in shallow-water waves via nonlinear medium transformation. *Journal of Fluid Mechanics*, 778, 273–287.

[191] Zareei, A. & Alam, M.-R. (2017). Broadband cloaking of flexural waves. *Phys. Rev. E*, 95, 063002.

[192] Zhang, H., Chen, Y., Liu, X., & Hu, G. (2020). An asymmetric elastic metamaterial model for elastic wave cloaking. *Journal of the Mechanics and Physics of Solids*, 135, 103796.

[193] Zhang, P. & Parnell, W. J. (2018). Hyperelastic antiplane ground cloaking. *The Journal of the Acoustical Society of America*, 143(5), 2878–2885.

[194] Zhao, S., Chen, J., Chang, Z., & Huang, G. (2023). Microstructure realization of a lattice-based polar solid for arbitrary elastic waveguiding. *Journal of the Mechanics and Physics of Solids*, 173, 105226.

4

3-D Elastic cloaking

In this Chapter, we propose a design for cloaking Rayleigh and Love surface waves, extending the results of Chapters 2 & 3. To such purpose, we utilize the invariance of the Navier elastodynamic equation under geometric transform by assuming identical displacements in original and transformed media (Cosserat gauge). In particular, we apply transformational elastodynamics to obtain the requisite mechanical properties for a 3-D prismatic and cylindrical carpet cloak of triangular and semi-circular cross section, respectively. By comparing the formulated 3-D elastic cloaking problem with

the superposition of the in-plane (Rayleigh) and out-of-plane (Love) cases, it reveals an extra set of elasticity components and additional broken symmetries of the elasticity tensor. Dispersion analysis and time-harmonic simulations are conducted to validate the performance of the cloak characterized by an elasticity tensor without minor symmetries (Cosserat medium). Finally, an original symmetrization technique of the elasticity tensor is applied, driven by the weak form solution of Love waves and the concept of generalized mean, to approximate the anisotropic and chiral properties of the cloak by isotropic Cauchy materials.

4.1 Introduction

Rayleigh and Love waves are elastic waves that propagate over the free surface of an elastic half-space. In stratified or heterogeneous media both types of waves are characterized by a dispersive nature where their velocity becomes dependent on the wavelength. The concept of bending these surface waves around an object (so-called cloaking) has been of major interest due to its ample applications in engineering. In particular, Rayleigh and Love waves are the predominant surface waves ignited upon an earthquake event. As a result, they can cause damages to structures placed on the earth surface. Thus, having the possibility to cloak targets from them would be a tremendous advancement towards seismic protection. Additionally, due to their proximity to the surface, these waves are easily generated and measured, thus finding applications in non-destructive testing and source identification [245,246,214].

The notion of invisibility has been a subject of profound research in recent years. Pioneering contributions by Pendry et al. [238] and Leonhart [222] established theoretical frameworks for cloaking electromagnetic waves, building upon the invariance of Maxwell's equations under arbitrary coordinate transformations [248]. Consequently, similar techniques were also applied in transformations optics [216,217,219,199,223,205], thermodynamics [251,232,218,242,252,200,241], cloaks for water waves [253,257,231,247] and acoustics [234,210,203]. However, in the context of elasticity Milton et al. [225] found that the Navier

elastodynamic equations are not form invariant under an arbitrary curvilinear transformation and are mapped to a more general system with non-scalar density and additional third-order tensors. As a result, all three components of the elastic waves are fully coupled in the transformed medium, making the cloaking problem in elasticity significantly more challenging than in optics or acoustics. Brun et al.[197] observed that choosing an identity map to connect the displacement fields (gauge) allows the Navier equation to retain its form invariance. However, this choice breaks the minor symmetries of the transformed elasticity tensor resulting in a so called Cosserat material form. Further contributions by Norris et al.[233] extended these ideas by deriving a more general system of transformed equations, dependent on both the transformation and the choice of gauge. Notably, the transformed equations can either take the form of Willis, where the elastic stress is symmetric but involves third-order tensors, or Cosserat, where the transformed equations maintain their structure but include non-symmetric constitutive relations. Hence, both scenarios impose significant constraints on realizing a 3-D elastodynamic cloak.

An interesting approach to address these challenge involves the direct architecture of lattice-based Cosserat or micropolar metamaterials[229,230,228,204,256,250,254] which can establish the necessary non-symmetric behavior by introducing an additional rotational degree of freedom or by applying symmetrization techniques to the elasticity tensor[212,243,208]. In similar fashion, mechanical cloaking designs enforcing direct lattice transformation have also shown promising cloaking applications[198,240,220]. Notably, an alternative technique pertains to the use of non-linear elastic pre-stress in hyperelastic materials[236,237,195,235,255].

While considerable research has been dedicated to cloaking of elastic waves, there exists a significant gap in exploring applications related to elastic surface waves. In the context of Love waves, some authors of this work investigated cloaking designs by means of transformational elastodynamics[202]. On the other hand, studies related to cloaking of Rayleigh waves include concealing of an embedded cylinder[221] or a triangular-shaped defect[204] incorporating micropolar elasticity or applying near-

cloaking techniques under quasi conformal mappings to uncouple the elastic wave potentials[239]. Recently, a near-cloaking strategy for Rayleigh waves was developed built upon the symmetrization of the elasticity tensor by using materials of classical symmetry and providing efficient cloaking performance[201]. However, none of the above works directly explore the potential for creating 3-D cloaks to effectively redirect both Rayleigh and Love waves around an object of interest. In contrast, a 3D acoustic cloak has been well understood and analyzed in numerous recent studies[203,209,226]. In this study, we explore such possibility and by assuming cylindrical symmetry we develop 3-D triangular and semi-circular carpet cloaks.

We structure our manuscript as follows: First we revisit the Navier equations concerning both the reference and the transformed semi-infinite layered media. By employing a Cosserat kinematic relation, we restore the form invariance of the transformed equation of motion and achieve the necessary non-symmetric mechanical properties for cloaking. The design involves applying cylindrical analogues of 2-D transformations studied in earlier works, with triangular and semi-circular cross-sections.

Remarkably, the 3-D problem differs from superimposing Love and Rayleigh waves due to its requirement for a heterogeneous system, as Love waves propagate exclusively in layered media, resulting in dispersive Rayleigh waves. By comparing the weak formulation of the 3-D equation with separate weak forms of Love and Rayleigh waves reveals additional coefficients in the transformed elasticity tensor. In addition, the symmetrization of the elasticity tensor impacts the effective shear moduli which is crucial for cloaking Love waves, a phenomenon absent in[202] due to the scalar Helmholtz equation's transformation lacking non-symmetric properties. To address this, we introduce a new symmetrization strategy, aligning symmetric coefficients with the weak-form solution of Love waves and symmetrizing the rest using the generalized mean. This approach seeks the optimal combination of symmetrization and cloak geometry for efficient cloaking.

To validate our designs, we perform time-harmonic simulations and dispersion analyses, compar-

ing the wave fields of cylindrical cloaks with pinched triangular and semi-circular cross-sections, under different symmetrization schemes and angles of incidence. In particular, we examine the transmitted displacement fields after the cloak and measure the scattering ratio of symmetrized and ideal cases. Next, the dispersive analysis employs a 3-D version of inverse participation ratio (IPR) used in[201] to recognize the localization level of the displacement fields, enabling the identification and counting of surface modes. Our findings indicate that a symmetrized semi-circular cylindrical cloak, using the "Maximal" mean, offers substantial cloaking protection across all tested frequencies compared to other designs.

4.2 Governing Equations

We consider a homogeneous, isotropic elastic layer of thickness h_1 and material properties $(\lambda_1, \mu_1, \rho_1)$ coupled to a semi-infinite medium with properties $(\lambda_2, \mu_2, \rho_2)$ where λ_i and μ_i are the Lamé coefficients and ρ_i the mass densities and the spatial coordinates for the reference domain are $\mathbf{X} = (X_1, X_2, X_3)$. The layered medium presents a surface defect that extends within the thickness of the upper layer. Then, the governing Navier elastodynamic equation reads:

$$\nabla_X \cdot \mathbf{C}^i : \nabla_X \mathbf{U}_i = \rho_i \mathbf{U}_{i,tt} \tag{4.1}$$

where $\mathbf{C}^i$ is the isotropic 2nd order elasticity tensor, $\mathbf{U}_i$ is the displacement and $\mathbf{U}_{i,tt}$ denotes the second order derivative in time of $\mathbf{U}$ of the layer ($i = 1$) and the semi-infinite medium ($i = 2$), respectively.

Following the cloaking strategy by[225,233] as in Chapters 2 & 3 and assuming $\mathbf{U} = \mathbf{u}$ (Cosserat gauge) for the displacements[197,211], we derive the governing equation in the transformed coordinate

system $\mathbf{x} = (x_1, x_2, x_3)$ as:

$$\nabla_x \cdot \mathbf{C}^{eff} : \nabla_x \mathbf{u}_i = \rho_i^{eff} \mathbf{u}_{i,tt} \tag{4.2}$$

where

$$\begin{aligned} C_{ijkl}^{eff} &= J^{-1} C_{IjKl} F_{iI} F_{kK} \\ \rho^{eff} &= \rho J^{-1} \end{aligned} \tag{4.3}$$

are the transformed mechanical parameters of the cloaked region on Einstein summation, $F = \nabla_X x$ is the deformation gradient and $J = det(F)$ its determinant.

4.2.1 Prismatic triangular carpet cloak

Let us consider a triangular carpet cloak, as the one in Figs. 4.1(a) and (b). For such configuration, we apply a prismatic $(x_3 = X_3)$ coordinate transformation $\Xi^P(\boldsymbol{X} \rightarrow \boldsymbol{x})$ as:

$$\Xi^P : \begin{cases} x_1 = X_1 \\ x_2 = (\frac{z_2(X_1) - z_1(X_1)}{z_2(X_1)}) X_2 + z_1(X_1) \\ x_3 = X_3 \end{cases} \tag{4.4}$$

stretching the field between $z = 0$ and $z = z_1(X_1)$ of the reference domain into the region between the curves $z_1(x_1)$ and $z_2(x_1)$ of the transformed domain (blue region). The Jacobian of the transformation in Cartesian coordinates is:

$$\mathbf{F}^T = \begin{bmatrix} \frac{\partial x_1}{\partial X_1} & \frac{\partial x_1}{\partial X_2} & \frac{\partial x_1}{\partial X_3} \\ \frac{\partial x_2}{\partial X_1} & \frac{\partial x_2}{\partial X_2} & \frac{\partial x_2}{\partial X_3} \\ \frac{\partial x_3}{\partial X_1} & \frac{\partial x_3}{\partial X_2} & \frac{\partial x_3}{\partial X_3} \end{bmatrix} = \begin{bmatrix} 1 & 0 & 0 \\ F_{21}^P & F_{22}^P & 0 \\ 0 & 0 & 1 \end{bmatrix} \tag{4.5}$$

where $F_{21}^p = sign(x_1)\frac{a}{c}$ and $F_{22}^p = det(\mathbf{F}^T) = \frac{b-a}{b}$ with a, b, c representing the geometric parameters of the pinched triangular cloak introduced in Chapters 1 & 2 Adopting the augmented Voigt notation for the 3-D problem as $\{1, 2, 3, 4, \overline{4}, 5, \overline{5}, 6, \overline{6}\} = \{11, 22, 33, 23, 32, 31, 13, 12, 21\}$, the transformed elastic tensor and material density properties within the cloak domain reads:

$$\mathbf{C}_{IJ}^{effP} = \begin{bmatrix} \frac{\lambda+2\mu}{F_{22}^p} & \lambda & \frac{\lambda}{F_{22}^p} & 0 & 0 & 0 & 0 & 0 & \frac{F_{21}^p}{F_{22}^p}(\lambda+2\mu) \\ \lambda & \frac{(F_{21}^p)^2\mu+(F_{22}^p)^2(\lambda+2\mu)}{F_{22}^p} & \lambda & 0 & 0 & 0 & 0 & \frac{F_{21}^p}{F_{22}^p}\mu & F_{21}^p(\lambda+\mu) \\ \frac{\lambda}{F_{22}^p} & \lambda & \frac{\lambda+2\mu}{F_{22}^p} & 0 & 0 & 0 & 0 & 0 & \frac{F_{21}^p}{F_{22}^p}\lambda \\ 0 & 0 & 0 & \frac{(F_{21}^p)^2\mu+(F_{22}^p)^2\mu}{F_{22}^p} & \mu & \frac{F_{21}^p}{F_{22}^p}\mu & \frac{F_{21}^p}{F_{22}^p}\mu & 0 & 0 \\ 0 & 0 & 0 & \mu & \frac{\mu}{F_{22}^p} & 0 & 0 & 0 & 0 \\ 0 & 0 & 0 & \frac{F_{21}^p}{F_{22}^p}\mu & 0 & \frac{\mu}{F_{22}^p} & \frac{\mu}{F_{22}^p} & 0 & 0 \\ 0 & 0 & 0 & \frac{F_{21}^p}{F_{22}^p}\mu & 0 & \frac{\mu}{F_{22}^p} & \frac{\mu}{F_{22}^p} & 0 & 0 \\ 0 & \frac{F_{21}^p}{F_{22}^p}\mu & 0 & 0 & 0 & 0 & 0 & \frac{\mu}{F_{22}} & \mu \\ \frac{F_{21}^p}{F_{22}^p}(\lambda+2\mu) & F_{21}^p(\lambda+\mu) & \frac{F_{21}^p}{F_{22}^p}\lambda & 0 & 0 & 0 & 0 & \mu & \frac{(F_{21}^p)^2(\lambda+2\mu)+(F_{22}^p)^2\mu}{F_{22}^p} \end{bmatrix} \tag{4.6}$$

$$\rho^{effP} = \rho(F_{22}^p)^{-1} \tag{4.7}$$

As shown in the previous Chapters, the effective properties of the triangular pinched cloak consist of homogeneous non-symmetric components of the elasticity tensor and constant effective density. In particular, it has 5 non-symmetric entries (instead of 3 in the plain strain problem), which in the

augmented 3D Voigt notation read:

$$\begin{cases} C_{16}^{effP} \neq C_{1\overline{6}}^{effP} \\ C_{26}^{effP} \neq C_{2\overline{6}}^{effP} \\ C_{36}^{effP} \neq C_{3\overline{6}}^{effP} \\ C_{44}^{effP} \neq C_{4\overline{4}}^{effP} \neq C_{\overline{4}\overline{4}}^{effP} \\ C_{45}^{effP} = C_{4\overline{5}}^{effP} \neq C_{\overline{4}5}^{effP} = C_{\overline{4}\overline{5}}^{effP} \\ C_{66}^{effP} \neq C_{6\overline{6}}^{effP} \neq C_{\overline{6}\overline{6}}^{effP} \end{cases} \tag{4.8}$$

4.2.2 Cylindrical circular carpet cloak

In the same vein, we formulate the scenario of a cylindrical semi-circular cloak located at the free-surface. We introduce a set of cylindrical polar coordinates centered at the cloaked region ($\mathbf{X} = \{R, \Theta, X_3\}, \mathbf{x} = \{r, \theta, x_3\}$) centered within the cloaked domain, where $R = \sqrt{{X_1}^2 + {X_2}^2}$, $r = \sqrt{{x_1}^2 + {x_2}^2}$, $\Theta = \arctan \frac{X_2}{X_1}[\pi]$ and $\theta = \arctan \frac{x_2}{x_1}[\pi]$.

For such a configuration, we utilize the 3-D cylindrical extension of radial quadratic transformation that was used for the case of Rayleigh waves in Chapter 2 as $\Xi^C \equiv \Xi^{C_2} : (R, \Theta, X_3) \rightarrow (r, \theta, x_3)$ that maps the origin (0,0) of the reference system onto an inner cylinder of radius $r_i = a$ in the physical one, and the outer cylinder $R_o = r_o = b$ to itself (see Figs. 4.1(c) and (d)):

$$\Xi^{C_2} : \begin{cases} r = A_2 R^2 + A_1 R + A_0 \quad 0 \leq R \leq R_o \\ \theta = \Theta \\ x_3 = X_3 \end{cases} \tag{4.9}$$

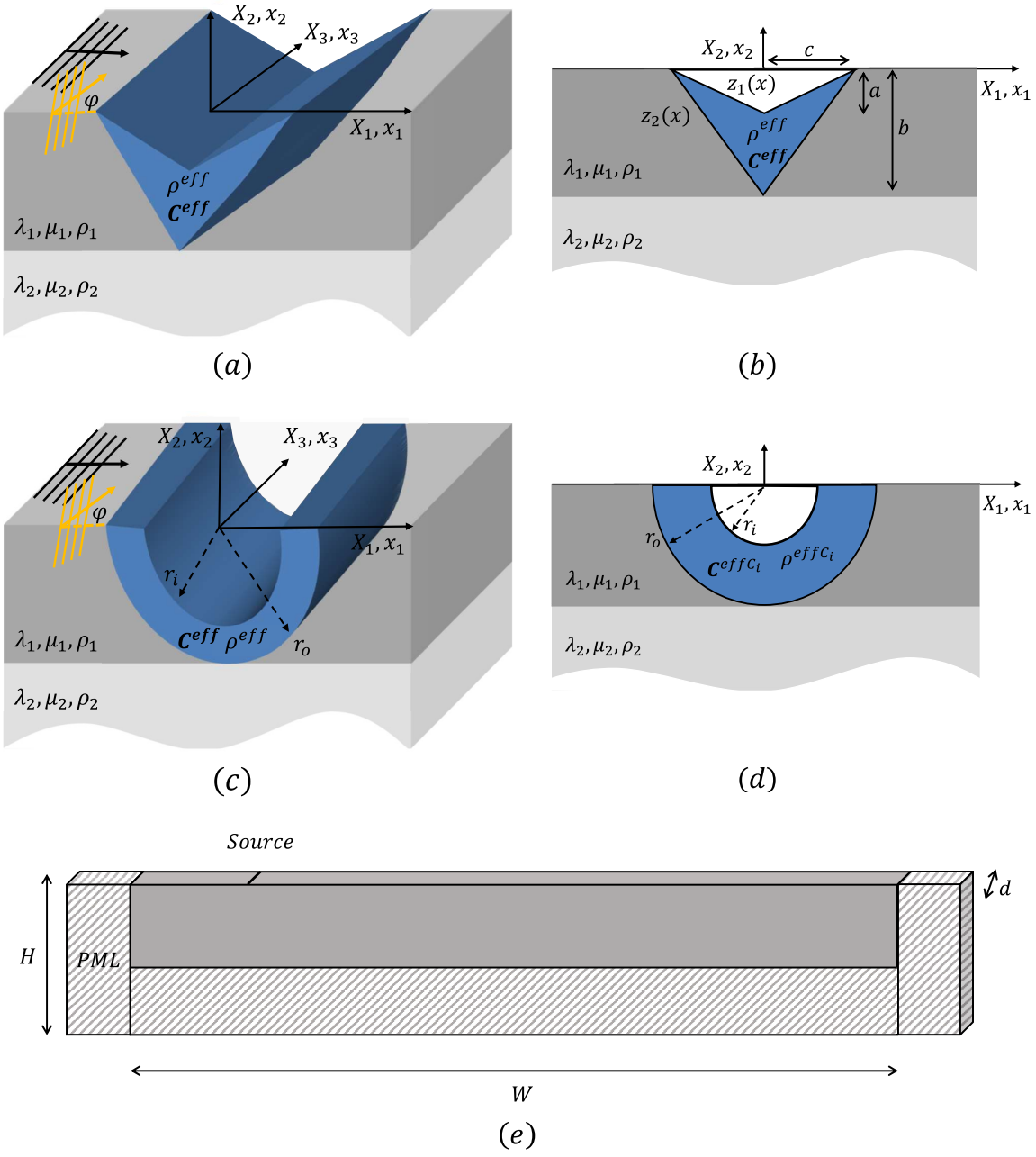

Fig. 4.1: (a) 3-D Schematic of a triangular carpet-pinched cylindrical cloak. (b) In-plane ($X_3 = 0$) model representation. (c) 3-D Schematic of a semi-circular carpet cylindrical cloak. (d) In-plane ($X_3 = 0$) model representation.

where:

$$A_2 = \frac{a}{b^2}, \quad A_1 = \frac{b-2a}{b}, \quad A_0 = a. \tag{4.10}$$

Now, the Jacobian of such transformation becomes:

$$\mathbf{F}^{C_2} = \begin{bmatrix} F_{11}^{C_2} & 0 & 0 \\ 0 & F_{22}^{C_2} & 0 \\ 0 & 0 & 1 \end{bmatrix} \tag{4.11}$$

Using the augmented Voigt notation for the 3-D problem in polar cylindrical coordinates: $\{1, 2, 3, 4, \overline{4}, 5, \overline{5}, 6, \overline{6}\} = \{rr, \theta\theta, x_3x_3, \theta x_3, x_3\theta, x_3r, rx_3, r\theta, \theta r\} =$

$\{11, 22, 33, 23, 32, 31, 13, 12, 21\}$, we obtain the following effective properties:

$$\mathbf{C}_{IJ}^{effC_2} = \begin{bmatrix} \frac{F_{11}^{C_2}}{F_{22}^{C_2}}(\lambda+2\mu) & \lambda & \frac{\lambda}{F_{22}^{C_2}} & 0 & 0 & 0 & 0 & 0 & 0 \\ \lambda & \frac{F_{22}^{C_2}}{F_{11}^{C_2}}(\lambda+2\mu) & \frac{\lambda}{F_{11}^{C_2}} & 0 & 0 & 0 & 0 & 0 & 0 \\ \frac{\lambda}{F_{22}^{C_2}} & \frac{\lambda}{F_{11}^{C_2}} & \frac{\lambda+2\mu}{F_{11}^{C_2}F_{22}^{C_2}} & 0 & 0 & 0 & 0 & 0 & 0 \\ 0 & 0 & 0 & \frac{F_{22}^{C_2}}{F_{11}^{C_2}}\mu & \frac{\mu}{F_{11}^{C_2}} & 0 & 0 & 0 & 0 \\ 0 & 0 & 0 & \frac{\mu}{F_{11}^{C_2}} & \frac{\mu}{F_{11}^{C_2}F_{22}^{C_2}} & 0 & 0 & 0 & 0 \\ 0 & 0 & 0 & 0 & 0 & \frac{\mu}{F_{11}^{C_2}F_{22}^{C_2}} & \frac{\mu}{F_{22}^{C_2}} & 0 & 0 \\ 0 & 0 & 0 & 0 & 0 & \frac{\mu}{F_{22}^{C_2}} & \frac{F_{11}^{C_2}}{F_{22}^{C_2}}\mu & 0 & 0 \\ 0 & 0 & 0 & 0 & 0 & 0 & 0 & \frac{F_{11}^{C_2}}{F_{22}^{C_2}}\mu & \mu \\ 0 & 0 & 0 & 0 & 0 & 0 & 0 & \mu & \frac{F_{22}^{C_2}}{F_{11}^{C_2}}\mu \end{bmatrix}, \tag{4.12}$$

$$\rho^{effC_2} = \frac{\rho}{det(\mathbf{F}^{C_2})} \tag{4.13}$$

for $I,J = \{1, 2, 3, 4, \bar{4}, 5, \bar{5}, 6, \bar{6}\}$. Again, the elastic tensor presents 3 sets non-symmetric components (instead of only 1 for the plain strain problem):

$$\begin{cases} C_{44}^{effC_2} \neq C_{4\bar{4}}^{effC_2} \neq C_{\bar{4}\bar{4}}^{effC_2} \\ C_{55}^{effC_2} \neq C_{5\bar{5}}^{effC_2} \neq C_{\bar{5}\bar{5}}^{effC_2} \\ C_{66}^{effC_2} \neq C_{6\bar{6}}^{effC_2} \neq C_{\bar{6}\bar{6}}^{effC_2} \end{cases} \tag{4.14}$$

Similarly with the separate cases of Love and Rayleigh waves in Chapters 2 & 3, respectively, the problem of 3-D cloaking is now shifted on finding the required materials to approximate the coefficients of the effective elastic tensor and the density. In particular, the effective parameters of the elasticity tensor are described by an anisotropic behaviour that is required to cloak incident Love waves as well as anisotropic and non-minor symmetric for the in-plane case of Rayleigh waves. We have already discussed the challenges to fabricate such materials in the in-plane scenario. Although micropolar metamaterials have been a proper candidate by exhibit such non-symmetries of the elasticity tensor[229,230,228], their mechanical instabilities (such as zero-modes) posses a major constrain towards their feasibility. In addition, the extension from a 2-D to a 3-D chiral metamaterial to support both Love and Rayleigh waves is not always straightforward as extra set of anisotropicities and non-symmetries will arise. This is further analyzed in the next section. Notably, Golgoon et al.[215] rigorously formulated the problem of elastic cloaking using principles of differential geometry. The authors showed that, in fact, elastodynamic cloaking in 2-D or 3-D in the general ideal case is not possible, even by using a micropolar continuum or Cosserat solids. They proved that the obstruction for cloaking is the violation of balance of angular momentum or the kinematic constrain for the acceleration terms in the non-linear regime. This suggest that near-cloaking techniques such as symmetrization of the elastic tensor are necessary. Then, the fully symmetric (major and minor) elasticity tensor and can be approximated by isotropic composite materials through homogenization theory[196].

4.3 3-D cloaking vs out-of-plane and in-plane cloaking

In this section, we compare the effective properties associated with the full 3-D cloaking problem and the separate cases of Love and Rayleigh waves that were investigated in [202,201], respectively. Our goal is to highlight the additional complexities associated with the full 3-D cloaking scheme and its symmetrization.

As showed previously, by adopting the kinematic constraint $\mathbf{U} = \mathbf{u}$ (Cosserat gauge) for the displacements, the cloaking formulation yields non-symmetric stresses and strains, leading to the coefficients of the elasticity tensor losing their minor-symmetries. The strain-stress constitutive relation of the effective medium is described as follows:

$$\begin{aligned} \sigma_{ij} &= C^{eff}_{ijkl} u_{l,k} \\ \varepsilon_{ij} &= u_{j,i} \end{aligned} \tag{4.15}$$

It it worth noting that strains and stresses are not symmetric, e.g. ($\sigma_{12} \neq \sigma_{21}$ and $\varepsilon_{12} \neq \varepsilon_{21}$). Considering a "smooth-enough" test function $\hat{u}$ and domain Ω the equation of motion (neglecting external forces and boundary terms) for the effective medium can be expressed using the divergence theorem as:

$$\int_\Omega \sigma : \nabla \hat{u} \, d\Omega = \int_\Omega \sigma : \hat{\varepsilon} \, d\Omega = \int_\Omega (C^{eff}_{ijkl} : \varepsilon) : \hat{\varepsilon} \, d\Omega = 0 \tag{4.16}$$

Let us now delve into the formulation of the equation of motion for Love and Rayleigh waves, independently.

4.3.1 Love waves-weak formulation

We first revisit the case of anti-plane shear waves (Love waves) covered in Chapter 1. For this reason, all the in-plane displacement are constrained i.e. $\mathbf{u} = (0, 0, u_3)$ and continuity along the out-of-plane di-

rection is imposed. In 3-D Voigt notation ($\{1,2,3,4,\overline{4},5,\overline{5},6,\overline{6}\} = \{11,22,33,23,32,31,13,12,21\}$) the vanishing strain terms read: $\varepsilon_1 = \varepsilon_2 = \varepsilon_3 = \varepsilon_{\overline{4}} = \varepsilon_5 = \varepsilon_6 = \varepsilon_{\overline{6}} = 0$. For the triangular carpet pinched cloak, taking into account Eq. (4.6) and Eq. (3.5), Eq. (4.16) in the Love setting becomes:

$$(C^{effP}_{44}\varepsilon_4 + C^{effP}_{4\overline{5}}\varepsilon_{\overline{5}})\hat{\varepsilon_4} + (C^{effP}_{\overline{5}4}\varepsilon_4 + C^{effP}_{\overline{55}}\varepsilon_{\overline{5}})\hat{\varepsilon_{\overline{5}}} = 0 \tag{4.17}$$

Note that the coefficients, C^{effP}_{44}, $C^{effP}_{4\overline{5}}$, $C^{effP}_{\overline{5}4}$, $C^{effP}_{\overline{55}}$ represent nothing more than the effective shear modulus of Eq. (2.9) written in Voigt notation.

In similar fashion, the weak formulation for a semi-circular cloak, considering Eq. (4.12) and Eq. (3.5) is:

$$(C^{effC_2}_{44}\varepsilon_4)\hat{\varepsilon_4} + (C^{effC_2}_{\overline{55}}\varepsilon_{\overline{5}})\hat{\varepsilon_{\overline{5}}} = 0 \tag{4.18}$$

4.3.2 Rayleigh waves-weak formulation

Next, we turn our attention to the in-plane case of Rayleigh waves that was explored in Chapter 2. As a result, the in-plane displacement vector reads $\mathbf{u} = (u_1, u_2, 0)$. Thus, all out-of-plane strains are zero: $\varepsilon_3 = \varepsilon_4 = \varepsilon_{\overline{4}} = \varepsilon_5 = \varepsilon_{\overline{5}} = 0$.

For the triangular cloak, using the transformed elastic tensor of Eq. (**??**), the weak formulation is:

$$\begin{aligned}(C^{effP}_{11}\varepsilon_1 + C^{effP}_{12}\varepsilon_2 + C^{effP}_{1\overline{6}}\varepsilon_{\overline{6}})\hat{\varepsilon_1} + (C^{effP}_{21}\varepsilon_1 + C^{effP}_{22}\varepsilon_2 + C^{effP}_{26}\varepsilon_6 + C^{effP}_{2\overline{6}}\varepsilon_{\overline{6}})\hat{\varepsilon_2} + \\ (C^{effP}_{62}\varepsilon_2 + C^{effP}_{66}\varepsilon_6 + C^{effP}_{6\overline{6}}\varepsilon_{\overline{6}})\hat{\varepsilon_6} + (C^{effP}_{\overline{6}1}\varepsilon_1 + C^{effP}_{\overline{6}2}\varepsilon_2 + C^{effP}_{\overline{6}6}\varepsilon_6 + C^{effP}_{\overline{66}}\varepsilon_{\overline{6}})\hat{\varepsilon_6} = 0\end{aligned} \tag{4.19}$$

For the semi-circular type cloaks the weak form using Eq. (4.12) is as follows:

$$\begin{aligned}(C^{effC_2}_{11}\varepsilon_1 + C^{effC_2}_{12}\varepsilon_2)\hat{\varepsilon_1} + (C^{effC_2}_{21}\varepsilon_1 + C^{effC_2}_{22}\varepsilon_2)\hat{\varepsilon_2} + \\ (C^{effC_2}_{66}\varepsilon_6 + C^{effC_2}_{6\overline{6}}\varepsilon_{\overline{6}})\hat{\varepsilon_6} + (C^{effC_2}_{\overline{6}6}\varepsilon_6 + C^{effC_2}_{\overline{66}}\varepsilon_{\overline{6}})\hat{\varepsilon_{\overline{6}}} = 0\end{aligned} \tag{4.20}$$

4.3.3 3-D CLOAKING PROBLEM-WEAK FORMULATION

Now, we focus on the full 3-D problem of cloaking a finite region, which is located at the free surface of an elastic medium, from incident elastic surface waves using cylindrical-shaped cloaking devices. In the absence of any constraints, the weak formulation of the elastodynamic equation of motion for the cloak with a triangular cross section is:

$$\begin{aligned}(C_{11}^{effP}\varepsilon_1 + C_{12}^{effP}\varepsilon_2 + C_{13}^{effP}\varepsilon_3 + C_{1\bar{6}}^{effP}\varepsilon_{\bar{6}})\hat{\varepsilon_1} + (C_{21}^{effP}\varepsilon_1 + C_{22}^{effP}\varepsilon_2 + C_{23}^{effP}\varepsilon_3 + C_{26}^{effP}\varepsilon_6 + C_{2\bar{6}}^{effP}\varepsilon_{\bar{6}})\hat{\varepsilon_2} + \\ (C_{31}^{effP}\varepsilon_1 + C_{32}^{effP}\varepsilon_2 + C_{33}^{effP}\varepsilon_3 + C_{3\bar{6}}^{effP}\varepsilon_{\bar{6}})\hat{\varepsilon_3} + (C_{44}^{effP}\varepsilon_4 + C_{4\bar{4}}^{effP}\varepsilon_{\bar{4}} + C_{45}^{effP}\varepsilon_5 + C_{4\bar{5}}^{effP}\varepsilon_{\bar{5}})\hat{\varepsilon_4} + \\ (C_{\bar{4}4}^{effP}\varepsilon_4 + C_{\bar{4}\bar{4}}^{effP}\varepsilon_{\bar{4}})\hat{\varepsilon_{\bar{4}}} + (C_{54}^{effP}\varepsilon_4 + C_{55}^{effP}\varepsilon_5 + C_{5\bar{5}}^{effP}\varepsilon_{\bar{5}})\hat{\varepsilon_5} + (C_{\bar{5}4}^{effP}\varepsilon_4 + C_{\bar{5}5}^{effP}\varepsilon_5 + C_{\bar{5}\bar{5}}^{effP}\varepsilon_{\bar{5}})\hat{\varepsilon_{\bar{5}}} + \\ (C_{62}^{eff}\varepsilon_2 + C_{66}^{effP}\varepsilon_6 + C_{6\bar{6}}^{effP}\varepsilon_{\bar{6}})\hat{\varepsilon_6} + (C_{\bar{6}1}^{effP}\varepsilon_1 + C_{\bar{6}2}^{effP}\varepsilon_2 + C_{\bar{6}3}^{effP}\varepsilon_3 + C_{\bar{6}6}^{effP}\varepsilon_6 + C_{\bar{6}\bar{6}}^{effP}\varepsilon_{\bar{6}})\hat{\varepsilon_{\bar{6}}} = 0\end{aligned} \tag{4.21}$$

whereas for the semi-circular cylindrical cloak we get:

$$\begin{aligned}(C_{11}^{effC_2}\varepsilon_1 + C_{12}^{effC_2}\varepsilon_2 + C_{13}^{effC_2}\varepsilon_3)\hat{\varepsilon_1} + (C_{21}^{effC_2}\varepsilon_1 + C_{22}^{effC_2}\varepsilon_2 + C_{23}^{effC_2}\varepsilon_3)\hat{\varepsilon_2} + \\ (C_{31}^{effC_2}\varepsilon_1 + C_{32}^{effC_2}\varepsilon_2 + C_{33}^{effC_2}\varepsilon_3)\hat{\varepsilon_3} + (C_{44}^{effC_2}\varepsilon_4 + C_{4\bar{4}}^{effC_2}\varepsilon_{\bar{4}})\hat{\varepsilon_4} + \\ (C_{\bar{4}4}^{effC_2}\varepsilon_4 + C_{\bar{4}\bar{4}}^{effC_2}\varepsilon_{\bar{4}})\hat{\varepsilon_{\bar{4}}} + (C_{55}^{effC_2}\varepsilon_5 + C_{5\bar{5}}^{effC_2}\varepsilon_{\bar{5}})\hat{\varepsilon_5} + (C_{\bar{5}5}^{effC_2}\varepsilon_5 + C_{\bar{5}\bar{5}}^{effC_2}\varepsilon_{\bar{5}})\hat{\varepsilon_{\bar{5}}} + \\ (C_{66}^{eff}\varepsilon_6 + C_{6\bar{6}}^{effC_2}\varepsilon_{\bar{6}})\hat{\varepsilon_6} + (C_{\bar{6}6}^{effC_2}\varepsilon_6 + C_{\bar{6}\bar{6}}^{effC_2}\varepsilon_{\bar{6}})\hat{\varepsilon_{\bar{6}}} = 0\end{aligned} \tag{4.22}$$

It should be noted that since the elasticity tensor is represented in the augmented Voigt notation, all its components are symmetric, i.e., $C_{ij}^{eff} = C_{ji}^{eff}$. With the formulation of all the equations of motion, we can now discuss the similarities and differences between the 3-D problem and the separate scenarios of Love and Rayleigh problems for both the triangular and semi-circular cloaks. By comparing Eqs. (4.17) and (4.19) with Eq. (4.21) it is evident that there exists an extra set of the following 15

elastic coefficients that were "eliminated" upon tackling the separate scenarios:

$$\{C_{13}^{effP}, C_{31}^{effP}, C_{23}^{effP}, C_{32}^{effP}, C_{33}^{effP}, C_{3\overline{6}}^{effP}, C_{\overline{6}3}^{effP}, C_{4\overline{4}}^{effP}, C_{\overline{4}4}^{effP}, C_{\overline{44}}^{effP}, C_{45}^{effP}, C_{54}^{effP}, C_{55}^{effP}, C_{5\overline{5}}^{effP}, C_{\overline{5}5}^{effP}\} \quad (4.23)$$

In the same vein, for the circular cloak, a comparison of Eqs. (4.18) and (4.20) with Eq. (4.22) points to an additional list of 11 parameters of the elasticity tensor stated bellow:

$$\{C_{13}^{effC_2}, C_{31}^{effC_2}, C_{23}^{effC_2}, C_{32}^{effC_2}, C_{33}^{effC_2}, C_{4\overline{4}}^{effC_2}, C_{\overline{4}4}^{effC_2}, C_{\overline{44}}^{effC_2}, C_{55}^{effC_2}, C_{5\overline{5}}^{effC_2}, C_{\overline{5}5}^{effC_2}\} \quad (4.24)$$

In 3-D cloaking, it is essential not to neglect the non-vanishing components mentioned above, as they play a crucial role in inducing additional anisotropic behaviours, such as C_{33}^{eff}, or extending the demands for symmetrization, as shown with $C_{\overline{44}}^{eff}$. Aside from the fact that 3-D cloaking is not a simple 'superposition' of the two distinct Love and Rayleigh wave phenomena, it also necessitates the presence of a heterogeneous system, as Love waves propagate exclusively in layered media. As a result, Rayleigh waves will also exhibit dispersive characteristics and will account for multiple modes. This differs from the scenario presented in Chapter 2, where Rayleigh waves were investigated upon a homogeneous medium, supporting only a single mode. Furthermore, the loss of minor symmetry of the elastic tensor along with its approximation using symmetric materials may mitigate the cloaking efficiency in the out-of-plane direction (Love waves). When studied independently, the effective cloaking requirements can be perfectly matched by isotropic materials, as we demonstrated in Chapter 2. Finally, it is worth mentioning that the statement of the problem in the full 3-D setting can now support wave shielding phenomena from multiple angles of incidence. This scenario could not be investigated in the previous Chapters, as in both we assumed 2-D geometry.

4.4 Carpet cloaking for Surface elastic waves: Symmetrization

In section 3.4 we used the arithmetic mean as a function to symmetrize the components of the elasticity tensor, building upon the fact that it minimized the variational problem of the PDEs between the ideal cloak and the cloak with symmetric elastic coefficients. This approach led to promising results and efficient shielding effect from incident Rayleigh waves. However, this metric does not guarantee optimum performance, especially in the elastodynamic regime, where the performance is highly dependent upon the frequency range. Since the 3-D problem consist of additional sets of non-symmetric components compared to the plane-strain scenario, it is of great importance to delve into the symmetrization problem by conducting a parametric study regarding the symmetrization function.

4.4.1 Generalized Mean

For a more comprehensive symmetrization approach, we utilize the concept of the generalized or power mean. We recall that if p is a real number and $x_1, ..., x_n$ are positive real numbers, then the power mean is defined as :

$$G_p(x_1, ..., x_n) = (\frac{1}{n}\sum_{i=1}^{n} x_i^p)^{1/p} \tag{4.25}$$

A few well-known specific cases include:the quadratic mean ($p = 2$), the arithmetic ($p = 1$), the geometric ($p = 0$) and the harmonic ($p = -1$), respectively. Moreover, $M = G_\infty(x_1, ..., x_n) = max(x_1, .., x_n)$ is the maximum and $m = G_{-\infty}(x_1, ..., x_n) = min(x_1, .., x_n)$ is the minimum value of the set. Another useful fact is that the power means are connected via the power mean inequality. If $p_1 \leq p_2$ then:

$$m = G_{-\infty}(x_1, ..., x_n) \leq G_{p_1}(x_1, ..., x_n) \leq G_{p_2}(x_1, ..., x_n) \leq G_\infty(x_1, ..., x_n) = M \tag{4.26}$$

with the equality condition applied if and only if all the variables are equal.

4.4.2 Love waves-driven symmetrization

This subsection is motivated to present an effective approach towards the symmetrization of the elasticity tensor in the 3-D scenario. Our goal is to discuss a possible "mixed" symmetrization technique that utilizes the generalized mean, but imposes constraints on specific elastic coefficients. We begin by recalling the non-symmetries of the elasticity tensor that resulted from the kinematic constrain (Gauge) of the displacement field and the applied transformation that connects the reference with the cloaked domain. For the triangular cloak T the non-symmetries are given in Eqs. (4.8). Thus, a symmetrized elastic tensor of a triangular-shaped cloak should satisfy the following requirements:

$$\begin{cases} C_{16}^{SymP} = C_{1\bar{6}}^{SymP} \\ C_{26}^{SymP} = C_{2\bar{6}}^{SymP} \\ C_{36}^{SymP} = C_{3\bar{6}}^{SymP} \\ C_{44}^{SymP} = C_{4\bar{4}}^{SymP} = C_{\bar{4}\bar{4}}^{SymP} \\ C_{45}^{SymP} = C_{4\bar{5}}^{SymP} = C_{\bar{4}5}^{SymP} = C_{\bar{4}\bar{5}}^{SymP} \\ C_{66}^{SymP} = C_{6\bar{6}}^{SymP} = C_{\bar{6}\bar{6}}^{SymP} \end{cases} \tag{4.27}$$

In order to "eliminate" the requirements for cloaking of Love waves, considering Eqs. (4.17), we set the symmetrized coefficients as follows:

$$\begin{cases} C_{44}^{SymP} = C_{4\bar{4}}^{SymP} = C_{\bar{4}\bar{4}}^{SymP} = C_{44}^{effP} \\ C_{45}^{SymP} = C_{4\bar{5}}^{SymP} = C_{\bar{4}5}^{SymP} = C_{\bar{4}\bar{5}}^{SymP} = C_{45}^{effP} \end{cases} \tag{4.28}$$

Similarly, for the semi-circular cylindrical cloak the requirements for symmetric tensor based on

Eqs. (4.14) read:

$$\begin{cases} C_{44}^{SymC_2} = C_{4\bar{4}}^{SymC_2} = C_{\bar{4}\bar{4}}^{SymC_2} \\ C_{55}^{SymC_2} = C_{5\bar{5}}^{SymC_2} = C_{\bar{5}\bar{5}}^{SymC_2} \\ C_{66}^{SymC_2} = C_{6\bar{6}}^{SymC_2} = C_{\bar{6}\bar{6}}^{SymC_2} \end{cases} \tag{4.29}$$

Thus, by letting the symmetrized coefficients to satisfy the Love wave governing equation given by Eqs. (4.18) we get:

$$\begin{cases} C_{44}^{SymC_2} = C_{4\bar{4}}^{SymC_2} = C_{\bar{4}\bar{4}}^{SymC_2} = C_{44}^{effC_2} \\ C_{55}^{SymC_2} = C_{5\bar{5}}^{SymC_2} = C_{\bar{5}\bar{5}}^{SymC_2} = C_{55}^{effC_2} \end{cases} \tag{4.30}$$

Having established the conditions for a symmetrized cloak to have identical shielding capabilities with the ideal scenario, we can now utilize the approach of generalized mean (Eqs. (4.25)) discussed above for the remaining coefficients and delve into the performance of such cloaks in the 3-D setting. This will be illustrated in the next section.

4.5 Numerical Results and comparisons

We analyze the propagation of Love and Rayleigh waves in a bi-layered medium that host a cylindrical-shaped defect of triangular or semi-circular cross section, respectively. This model of a half-space, introduced in Chapter 2, is the simplest possible configuration that permits the existence of Love waves. For both cross section configurations, the carpet cloaks are located inside the soft layer of a double-layered semi-infinite medium and the mechanical parameters are given according to the Eq. (4.4) and Eq. (4.9). For this particular study, numerical of geometrical and mechanical quantities are depicted in Table 4.1.

To facilitate the discussion and analysis of our results, we introduce the following normalized quantities:

Layer	Shear velocity	Pressure velocity	Density	Depth
1	c_{s1}=300 m/s	$c_{p1} = \sqrt{3}c_{s1}$ m/s	1600 kg/m^3	h_1=40 m
2	c_{s2}=800 m/s	$c_{p2} = \sqrt{3}c_{s2}$ m/s	1600 kg/m^3	∞

Table 4.1: Mechanical and geometrical properties of the double-layered substrate.

- We normalize the wavelength, denoted as $\lambda^\star = b$, to be equal to the depth of the cloak, resulting in a normalized wave number $k^\star = \frac{2\pi}{\lambda^\star}$.
- The normalized frequency, denoted as $f^\star = \frac{c_R}{\lambda^\star}$, where c_R is Rayleigh wave velocity, which can be approximated by the following formula: $c_R = c_s \frac{0.826+1.14\nu}{1+\nu}$ where ν is the Poisson's ratio.
- $f_{L1} = \frac{\omega_{L1}}{2\pi} = \frac{1}{2h_1\sqrt{\frac{1}{\omega_1^2}-\frac{1}{\omega_2^2}}}$ which is the cut-off frequency of the first higher-order Love wave mode. In our example, we have $\frac{f^\star}{f_{L1}} \approx 1.7$;

To evaluate the capabilities of the cloaking devices, we conduct time-harmonic simulations utilizing the finite element software COMSOL Multiphysics. For these simulations, we model a 3-D strip of the medium with dimensions $W \times H \times d$ along the Cartesian axes (x_1, x_2, x_3) (see Fig. 4.1*e*). The dimensions of the model are chosen as $W = 12.35\lambda^\star$, $H \approx 4.75\lambda^\star$ and $d = 0.2\lambda^\star$. Fixed constraints are applied to the bottom of the model, continuity boundary conditions are imposed along the out-of-plane x_3 direction and the surface is stress-free. Additionally, Perfectly Matched Layers are applied at the boundaries of the model to diminish reflections. Rayleigh and Love waves are generated by imposing at the surface of the model a time-harmonic line source along the x_3 direction located at $0.35W$ distance from the origin. The cylindrical inclusion of triangular cross-section which has a height $a = 0.4h_1 \approx 0.0842H$, width $2c = 0.7h_1 \approx 0.2947H$ and thickness d, is shielded by a cloak of identical shape which extends up to the depth of the soft layer ($b = h_1$). On the other hand, the semi-circular shaped cylindrical defect has radius a, and its surrounding semi-circular cloak has radius b, both expanded along the domain's thickness d.

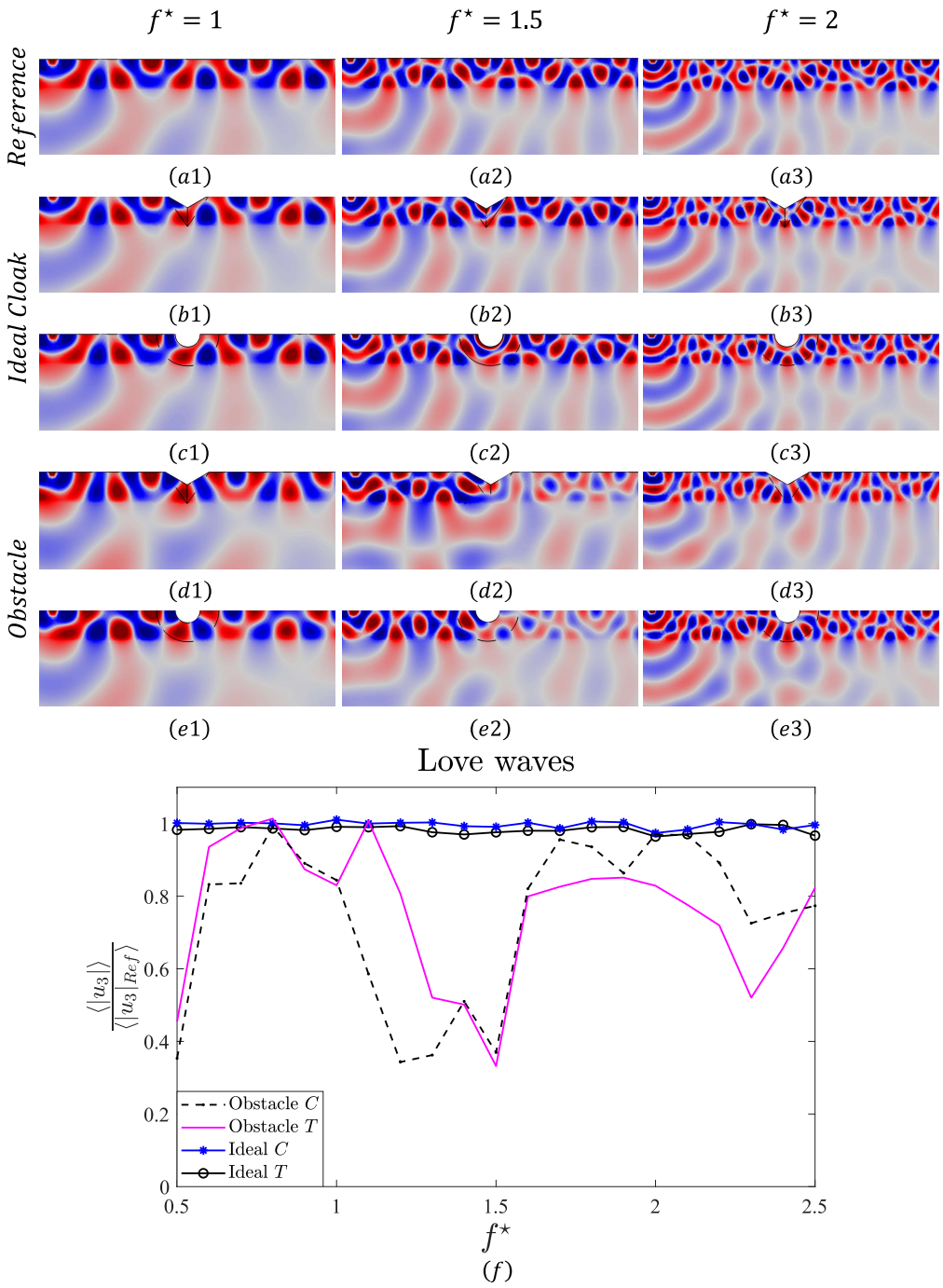

Fig. 4.2: Out-of-plane Displacement fields for the Reference $(a1) - (a3)$, Ideal Cloak $(b1) - (c3)$ and Obstacle $(d1) - (e3)$ configurations, of the triangular T and the circular C type of cloaks, computed at frequencies $f^\star = [1, 1.5, 2]$, respectively. (f) Performance of the ideal cloaks and the obstacle cases, computed by using the average of the total displacement of the transmitted field along the surface beyond the cloaked region at 21 frequencies in the range $f^\star = [0.5, 1.5, 2]$.

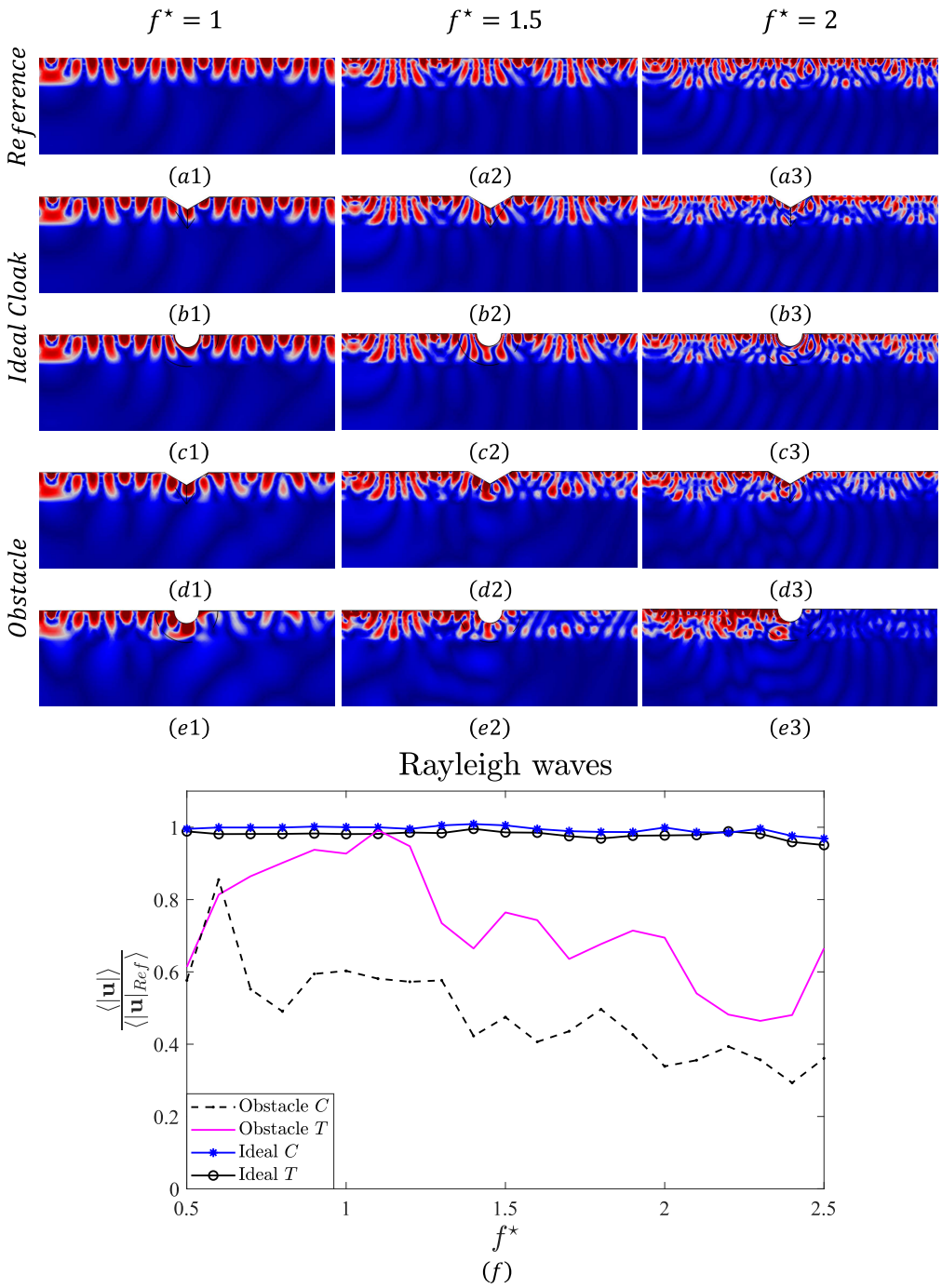

Fig. 4.3: In-plane Displacement fields for the Reference $(a1) - (a3)$, Ideal Cloak $(b1) - (c3)$ and Obstacle $(d1) - (e3)$ configurations, of the triangular T and the circular C type of cloaks, computed at frequencies $f^\star = [1, 1.5, 2]$, respectively. (f) Performance of the ideal cloaks and the obstacle cases, computed by using the average of the total displacement of the transmitted field along the surface beyond the cloaked region at 21 frequencies in the range $f^\star = [0.5, 0.1, 2.5]$.

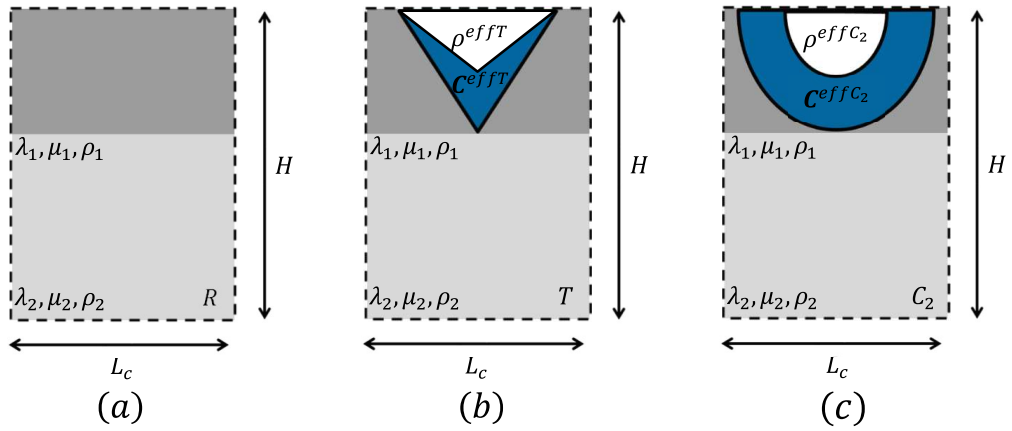

Fig. 4.4: Schematics of the cross-section of the unit cell for the reference R (*a*), triangular T (*b*) and circular C_2 (*c*) cloak configurations, respectively. All the unit cells have thickness d.

4.5.1 Ideal Cloaks

Adopting a similar approach with the previous Chapters, we begin our study by testing the performance of the "Ideal Cloaks" in the 3-D setting. These cloaks are characterized by mechanical parameters defined according to the to the transformation detailed in Eqs. (4.3). Our objective is to confirm whether such Cosserat (non-symmetric) cylindrical cloaks can effectively conceal cylindrical surface defects from incident Love and Rayleigh waves across a broad range of frequencies.

Harmonic Analysis

Thus, we conduct time-harmonic simulations to compare the surface displacement field of the system in three scenarios: (i) the pristine configuration, denoted as "Reference", (ii) the domain equipped with the cloaked defect, referred to as "Ideal Cloak", and (iii) the domain containing the bare defect, referred to as "Obstacle.". Specifically, we present the computed displacement fields for harmonic excitation at frequencies $f^* = [1, 1.5, 2]$. To make our claims more clear, instead of calculating the total modulus of the displacement fields, we split the portrayed displacement field into an out-of-plane

scenario which is generated by incident Love waves (Fig. 4.2 and an in-plane case that amounts for Rayleigh waves (Fig. 4.3. We remark that both Love and Rayleigh waves now exhibit as a dispersive nature, as expected from the theory. For Love waves (Fig. 4.2(a1)-(e3) the reference domain (Fig. 4.2(a1)-(a3) is almost perfectly approximated by both cylindrical cloaks of triangular and semi-circular shaped cross sections (Fig. 4.2(b1)-(c3). On the other hand, the uncloaked scenarios (Fig. 4.2(d1)-(e3) exhibit scattering effects across the bi-layered domain, with more severe effects being observed at frequency $f^{\star} = 1.5$. In addition, we provide the normalized transmitted out-of-plane displacement field $\frac{\langle |u_3| \rangle}{\langle |u_3|_{Ref} \rangle}$, as the ratio between the average out-of-plane displacement at the surface $\langle |u_3| \rangle$ computed beyond the obstacle for the ideal cloaks and the obstacle cases, and the same average displacement computed for the reference configuration as well $\langle v_{Ref} \rangle$. The results depicted in Fig. 4.2f near flawless performance of the ideal cloaks with $\frac{\langle |u_3| \rangle}{\langle |u_3|_{Ref} \rangle}$ approaching unity. In stark contrast, scenarios involving defects without the cloaking device exhibit significant inefficiency, as evidenced by the substantial reduction in the transmitted surface field compared to the reference configuration. In similar fashion, the displacement fields for the now dispersive propagating Rayleigh waves (Fig. 4.3(a1)-(e3), confirm near exact matching of the pristine medium (Fig. 4.2(a1)-(a3) with both cylindrical cloaking devices of triangular and semi-circular shape ((Fig. 4.3(b1)-(c3). As expected, the bare obstacle cases (Fig. 4.3(d1)-(e3) display scattering effects and thus, inefficient protection. Furthermore, we present the normalized displacement field at the $u_1 - u_2$ plane, denoted as $\frac{\langle |\boldsymbol{u}| \rangle}{\langle |\boldsymbol{u}|_{Ref} \rangle}$, where $|\boldsymbol{u}| = \sqrt{u_1^2 + u_2^2}$ is the displacement modulus using the Euclidean metric, in the same spirit as the case of Love waves. The results, as illustrated in Fig. 4.3f, reveal the remarkable effectiveness of ideal cloaks, with $\frac{\langle |\boldsymbol{u}| \rangle}{\langle |\boldsymbol{u}|_{Ref} \rangle} \approx 1$. For both geometries, the cases involving only an obstacle had a significant loss of performance, especially in the higher frequency regime.

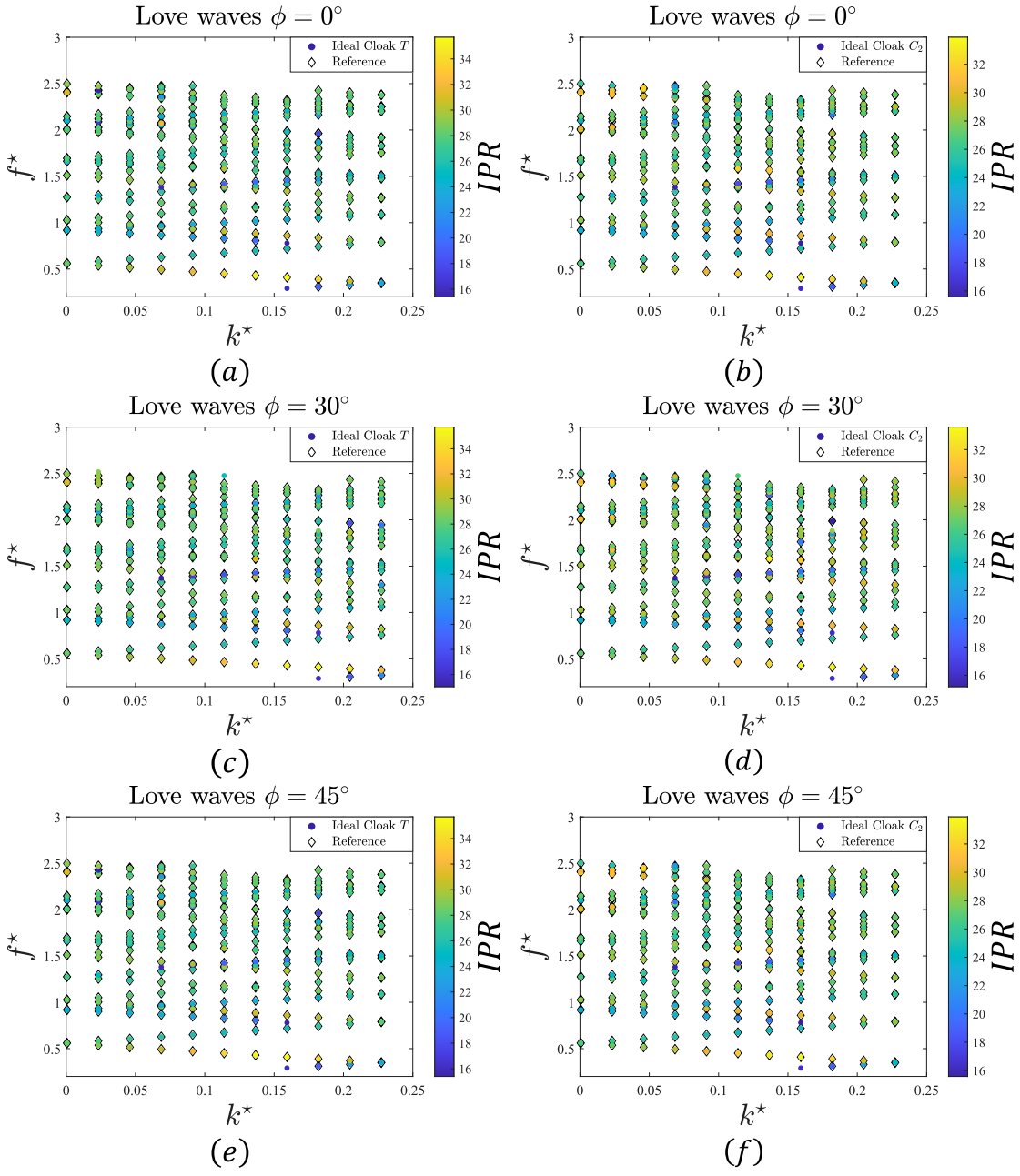

Fig. 4.5: Dispersion curves of Love wave surface modes for the reference (diamond dots), and ideal cloaks (contour circle dots) of triangular (left column) and semi-circular cross-sections (right column), respectively, computed at different angles of incidence $\varphi = [0°, 30°, 45°]$

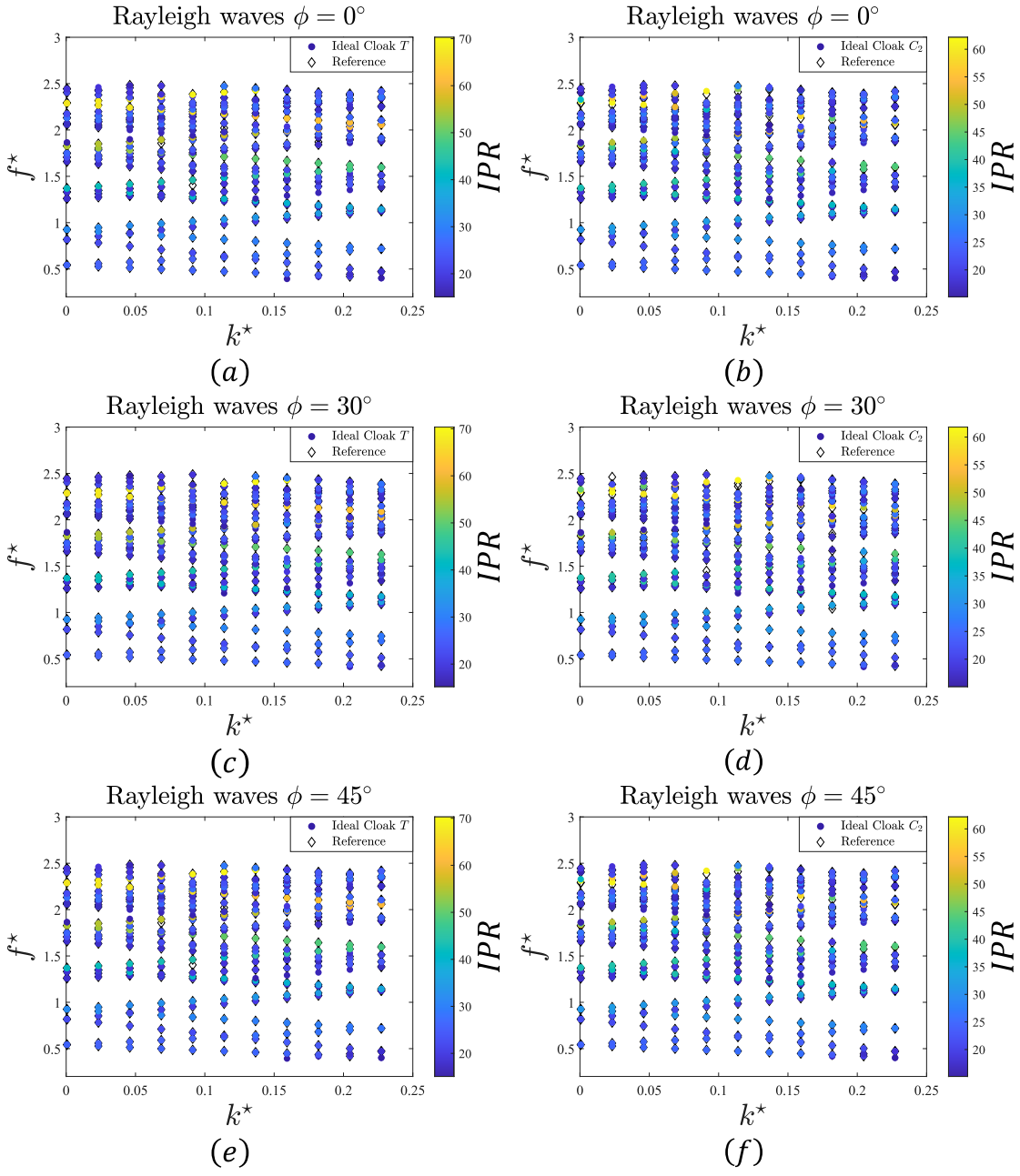

Fig. 4.6: Dispersion curves of Rayleigh wave surface modes for the reference (diamond dots), and ideal cloaks (contour circle dots) of triangular (left column) and semi-circular cross-sections (right column), respectively, computed at different angles of incidence $\varphi = [0°, 30°, 45°]$

Dispersive Analysis

To further demonstrate the broadband capabilities of the proposed carpet cloaks, we compare the dispersive characteristics of Love and Rayleigh waves propagating through both the pristine and the cloaked double-layered medium. The primary objective of this study is to establish that within the cloaked configuration with effective properties given by Eqs. (**??**) or (4.12) and their related geometrical transformations, as outlined in Eqs. (4.4) or (4.9), the cloak enable an accurate replication of the dispersive properties observed in the pristine layered medium. To achieve this, we employed a finite element modeling using COMSOL Multiphysics environment to simulate a 3-D unit cell of the cloak and the reference, respectively. The unit cells have dimensions $L_c \times H \times d$, with $L_c = 2.2b$ (See Fig. 4.4(a)-(c)). Fixed boundary conditions are imposed at the base of the unit cell, continuity conditions are implemented along the x_2 direction and Bloch-Floquet boundary conditions are applied along the x_1 direction. Moreover, an equivalent unit cell is used to model the "Reference" configuration. In all scenarios, the dispersive properties were determined through an eigenvalue analysis, involving variations in the wavenumber within the first Brillouin zone, specifically $k_{x_1} = [\frac{\pi}{400L_c}; \frac{\pi}{L_c}]$, with subsequent extraction of the frequency f. According to the results discussed in section 3.5.1, the length of the unit cell must be at least equal with the size of the cloak (we set $L_c = 2.2b$) to avoid overlapping transformations, see[224]. However, this restriction has the consequence of limiting the size of the first Brillouin zone (FBZ). As a result, to calculate frequencies up to $f^* = 2.5$, multiple modes (>200) must be computed for each wavenumber. To address the issue of separating the surface modes from rest of the wave solutions, we again employ the concept of the inverse participation ratio (IPR)[249,213,227,244,226] for the 3-D model as:

$$IPR = \frac{\iiint_{V^*} \|\mathbf{u}\|^4 \, dx_1 \, dx_2 \, dx_3}{(\iiint_{V^*} \|\mathbf{u}\|^2 \, dx_1 \, dx_2 \, dx_3)^2} |V^*| \tag{4.31}$$

where we normalize the ratio by multiplying it with the volume of the model $|V^{\star}|$ and $\|\mathbf{u}\| = \sqrt{u_1^2 + u_2^2 + u_3^2}$ is the total displacement. For our case-study an IPR$>$ 15 allows us to clearly differentiate surface modes from bulk ones. Furthermore, to obtain a better understanding of the results from the proposed strategy we split the collected surface modes into two subsets according to the absolute value of the out-of-plane component u_3 of the displacement field. We found that the condition $\langle |u_3| \rangle > 10^{-4} m$, where the average is taken over the surface line, extending across the length L_c of the unit cell, is sufficient to isolate the Love from the Rayleigh wave solutions. Figs. 4.5 and 4.6 depict the surface modes of Love and Rayleigh type, respectively traveling within the triangular T (left column) and the semi-circular cloak C_2 (right column), using coloured dots based upon their IPR values. In addition, the 3-D scenario gives us the leverage to test the performance of the cloaks upon multiple angles of incidence, $\varphi = [0^{\circ}, 30^{\circ}, 45^{\circ}]$, where φ is the angle on the $x_1 - x_3$ plane (see Figs. 4.1(a) and (c)), as shown in each row of Figs. 4.5 and 4.6. This phenomenon significantly improves the quality of the cloaking effect and unlocks further the potential applications. Overall, this visualization allows the reader to observe the correspondence between surface modes within the cloaked domains and the surface wave solution within the reference field, thereby highlighting the broadband cloaking capabilities of the non-symmetric cloaks under investigation.

4.5.2 Symmetrized Cloaks

Following the excellent performance of the ideal cloaks and the benefits of a 3-D study of cloaking, we will delve into the behavior of symmetrized cloaks featuring triangular (T) and semi-circular (C_2) transformations, respectively. In accordance with Chapter 2, our primary objective is to identify the combination of symmetrization and cloak geometry that yields optimal cloaking efficiency. For this reason, we will adopt the strategy described in Section 4.4. In particular, we start by symmetrizing the coefficients of the effective elasticity tensor according to the Love wave solution given by Eqs. (4.28) and (4.30), for both the triangular and the semi-circular cloak, respectively. Then, the remaining

components in Eqs. (4.27) and (4.29) are symmetrized by employing different values of the generalized mean given by (4.25). For our study we will use the following statistical means: 'Harmonic' ($p = -1$), 'Geometric' ($p = 0$), 'Arithmetic' ($p = 1$), 'Quadratic' ($p = 2$) and the 'Maximum' mean ($p = \infty$).

Harmonic Analysis

We begin by computing the ratio of the the out-of-plane (Fig. 4.7(a)-(b)) (Love waves) and the in-plane (Rayleigh) (Fig. 4.7(c)-(d)) transmitted displacement field of the symmetrized cloaks over the ideal ones for the triangular and the semi-circular cloaks, respectively. The reader can appreciate the excellent ($\frac{\langle |u_3|_{Sym} \rangle}{\langle |u_3|_{Ideal} \rangle} \approx 1$) out-of-plane performance of the symmetrized cloaks across all frequencies (see Figs. 4.7(a)-(b)), as predicted by Section 4.4.2. Now we turn our attention to the case of Rayleigh waves. The performance of the triangular-shaped cylindrical cloak with symmetric elastic tensor is illustrated in Fig. 4.7(c). We remark that due to the presence of a layered substrate with depth equal to the size of the cloak, the transmitted field can be impacted by reflections across the boundaries between the substrate and the half-space. This can lead to values $\frac{\langle |\boldsymbol{u}|_{Sym} \rangle}{\langle |\boldsymbol{u}|_{Ideal} \rangle} > 1$. To avoid any confusions in the plots, all such values will be replaced by their reciprocals. From Fig. 4.7(c), it is clear that the 'Maximum' mean ($p = \infty$), portrayed with red circles, fails to deliver sufficient cloaking protection, performing worse than the obstacle case in at most of the examined frequencies. For frequencies up to $f^* = 1.4$, it is observed that the 'Quadratic' mean ($p = 2$) demonstrates a better overall performance that the other designs. However, a shift in performance can be seen for higher frequencies ($f^* \geq 1.4$) as the triangular cloak design based on the 'Arithmetic' mean prevails over the rest of the cloaks. This unstable behaviour of the symmetrized triangular cloaks, questions their practical realization for a wide range of operating frequencies. Moreover, we point out that the cases pertaining the 'Harmonic' ($p = -1$) and the 'Geometric' ($p = 0$) means produced inefficient solutions (not shown here) and were excluded from the investigation. On the other hand, the symmetrized semi-

circular cylindrical cloak exhibits a more well-rounded performance (see Fig. 4.7(d)). Overall, most of the applied symmetrization techniques achieved superior performance to the 'Obstacle' case, thus providing a clear shielding effect. This can be attributed to the smaller number of conditions (3) required for its symmetrization compared to the triangular scenario (6), as outlined in Eqs. (4.27) and (4.29). In particular, the symmetrized construction driven by the 'Maximum' mean, represented by circle-marked red line in Fig. 4.7(d), leads to the most efficient cloaking protection across the majority of the frequency range.

Furthermore, to better asses the efficacy of the invisibility cloaks we utilize another quantifiable measure. For the present work, we will use the scattering measure for the transmission field used in [207,206], as a tool to quantify the effectiveness of the cloak as:

$$\Delta^i = \frac{\sqrt{\sum(|\boldsymbol{u}|_i - |\boldsymbol{u}|_{Ideal})^2}}{\sqrt{\sum |\boldsymbol{u}|_{Ideal}{}^2}} \tag{4.32}$$

where the index i corresponds to the symmetrized cloak (Sym) or the obstacle (Obs), and (Ideal) stands for the ideal cloak. The summation is computed over 5000 uniformly distributed points on the line segment located at the free surface of the transmitted field. We recall that a perfect cloaking performance is translated to a vanishing scattering field i.e. $\Delta^i \approx 0$. The results displayed in Figs. 4.7(e)-(f) for the triangular and the semi-circular cloaks, respectively, further corroborate the previous findings, as the symmetrized triangular cloak fails to provide an efficient and consistent protection, with scattering measures up to 20 times of a bare obstacle. In stark contrast, the semi-circular cloaking designs provide an adequate suppression of the scattering effects, especially utilizing the "Maximum" mean solution, which enhances the protection upon all the calculated frequencies. Finally, The reader can appreciate the in-plane wavefield of the symmetrized cloaks for 3 calculated frequencies in Fig. 4.8. Indeed, by comparing the "Reference" (Fig. 4.8($a1$)-($a3$)) with the cloaks symmetrized through 'Arithmetic' ($p = 1$) (Fig. 4.8($b1$)-($c3$)), 'Quadratic' ($p = 2$) (Fig. 4.8($d1$)-($e3$)) and the 'Maximum' mean

($p = \infty$) (Fig. 4.8($f1$)-($g3$)), it is clear that the semi-circular cloaks provide superior cloaking efficiency compared to the triangular cloaking designs.

Dispersion Analysis

We conclude our investigation by conducting a dispersive analysis, incorporating unit cells composed of symmetrized cloaks. At this stage, we restrict the investigation to the study of the semi-circular C_2 cylindrical cloak symmetrized acoording to the 'Maximum' mean function. Our goal is assess how well the symmetrized cloak is able approximate the dispersive characteristics of a pristine "Reference" medium, upon different angles of incidence. The results are depicted in Fig. 4.9 for $\varphi = 0°$ (Figs. 4.9(a)-(b)), $\varphi = 30°$ (Figs. 4.9(c)-(d)) and $\varphi = 45°$ (Figs. 4.9(e)-(f)), respectively. It is evident that for the Love waves scenario, the dispersive properties of the symmetrized cloak match the ones of the reference, as expected by our symmetrization strategy (see Figs. 4.9(a),(c) and (e)). In addition, for case of Rayleigh waves, the symmetrized cloak obtained through a C_2 type cylindrical transformation and symmetrized according to the maximum function is able to well-approximate the Rayleigh modes of the reference medium, replicating 224 out of 377 reference modes for $\varphi = 0°$ (Fig. 4.9(b)), 216 out of 376 reference modes for $\varphi = 30°$ and 224 out of 377 reference modes for $\varphi = 45°$, all upon the same IPR value (> 15). These results further validate the concept that a cylindrical quadratic (C_2) cloak with a semi-circular cross-section, utilizing the 'Maximum' mean function (where $p = \infty$), provides an effective form of cloaking protection against incident surface elastic waves.

4.6 Conclusion

In this study, we introduced a method for designing three-dimensional carpet cloaks that suppress scattering effects and mechanical vibrations caused by the propagation of Love and Rayleigh waves around defects. Our approach utilized geometric transformations on the Navier elastodynamic equa-

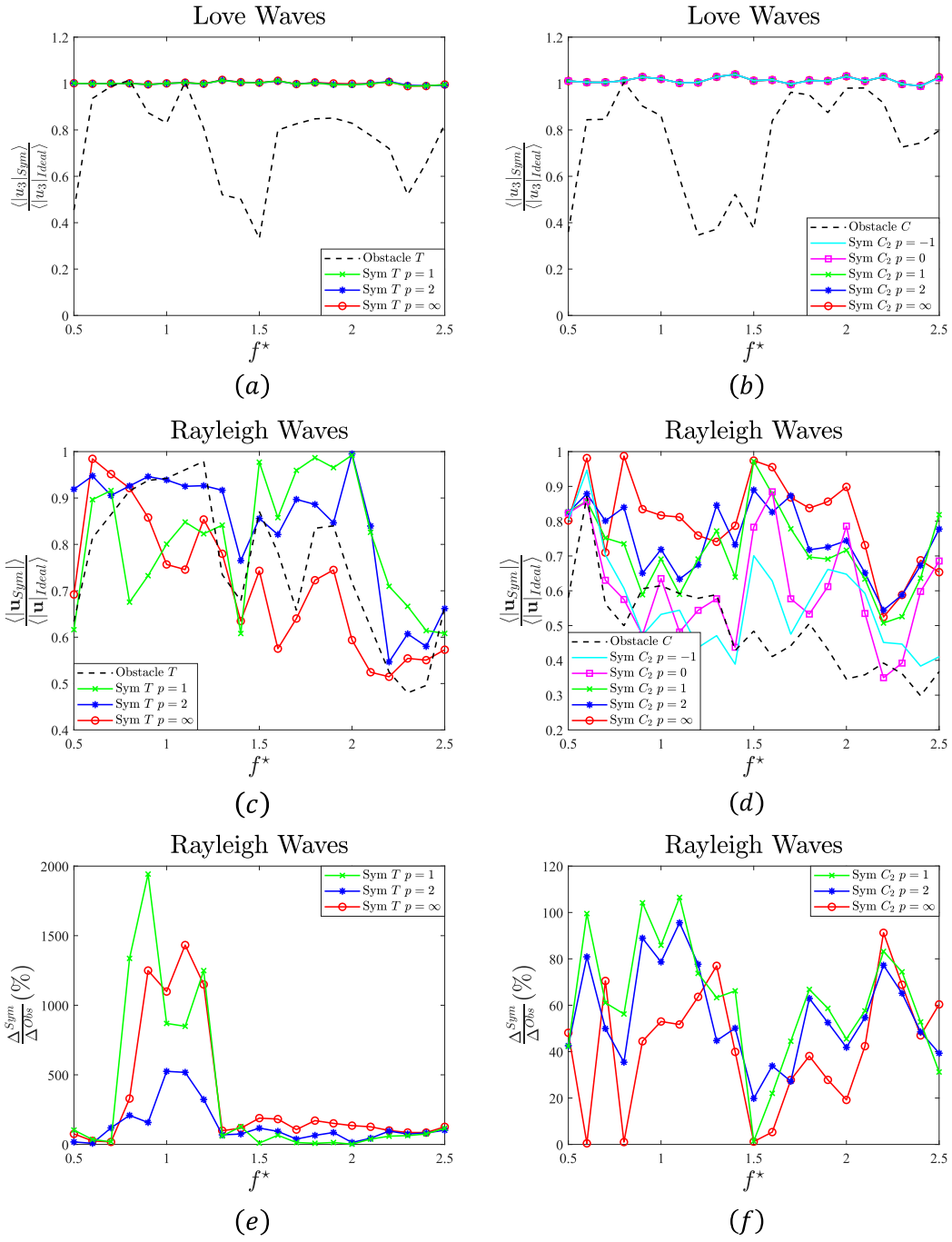

Fig. 4.7: (a)-(d) Performance of the cloaks using the ratio of the transmitted field of the symmetrized cloaks over the ideal one, for Love (a)-(b) and Rayleigh (c)-(d) waves, respectively. (e)-(f) Scattering percentage ratio of the symmetrized cloaks over the obstacle configuration for the triangular (e) and the semi-circular (f) shaped cloaks, respectively. The results are calculated at normalized frequencies $f^\star = [0.5 - 2.5]$.

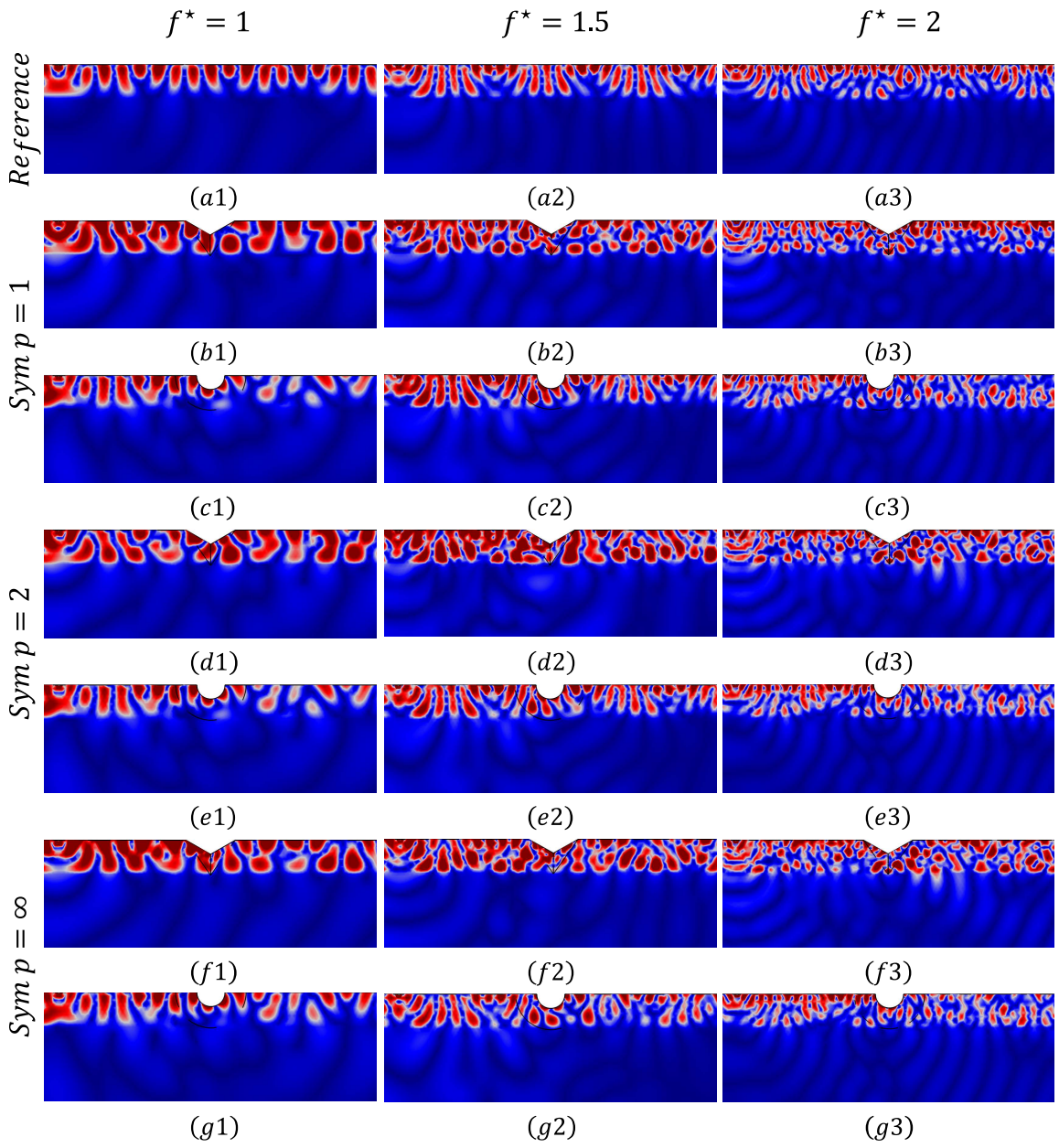

Fig. 4.8: In-plane Displacement fields for the Reference $(a1) - (a3)$, and symmetrized cloaks obtained through the 'Arithmetic' $(p = 1)$ $(b1) - (c3)$, 'Quadratic' $(p = 2)$ $(d1) - (e3)$ and 'Maximum' mean $(p = \infty)$ $(f1) - (g3)$, of triangular and semi-circular cross sections, respectively. The harmonic simulations are performed at 3 different normalized frequencies $f^\star = [1, 1.5, 2]$.

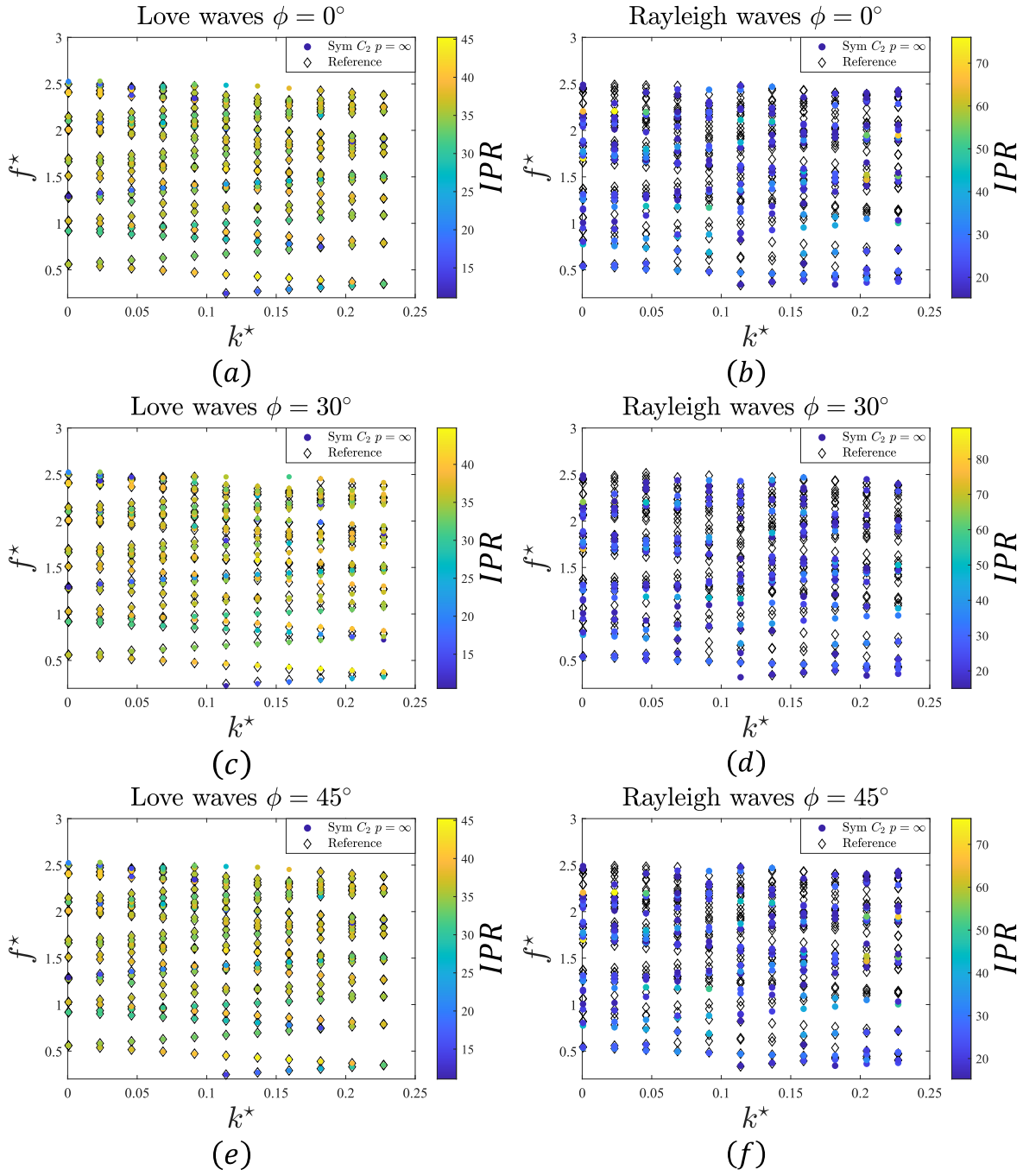

Fig. 4.9: Dispersion curves of Love (Left column) and Rayleigh (right column) surface modes, for the reference (diamond dots) and the symmetrized ($p = \infty$) semi-circular C_2 cloak (contour circle dots), respectively, computed at different angles of incidence $\varphi = [0°, 30°, 45°]$

tion that encompasses a Cosserat gauge for the displacements, in order to maintain the invariance of the governing equation. However, the 3-D cloaking problem includes additional terms in the effective elasticity tensor compared to the Rayleigh and Love isolated cases and yields to an increased number of non-symmetric entries. Due to this complexity, practical applications may seem challenging. Hence, we restricted ourselves into near-cloaking regimes and concentrated on the symmetrization of the elasticity tensor. Specifically, we allowed the "Love wave" coefficients dictate the symmetrization for the out-of-plane effective components, focusing exclusively on in-plane cloaking performance. To assess the efficacy of our designs, we conducted time-harmonic simulations utilizing finite element methods for cloaks with various symmetrized configurations. We compared the transmitted displacement fields and calculated the scattering measure ratio of the cloaks over the obstacle. To gain a more comprehensive understanding of these results, we conducted dispersive analyses, employing symmetrized semi-circular cloaks, and examined their performance under three different angles of incidence. Our findings indicate that a semi-circular cloak symmetrized using the maximum function provided the most accurate approximation of the ideal cloak.

References

[195] Barnwell, E. G., Parnell, W. J., & David Abrahams, I. (2016). Antiplane elastic wave propagation in pre-stressed periodic structures; tuning, band gap switching and invariance. *Wave Motion*, 63, 98–110.

[196] Bensoussan, Lions, P. (1978). *Asymptotic Analysis of Periodic Structures*. North Holland.

[197] Brun, M., Guenneau, S., & Movchan, A. B. (2009). Achieving control of in-plane elastic waves. *Applied Physics Letters*, 94(6), 061903.

[198] Bückmann, T., Kadic, M., Schittny, R., & Wegener, M. (2015). Mechanical cloak design by direct lattice transformation. *Proceedings of the National Academy of Sciences*, 112(16), 4930–4934.

[199] Cai, W., Chettiar, U. K., Kildishev, A. V., & Shalaev, V. M. (2007). Optical cloaking with metamaterials. *Nature Photonics*, 1(4), 224–227.

[200] Cassier, M., DeGiovanni, T., Guenneau, S., & Guevara Vasquez, F. (2021). Active thermal cloaking and mimicking. *Proceedings of the Royal Society A: Mathematical, Physical and Engineering Sciences*, 477(2249), 20200941.

[201] Chatzopoulos, Z., Palermo, A., Diatta, A., Guenneau, S., & Marzani, A. (2023). Cloaking rayleigh waves via symmetrized elastic tensors. *International Journal of Engineering Science*, 191, 103899.

[202] Chatzopoulos, Z., Palermo, A., Guenneau, S., & Marzani, A. (2022). Cloaking strategy for love waves. *Extreme Mechanics Letters*, 50, 101564.

[203] Chen, H. & Chan, C. T. (2007). Acoustic cloaking in three dimensions using acoustic metamaterials. *Applied Physics Letters*, 91(18), 183518.

[204] Chen, Y., Nassar, H., & Huang, G. (2021). Discrete transformation elasticity: An approach to design lattice-based polar metamaterials. *International Journal of Engineering Science*, 168, 103562.

[205] Choi, J. S. & Howell, J. C. (2014). Paraxial ray optics cloaking. *Opt. Express*, 22(24), 29465–29478.

[206] Colquitt, D., Brun, M., Gei, M., Movchan, A., Movchan, N., & Jones, I. (2014). Transformation elastodynamics and cloaking for flexural waves. *Journal of the Mechanics and Physics of Solids*, 72, 131–143.

[207] Colquitt, D. J., Jones, I. S., Movchan, N. V., Movchan, A. B., Brun, M., & McPhedran, R. C. (2013). Making waves round a structured cloak: lattices, negative refraction and fringes. *Proceedings of the Royal Society A: Mathematical, Physical and Engineering Sciences*, 469(2157), 20130218.

[208] Craster, R., Diatta, A., Guenneau, S., & Hutridurga, H. (2021). On near-cloaking for linear elasticity. *Multiscale Modeling and Simulation*, 19(2), 633–664.

[209] Cummer, S. A., Popa, B.-I., Schurig, D., Smith, D. R., Pendry, J., Rahm, M., & Starr, A. (2008). Scattering theory derivation of a 3d acoustic cloaking shell. *Phys. Rev. Lett.*, 100, 024301.

[210] Cummer, S. A. & Schurig, D. (2007). One path to acoustic cloaking. *New Journal of Physics*, 9(3), 45.

[211] Diatta, A. & Guenneau, S. (2014). Controlling solid elastic waves with spherical cloaks. *Applied Physics Letters*, 105(2), 021901.

[212] Diatta, A., Kadic, M., Wegener, M., & Guenneau, S. (2016). Scattering problems in elastodynamics. *Phys. Rev. B*, 94, 100105.

[213] Evers, F. & Mirlin, A. D. (2000). Fluctuations of the inverse participation ratio at the anderson transition. *Phys. Rev. Lett.*, 84, 3690–3693.

[214] Fan, J., Ma, T., Zhang, W., Zhu, Y., & Wang, H. (2022). Inner dimension detection of open and buried crack in asphalt pavement based on rayleigh wave method. *Construction and Building Materials*, 328, 127003.

[215] Golgoon, A. & Yavari, A. (2019). Nonlinear and linear elastodynamic transformation cloaking. *Archive for Rational Mechanics and Analysis*, 234, 211–316.

[216] Greenleaf, A., Kurylev, Y., Lassas, M., & Uhlmann, G. (2009). Cloaking devices, electromagnetic wormholes, and transformation optics. *SIAM Review*, 51(1), 3–33.

[217] Greenleaf, A., Kurylev, Y., Lassas, M., & Uhlmann, G. (2011). Cloaking a sensor via transformation optics. *Phys. Rev. E*, 83, 016603.

[218] Han, T., Bai, X., Gao, D., Thong, J. T. L., Li, B., & Qiu, C.-W. (2014). Experimental demonstration of a bilayer thermal cloak. *Phys. Rev. Lett.*, 112, 054302.

[219] Kadic, M., Bückmann, T., Schittny, R., & Wegener, M. (2015). Experiments on cloaking in optics, thermodynamics and mechanics. *Philosophical Transactions of the Royal Society A: Mathematical, Physical and Engineering Sciences*, 373(2049), 20140357.

[220] Kadic, M., Wegener, M., Nicolet, A., Zolla, F., Guenneau, S., & Diatta, A. (2020). Elastodynamic behavior of mechanical cloaks designed by direct lattice transformations. *Wave Motion*, 92, 102419.

[221] Khlopotin, A., Olsson, P., & Larsson, F. (2015). Transformational cloaking from seismic surface waves by micropolar metamaterials with finite couple stiffness. *Wave Motion*, 58, 53–67.

[222] Leonhardt, U. (2006). Optical conformal mapping. *Science*, 312(5781), 1777–1780.

[223] McCall, M. (2013). Transformation optics and cloaking. *Contemporary Physics*, 54(6), 273–286.

[224] Meirbekova, B. & Brun, M. (2020). Control of elastic shear waves by periodic geometric transformation: cloaking, high reflectivity and anomalous resonances. *Journal of the Mechanics and Physics of Solids*, 137, 103816.

[225] Milton, G. W., Briane, M., & Willis, J. R. (2006). On cloaking for elasticity and physical equations with a transformation invariant form. *New Journal of Physics*, 8(10), 248–248.

[226] Monthus, C. & Garel, T. (2010). Anderson localization of phonons in dimension $d = 1, 2, 3$: Finite-size properties of the inverse participation ratios of eigenstates. *Phys. Rev. B*, 81, 224208.

[227] Murphy, N. C., Wortis, R., & Atkinson, W. A. (2011). Generalized inverse participation ratio as a possible measure of localization for interacting systems. *Phys. Rev. B*, 83, 184206.

[228] Nassar, H., Chen, Y., & Huang, G. (2019). Isotropic polar solids for conformal transformation elasticity and cloaking. *Journal of the Mechanics and Physics of Solids*, 129, 229–243.

[229] Nassar, H., Chen, Y. Y., & Huang, G. L. (2018). A degenerate polar lattice for cloaking in full two-dimensional elastodynamics and statics. *Proceedings of the Royal Society A: Mathematical, Physical and Engineering Sciences*, 474(2219), 20180523.

[230] Nassar, H., Chen, Y. Y., & Huang, G. L. (2020). Polar metamaterials: A new outlook on resonance for cloaking applications. *Phys. Rev. Lett.*, 124, 084301.

[231] Newman, J. (2014). Cloaking a circular cylinder in water waves. *European Journal of Mechanics - B/Fluids*, 47, 145–150. Enok Palm Memorial Volume.

[232] Nguyen, D. M., Xu, H., Zhang, Y., & Zhang, B. (2015). Active thermal cloak. *Applied Physics Letters*, 107(12), 121901.

[233] Norris, A. & Shuvalov, A. (2011). Elastic cloaking theory. *Wave Motion*, 48(6), 525–538. Special Issue on Cloaking of Wave Motion.

[234] Norris, A. N. (2008). Acoustic cloaking theory. *Proceedings of the Royal Society A: Mathematical, Physical and Engineering Sciences*, 464(2097), 2411–2434.

[235] Norris, A. N. & Parnell, W. J. (2012). Hyperelastic cloaking theory: transformation elasticity with pre-stressed solids. *Proceedings of the Royal Society A: Mathematical, Physical and Engineering Sciences*, 468(2146), 2881–2903.

[236] Parnell, W. J. (2012). Nonlinear pre-stress for cloaking from antiplane elastic waves. *Proceedings of the Royal Society A: Mathematical, Physical and Engineering Sciences*, 468(2138), 563–580.

[237] Parnell, W. J. & Shearer, T. (2013). Antiplane elastic wave cloaking using metamaterials, homogenization and hyperelasticity. *Wave Motion*, 50(7), 1140–1152. Advanced Modelling of Wave Propagation in Solids.

[238] Pendry, J. B., Schurig, D., & Smith, D. R. (2006). Controlling electromagnetic fields. *Science*, 312(5781), 1780–1782.

[239] Quadrelli, D. E., Craster, R., Kadic, M., & Braghin, F. (2021). Elastic wave near-cloaking. *Extreme Mechanics Letters*, 44, 101262.

[240] Sanders, E. D., Aguiló, M. A., & Paulino, G. H. (2021). Optimized lattice-based metamaterials for elastostatic cloaking. *Proceedings of the Royal Society A: Mathematical, Physical and Engineering Sciences*, 477(2253), 20210418.

[241] Schittny, R., Kadic, M., Guenneau, S., & Wegener, M. (2013). Experiments on transformation thermodynamics: Molding the flow of heat. *Phys. Rev. Lett.*, 110, 195901.

[242] Shen, X., Li, Y., Jiang, C., Ni, Y., & Huang, J. (2016). Thermal cloak-concentrator. *Applied Physics Letters*, 109(3), 031907.

[243] Sklan, S. R., Pak, R. Y. S., & Li, B. (2018). Seismic invisibility: elastic wave cloaking via symmetrized transformation media. *New Journal of Physics*, 20(6), 063013.

[244] Tsukerman, E. (2017). Inverse participation ratios in the xx spin chain. *Phys. Rev. B*, 95, 115121.

[245] Wakata, S., Hosoya, N., Hasegawa, N., & Nishikino, M. (2022). Defect detection of concrete in infrastructure based on rayleigh wave propagation generated by laser-induced plasma shock waves. *International Journal of Mechanical Sciences*, 218, 107039.

[246] Wang, D. & Lv, L. J. (2023). Analysis of rayleigh wave response characteristics in complicated cave system and detection methods. *Mechanical Systems and Signal Processing*, 185, 109806.

[247] Wang, Z., Li, C., Zatianina, R., Zhang, P., & Zhang, Y. (2017). Carpet cloak for water waves. *Phys. Rev. E*, 96, 053107.

[248] Ward, A. J. & Pendry, J. B. (1996). Refraction and geometry in maxwell's equations. *Journal of Modern Optics*, 43(4), 773–793.

[249] Wegner, F. (1980). Inverse participation ratio in $2+\varepsilon$ dimensions. *Zeitschrift für Physik B Condensed Matter*, 36, 270–287.

[250] Wu, Q. & Huang, G. (2022). Omnidirectional wave polarization manipulation in isotropic polar solids. *International Journal of Solids and Structures*, 241, 111481.

[251] Xu, H., Shi, X., Gao, F., Sun, H., & Zhang, B. (2014). Ultrathin three-dimensional thermal cloak. *Phys. Rev. Lett.*, 112, 054301.

[252] Yue, X., Nangong, J., Chen, P., & Han, T. (2021). Thermal cloak: Theory, experiment and application. *Materials*, 14(24).

[253] Zareei, A. & Alam, M.-R. (2015). Cloaking in shallow-water waves via nonlinear medium transformation. *Journal of Fluid Mechanics*, 778, 273–287.

[254] Zhang, H., Chen, Y., Liu, X., & Hu, G. (2020). An asymmetric elastic metamaterial model for elastic wave cloaking. *Journal of the Mechanics and Physics of Solids*, 135, 103796.

[255] Zhang, P. & Parnell, W. J. (2018). Hyperelastic antiplane ground cloaking. *The Journal of the Acoustical Society of America*, 143(5), 2878–2885.

[256] Zhao, S., Chen, J., Chang, Z., & Huang, G. (2023). Microstructure realization of a lattice-based polar solid for arbitrary elastic waveguiding. *Journal of the Mechanics and Physics of Solids*, 173, 105226.

[257] Zou, S., Xu, Y., Zatianina, R., Li, C., Liang, X., Zhu, L., Zhang, Y., Liu, G., Liu, Q. H., Chen, H., & Wang, Z. (2019). Broadband waveguide cloak for water waves. *Phys. Rev. Lett.*, 123, 074501.

5

Conclusions & future outlook

In this Ph.D. thesis we investigated the conception and design of a novel device, termed elastic carpet cloak, which can protect structures from surface elastic waves, by smoothly detouring the waves around it, without any scattering effect or loss of energy. The wave guiding was achieved by properly designing the material properties of the cloak, based on principles from transformation elastodynamics.

5.0.1 Main conclusions

In Chapter 2, we examined the elastodynamic equations for cloaking of Love waves in an isotropic layered medium. Exploiting the invariance of the equations under a curvilinear coordinate transformation, it is possible to map the properties of the initial system to the transformed one. We proved, via numerical finite element simulations, the validity of the proposed mapping, showing both the invariance of the dispersive properties of Love waves and the near zero scattering for configurations with cloaked defects. Next, for a surface triangular defect, we applied a straightforward homogenization technique to map the material properties of the ideal cloak onto a monoclinic double-material unit cell. The unit cell allows the realization of a layered cloak with a feasible microstructure. We confirmed the validity of the adopted homogenization step by comparing the performances of the layered cloak with those of the ideal cloak. In addition, by performing parametric analyses with respect to the size of the unit cell, we concluded that the layered cloak's dispersion curves converged to the ideal one, as the length of the unit cell decreased. This methodology showcased excellent performance and feasibility for cloaking Love waves.

As a further step, in Chapter 3, we explored the possibility of cloaking Rayleigh waves. In particular, the ability to cloak incident Rayleigh waves would represent a significant scientific advancement toward seismic and vibrations isolation of structures. In this study, we developed a strategy to cloak surface defects from incident Rayleigh waves by means of symmetrized anisotropic elastic tensors. To this purpose, we used transformation elastodynamics and exploit the invariance of the Navier elastodynamic equation by assuming a Cosserat kinematic constrain (gauge) between the displacement fields. The obtained transformed cloaked region is thus characterized by a non-symmetric elastic tensor. For this reason, we adopted a symmetrization technique exploiting the arithmetic mean to approximate the non-symmetric Cosserat material with a composite material of symmetric elastic tensors. We investigated the efficacy of the proposed design by performing time-harmonic numerical

simulations and dispersion analyses, analyzing cloaks with a triangular shape and semi-circular ones with different radial distributions (linear and non-linear). Among these designs, the symmetrized semi-circular cloak with effective properties obtained from quadratic transformation demonstrated the most effective cloaking performance.

Finally, in Chapter 4, we delved into the possibility of designing a full 3-D cloak for Rayleigh and Love waves. As in the previous chapter, we employed a Cosserat kinematic relation for the displacements to acquire the requisite mechanical properties for cloaking. Assuming only cylindrical symmetry we designed cylindrical cloaks of triangular and semi-circular cross sections, respectively. Notably, the 3-D problem proved distinct from the superposition of Love and Rayleigh waves since it required a heterogeneous system due to the exclusive propagation of Love waves in layered media, resulting in Rayleigh waves with dispersive characteristics. In addition, by comparing the weak formulation for the 3-D equation of motion and the separate weak form solutions of Love and Rayleigh waves, we denoted the presence of an extra set of coefficients in the transformed elasticity tensor that was eliminated at each of the previously examined cases. Under this 3-D setting, we proposed a symmetrization strategy involving constraining the related symmetric coefficients to satisfy the weak-form solution of Love waves and symmetrize the remaining terms according to the generalized mean. This strategy aimed to identify the combination of symmetrization and cloak geometry that yields optimal cloaking efficiency. Time-harmonic simulations and dispersion analyses were conducted to validate the performance of the cloaks designed according to the developed framework. In contrast with the previous chapters, where the assumption of a 2D geometry restricted the dynamics of the cloak to plane waves with orthogonal incidence w.r.t the cloak, through this 3-D formulation we tested the dispersive properties of the proposed cloaks upon multiple angles of incidence. Through the analyses, we showed that a symmetrized semi-circular cylindrical cloak, constructed by the so-called "Maximal" mean, provided significant cloaking protection across all the computed frequencies.

In summary, this Ph.D. thesis represents a significant contribution to the field of wave protection,

demonstrating innovative methods for cloaking both Love and Rayleigh waves. Through meticulous analysis, numerical simulations, and material design, this research could pave the way for practical applications in seismic and structural engineering, potentially revolutionizing seismic protection for structures and infrastructure.

5.0.2 Future outlook

As a sequel of this work, we envisage many possible future studies, including:

- Exploring three-dimensional cloaking shapes beyond cylindrical structures, such as a pyramid or a sphere. It will be interesting to compare the impact of symmetrization in such cases, since both cloaks will exhibit a higher number of non-symmetric entries in the elasticity tensor.

- In our current analyses, we focused exclusively on piece-wise isotropic semi-infinite mediums. Further developments could revolve around extending our cloaking strategies to arbitrary waveguides, considering diverse shapes and distributions of the mechanical parameters.

- Cloaking in the elastodynamic regime is inherently connected to the frequency of interest, making it challenging to establish a single performance metric to achieve broadband cloaking capabilities. An extension of our research could pertain to derive the elastic scattering coefficients for both ideal and symmetrized cloaks, with a goal of identifying the most suitable, if any, symmetrization function.

- It is important to acknowledge that the concept of cloaking is essentially a complex, multivariable problem that depends on the given geometry, the mechanical parameters and also in the frequency range of interest. Consequently, formulating an optimal design strategy for elastodynamic cloaks is imperative.